This is to certify that the
dissertation entitled

Formation and Characterization of Air Stable Phospholipid Adlayers on Modified Substrates

presented by

Benjamin Oberts

has been accepted towards fulfillment
of the requirements for the

Doctoral degree in Chemistry

Major Professor's Signature

9/14/2009

Date

FORMATION AND CHARACTERIZATION OF AIR STABLE PHOSPHOLIPID ADLAYERS ON MODIFIED SUBSTRATES

By

Benjamin Oberts

A DISSERTATION

Submitted to
Michigan State University
in partial fulfillment of the requirements
for the degree of

DOCTOR OF PHILOSOPHY

Chemistry

2009

ABSTRACT

FORMATION AND CHARACTERIZATION OF AIR STABLE PHOSPHOLIPID ADLAYERS ON MODIFIED SUBSTRATES

By

Benjamin Oberts

Plasma membranes are essential to the function of cellular systems. As a consequence of this fact many proteins and other biological species are not active outside of their native environment. It would be ideal to create an artificial structure that could house selected biomolecules in their active forms, enabling their use in applications such as bio-sensing, for example. As the understanding of these complex and dynamic bilayer structures increases, it has become clear that their stability in air is not sufficient for use in many chemical sensing applications. For this reason, the work presented here was undertaken to find ways to optimize interactions between lipids and planar substrates, enabling the formation of air-stable lipid adlayers. Several phospholipids were explored; 1,2-dimyristoyl-sn-glycero-3-phosphatidic acid (DMPA), 1,2-dimyristoyl-sn-glycero-3-phosphocholine (DMPC), 1,2-dimyristoyl-sn-glycero-3-phosphoethanolamine (DMPE), 1,2-dimyristoyl-sn-glycero-3-[phospho-rac-(1-glycerol)] (DMPG), and 1,2-dimyristoyl-sn-glycero-3-[phospho-L-serine] (DMPS). These lipids, in vesicle form, were exposed to chemically modified substrates and underwent vesicle fusion to create lipid adlayers. The Au substrates on which the adlayers were deposited were modified to interact with the phospholipid headgroups. The resulting lipid adlayer was stable with respect to transport across the water/air boundary. The chemical modification of the interface was

accomplished using 6-mercapto-1-hexanol to form a self-assembled monolayer characterized by a polar, hydrophilic interface. The 6-mercapto-1-hexanol monolayer was reacted with $POCl_3$ and water to create a phosphate-terminated interface. The phosphate functionalities were populated with Zr^{4+} ions, rendering them capable of complexation with phospholipid phosphate moieties. Other metal salts were also used to gain insight into the effect of metal ion identity on the binding of phospholipids. To characterize the lipid adlayers, time correlated ellipsometry, water contact angle, cyclic voltametery, XPS, ^{31}P-NMR and FTIR measurements where used. All of the analyses performed were *ex-situ* from the lipid deposition vessel, demonstrating air-stable adlayer formation. Each technique interrogated a different adlayer property. The discovery of a novel family of self-assembling adlayer comprised of biologically important molecules opens the possibility of future success in the creation of robust biomimetic interfacial structures.

To my wife Carrie
and our cat Lucky

To my wife Carrie
and our cat Lucky

Acknowledgements

I would like to first thank my advisor Gary Blanchard for his support and guidance through out my time in graduate school. He has been a guide through these tough years and has always been there to point me in the right direction or supply a new idea. I have learned a lot from his teachings and will carry with me the experience and confidence that he has instilled in me. As he once said to me "the best way to learn how something works it to take it apart and put it back together." This holds true and I will apply this mentality were ever I end up and toward any problem I face. I have been very fortunate to have known him and work with him.

I would also like to thank my friends and fellow group mates as they have always been there for me through failed experiments and new discoveries. I will miss our weekly lunches out as well as the time we spent together in the lab. Being friends with and working with such talented and knowledgeable people made it a joy to get in the lab and made it easier to work the long hours that some experiments required.

I would like to say thanks to my parents Chuck and Leslie Oberts, who have always been there to support me through all my endeavours. They have always gone far beyond what was necessary to help me. Much of what I am today I owe to them and their continued support.

Finally, my greatest thanks goes to my wife Carrie. From moving to Michigan to constantly reassuring me that I will figure out the next problem she has been my rock. Her patience and constant belief in me, even when I did not believe in myself, has been the driving force behind my success. I truly would not have gotten my degree with out her. Out of all the things in my life I am most proud and thankful to be her husband and to have her at my side through it all.

TABLE OF CONTENTS

LIST OF TABLES

LIST OF FIGURES

Figur

Figur

Figur

Figur

Chapter 1

Introduction

Biological systems are complex and dynamic, and consequently it is difficult to gain molecular scale insight into their behavior. The cellular level is the typical starting point for the evaluation of biological function, but progress in our ability to measure complex molecular structures at low concentrations has lead to further questions on how such molecular complexity serves to produce functional biological systems. Mammalian cells contain components such as mitochondria, a nucleus (except for erythrocytes), and a cell membrane, among others. Each of the sub-structures within a cell is characterized by significant molecular complexity and there is much current research activity in the area of detailed characterization of the component parts of cellular systems. Plasma membranes serve as an excellent example of this complexity. The lipid bilayer structure that defines the plasma membrane serves a critical role in supporting trans-membrane proteins, which regulate cellular functions such as transport of ions and other species into and out of the cell. Perhaps the most basic function of the plasma membrane is to maintain cellular integrity and serve as an impediment to pathogens. Mammalian plasma membranes are composed of more than 100 different components,[1] including glycerophospholipids, sphingolipids and cholesterol, which make up ~50% of the cell wall. The balance of the plasma membrane is comprised of integral and peripheral proteins, and a detailed inventory of plasma membrane components varies according to cell function.[2,3] The complexity of the plasma membrane poses a substantial challenge to achieving a detailed understanding of membrane form and function. It is thought that this compositional complexity plays a role in stabilizing the folding of transmembrane proteins and thus mediating their function. It is clear that the relationship between molecular-scale

membrane composition and dynamics and transmembrane protein function is a prerequisite to the broad-based use of synthetic lipid bilayers in applications ranging from cellular function to chemical and/or biological sensing. It is not the purpose of this dissertation to achieve a connection between bilayer composition and transmembrane protein function. The focus of this work is on the more fundamental issue of how bilayer composition and interactions with interfaces can serve to mediate lipid dynamics and organization.

1-1: Understanding Lipid Bilayers

A prerequisite for the study of lipid bilayer structures is the ability to form such structures in a reproducible manner. Given the complexity of plasma membranes and the desire to construct biomimetic structures that are compositionally simpler, the primary focus of this work will be on phospholipids. The choice of phospholipids has been made because this family of molecules comprises the largest fraction of plasma membranes and because phospholipids can form bilayer structures without the addition of other components, such as sterols, for example. Phospholipids are amphipathic, containing two hydrophobic carbon tails that are bound to any of several hydrophilic head group functionalities through a phosphate linkage. Fig. 1-1 shows a phosphocholine as an example

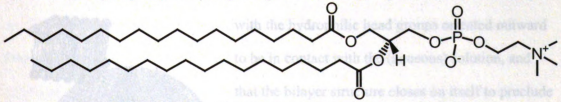

Fig. 1-1: 1,2-Distearoyl-*sn*-Glycero-3-Phosphocholine (DSPC)

phospholipid. The head group (choline is shown in Fig. 1.1) can vary in size, polarity, and charge while the acyl chains vary in length and the presence of unsaturation(s). The acyl chains can either be identical or different, both in length and in the presence of unsaturations. This structural variability allows for complex mixtures of phospholipids in

bilayer structures, yielding a commensurate complexity in terms of understanding bilayer organization and stability. Lipid bilayers are quasi-two dimensional structures characterized by compositional heterogeneity and fluidity, and it is this latter property that adds significant complexity to the study of these systems.[4-16] The work presented in this dissertation focuses on comparatively simple lipid mono- and bilayer structures, which are intended as starting points in developing supported biomimetic structures for potential use in areas such as chemical sensing and selective lipid detection.[17] It should also be noted that while this dissertation focuses on planer supported lipid bilayers on modified interfaces, it is expected that the dynamics and molecular interactions of non-supported bilayers are going to carry over to supported bilayers. It is then important to first discuss these interactions.

1-2: Phospholipid Vesicles

Phospholipid vesicles where devised as a possible means of simulating a plasma membrane. In an aqueous medium, phospholipids will self-assemble to form a bilayer structure called a vesicle (Fig. 1-2). The key structural features of the vesicle are that the lipid tail region for each lipid layer is directed inward, toward the center of the bilayer, with the hydrophilic head groups oriented outward to be in contact with the (aqueous) solution, and that the bilayer structure closes on itself to preclude exposure of the acyl chain region to an aqueous environment. The presence of the inner lipid layer differentiates a vesicle from a micelle structure.

Fig 1-2: Model vesicle structure

Through the study of bilayer structures, mostly in the form of vesicles, it has been found

that even for binary and ternary systems, phase separation between the constituents can occur.[8,15,18-20] The phase separation of different lipids and/or lipids and sterols plays a major role in determining the organization and fluidity of the vesicles. For such comparatively simple systems to provide meaningful insight into organization in the substantially more complex plasma membranes, it is important to understand first the organizational behavior of the model system. It is thought that the phase separation and fluidity that is characteristic of plasma membranes mediate the function of transmembrane protein.[21,22]

The issue of bilayer composition is inherently related to bilayer fluidity. Bilayers exhibit phase transitions between a variety of phases, depending on the composition of the bilayer and the temperature. It has been observed that several phase transitions occur with increasing temperature. At a low temperature for a given lipid, a bilayer will exist in a crystalline gel phase (L_c), which undergoes a transition to lamellar gel phase (L_β), which can undergo a further transition to a rippled gel phase (P_β) with increasing temperature.[23] The gel-to-fluid phase transition, which occurs with a further increase in temperature, is labeled the gel-to-fluid phase transition temperature (T_m), and is thought to proceed because of the acyl chains undergoing a structural change from predominantly all-trans to a conformation with a significant contribution from trans-gauche conformers.[24] The rationale for phase transitions in bilayer systems is the balance between thermal energy and the attractive inter-chain interactions that operate in the acyl chain region of the bilayer. It is clear on physical grounds that the value of T_m, or any of the preceding transitions will be influenced by the length and degree of unsaturation of the lipid acyl chains. The measurement of T_m is a well established means of characterizing bilayer structures.[21,22,25-27] The relative ease of measuring T_m compared to other phase transitions, and the sensitivity of the transition temperature to impurities within the bilayer, provides an important gauge of lipid purity and suggests that impurities may play

an important if underestimated role in determining the range of literature values that have been reported for a given system.

1-2.1: Fluidity and the Effect of Impurities on Lipid Vesicles

Koan and coworkers[28] examined the effect of impurities on the phase transition temperature of the C_{14} phosphocholine DMPC using time-resolved fluorescence measurements. These experiments reported on the anisotropy decay dynamics of a chromophore inserted into the acyl chain region of the vesicles as function of the amount of impurity (14:1 PC) present in the bilayer. It is useful to review this measurement to understand how T_m is extracted from the anisotropy decay data. The induced orientational anisotropy function, which is a measurement of the orientational relaxation of molecules excited by polarized light to a random distribution, can be performed using time-correlated single photon counting (TCSPC) spectroscopy. Data collected from this measurement contains information pertaining to the motion of a chromophore within the lipid bilayer, which is present in this case in the form of a vesicle. The goal of anisotropy decay measurements is to acquire molecular reorientation information, specifically the reorientation time constant(s), which depend on the identity of the chromophore and the environment in which it resides. In the case of this work, temperature-dependent changes in the reorientation time constant reveal the temperature, T_m, at which the gel-to-fluid phase transition occurs. The chromophore local environment will affect the functional form of induced orientational anisotropy decay. Calculation of the anisotropy decay function with equation 1-1 is accomplished by taking the normalized difference between the fluorescence transients polarized parallel and perpendicular to the incident vertically polarized excitation pulse. In its

$$r(t) = \frac{I_{\parallel}(t) - I_{\perp}(t)}{I_{\parallel}(t) + 2I_{\perp}(t)} \qquad (1\text{-}1)$$

$$r(t) = r(0)\exp\left(\frac{-t}{\mathrm{t}_{OR}}\right) \qquad (1\text{-}2)$$

$$\mathrm{t}_{OR} = \frac{\mathrm{h}Vf}{k_B TS} = \frac{1}{6\mathrm{D}} \qquad (1\text{-}3)$$

simplest interpretation, the anisotropy decay function is fit to equation 1-2 to extract the reorientation time, τ_{or}. In equation 1-2, r(0) is the initial anisotropy, which is related to the angle between the excited and emittng transition dipole moments, and can range from -0.2 to 0.4. Measurement of the reorientation time allows the calculation of the viscosity h according to the modified Debye-Stokes-Einstein equation (equation 1-3).[29-31] In this equation, *V* is the hydrodynamic volume of the chromophore, calculated according to Edward's formulation,[32] k_b is the Boltzmann constant, T is the temperature in K, *f* is the "friction" coefficient for the solvent-solute interaction boundary condition, and *S* is the shape factor to account for non-spherical shapes, which ranges from 0 to 1. This data yields a general picture of the system.

Koan et al,[28] used perylene as the "probe" chromophore. Perylene has a well characterized linear response and is a planar polycyclic aromatic hydrocarbon, a structure useful for the interrogation of the lipid bilayer acyl chain region. A time-correlated single photon counting apparatus was used and the results from this system allowed detailed information to be obtained on the chromophore local environment.[33,34] The bilayer system used was composed of two different lipids; 1,2-dimyristoyl-sn-phosphatidylcholine (14:0 PC) and an "impurity" of 1,2-dimyristoyl-sn-glycero-3-phophocholine (14:1 PC). Fluorescence lifetime and anisotropy data was collected for perylene in vesicles containing controlled ratios of 14:0 PC to 14:1 PC at several temperatures. These data exhibited a discontinuous change in τ_{or} at T_m which is interpreted in the context of a change in the molecular scale organization of the lipid bilayers.

Results from this work indicate that impurities can significantly influence the phase transition temperature T_m.[28] Vesicles of 14:0 PC exhibited T_m at 24°C, in agreement with the literature.[35] Upon addition of 14:1 PC "impurity", T_m decreased considerably. For 0.3 mol% of 14:1 PC, Tm decreased by ~15°.[28] Increasing the concentration

of 14:1 PC further lowered T_m, but the change in T_m with 14:1 PC not as great as it was for the initial addition. T_m changes with increasing 14:1 PC concentration exhibit a monotonic decrease, demonstrating that a relatively small amount of impurity gives rise to large changes in the organization of the bilayer. It is interesting to note that while the value of T_m changed significantly with the presence of the impurity, the viscosities sensed by the chromophore did not. For the fluid phase viscosities were in the range of 8.5 ± 1.5 cP and the gel phase viscosities lied in the range of 14.5 ± 2.5 cP.[27] While the impurities may perturb the organization of the bilayers, the interactions responsible for maintaining bilayer structure do not change.

The overall conclusion to be drawn by this work is that even the simplest systems pose problems in understanding their intrinsic complexity at the molecular scale, and further work is necessary to develop an understanding before it will be possible to create systems that can function as biomimetic plasma membrane structures. While this study focused on the bilayers in the form of vesicles, the interactions probed are pertinent to supported bilayer structure described in this work.

1-2.2: Lipid Rafts

Lipid heterogeneity in vesicle systems has lead to further observations and challenges in regard to the complexity of these systems. Binary mixtures of cholesterol and phospholipids are found to be miscible however, when cholesterol is mixed with two phospholipids of varying melting temperature (T_m) to form a ternary mixture, cholesterol can complex preferably with one phospholipid creating "rafts" or condensed complexes that phase separate.[36-39] Rafts have been observed as distinct domains with reduced diffusion within cell membranes.[38] These physical properties may suggest that these organized regions could be locations for specific proteins to interact with the membrane,

which could lead to further bilayer satiability. It has also been theorized that some proteins require the presence of raft structures and, as such, pure phospholipid bilayers will not provide the required biomimetic environments for functional biomolecules.[38] These theories suggest that lipid rafts are important due to their putative role in mediating protein functionality as well as other cellular functions.[38,39]

It has been proposed that the cholesterol rafts will form between mixtures of cholesterol and saturated lipids because cholesterol is immiscible in unsaturated lipids.[38] Mixtures of cholesterol and two lipids with different melting points have exhibited two liquid phases, particularly if the T_m's for the two different lipids are widely different.[19,40-42] To observe and characterize these lipid-cholesterol domains, Veatch and coworkers[43] utilized ^{1}H-NMR techniques and fluorescence microscopy. Giant unilamellar vesicles (GUVs) were created that were composed of 30% cholesterol and varying ratios of 1,2-dioleoyl-sn-glycero-3-phosphocholine (DOPC) and 1,2-dipaplmitoyl-sn-glycero-3-phosphocholine (DPPC). ^{1}H-NMR data reveal that not only are domains being formed but it is possible to map the phase boundary of the domains from one relatively homogenous domain in the vesicles, to two liquid domains containing lipid and cholesterol or lipid only. Fluorescence microscopy was utilized to image the GUVs for that investigation. Fig. 1-3 shows the fluorescence micrographs of the GUVs at different ratios of lipids.[43] It is clearly visible from Fig. 1-3 that lipid domains are being formed, as well as upon larger concentrations of the miscible lipid DPPC, the domains become larger until they encompass the majority of the

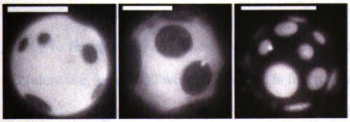

Fig. 1-3: Fluorescence micrographs of GUVs at 25°C and compositions of 30% cholesterol mixed with 2:1 DOPC/DPPC, 1:1 DOPC/DPPC, and 1:2 DOPC/DPPC. The scale bars indicate 20 μm. Figure adapted from Veatch and coworkers.[42]

GUV, leaving DOPC minor domains. Both the ^{1}H-NMR and fluorescence data indicate the formation of two phase domains. From this work it was found that the domains can be as small as ca. 80 nm and projected phase diagrams are consistent with other studies.[43]

To quantify the results reported by Veatch and coworkers,[43] a thermodynamic model was developed by Radhakrishnan and McConnell.[36,37] In their model it is assumed that there are four different species in the liquid phase of the bilayer at equilibrium. These consist of un-reactive lipids (DOPC), reactive lipids (DPPC), free cholesterol, and the reactive lipid-cholesterol complex. Assuming all species are present in equimolar amounts, the Gibbs free energy can be express as Equations 1-4.[37] In this equation μ_i^0

$$G = \sum_i x_i(\mu_i^0 + kT \ln x_i) + 2k\sum_{i<j} x_i x_j T_{ij}^0 \qquad (1-4)$$

is the chemical potential of pure component i and x_i is the equilibrium mole fraction. In the simplest model, all of the chemical potentials would be constant except that of the complex, which would leave $-kT \ln K$, while all of the critical temperatures (T_{ij}^0) are assumed to be below 298 K with the exception of the binary un-reactive/complex pair labeled T_c^0.[37] From these assumptions it is then possible to model the phase behavior of the DOPC/DPPC/Cholesterol system for varying temperatures and equilibrium constants for the complex (K). This approach allows for a qualitative model to account for the experimental data.

To further understand these multi-component systems, allowing for their potential future use, significant work to incorporate functioning proteins in to these structures has been investigated. Evidence that rafts could be the site of important protein lipid interactions has surfaced.[45] One such study focused on the disorder of extracellular inorganic phosphates. It has been observed that type IIa renal apical brush border membrane (BBM) sodium/phosphate co-transporter (Na/Pi) protein systems play a major role

in mediation of the renal proximal tubular BBM Na/Pi transport which helps prevent hypophosphatemia or hyerphosphatemia by regulating renal and gastrointestinal phosphate reabsorption.[44] Finding the mediating factors of the Na/Pi would allow a better understanding of how to address the reabsorption of the renal phosphate. While the bulk of this work is not pertinent to the discussion at hand, it was found that samples taken from control rats indicated that the majority of the Na/Pi in the samples was found to be located by highly enriched areas of cholesterol, sphingomyelin, and glycosphingolipids.[45] This is indicative of the impact of these lipid rafts on the function of cellular systems and shows that further work is still necessary for a further understanding to be had with this multicomponent lipid rafts.

What these studies show is that lipid heterogeneity in plasma membranes is a crucial factor that leads to bilayer stability as well as bilayer interactions with other species. While the supported bilayers discussed in this dissertation focus on much simpler systems, future work on supported bilayers will explore interactions of analogous complexity in vesicle systems, and having an understanding of these systems is thus germane to the design of future expemiments.

1-3: Supported Lipid Bilayers

With a working understanding of lipid vesicle systems it is possible to move on to supported lipid bilayers. Vesicles are limited to some extent because of the variability associated with the curvature intrinsic of vesicles, which can differ widely from the curvature of a typical plasma membrane. Vesicles are also suspended in solution, and for applications such as chemical or biological sensing, a planar, supported bilayer structure is of more immediate interest.

Supported lipid bilayers (SLBs) are interesting not only because they provide a

structural motif that may be useful for chemical sensing, but also because the connection of the bilayer to a planar substrate can pose a significant chemical and physical challenge, and the properties of the resulting bilayer structure may be perturbed by the presence of the substrate. Supported lipid bilayers are typically deposited on a planar substrate which removes issues arising from the radius of curvature that lipid vesicles give rise to. Additionally, these same characteristics have been thought to lend the SLBs to be a more ideal model systems for plasma membranes opposed to vesicles.[46-50] It should be noted that real cells are curved so while vesicles may mimic this aspect of plasma membranes. Since the lipids are supported in the SLBs, they are easier to work with and lead to several possible materials applications, including the ability to be utilized as biochips or biosensors utilizing naturally existing biomolecules as well as for multiple uses including medical diagnosis and drug discovery.[50-54] For one possible example of a future application, it has been observed that many biomolecules lose their activity away from their native environment, one means of getting around this is to fabricate an artificial environment that mimics the native environment such as a SLB.[55-57] Therefore it is beneficial to have a quick and efficient way to develop SLBs that can then be used for further analysis. One down side to SLBs though is that they are harder to fabricate.

1-3.1: SLB Formation

There are two primary ways that SLBs are formed. The first is Langmuir-Blodgett (LB) deposition followed by Langmuir-Schaefer (LS) deposition.[57] LB-LS lipid deposition (Fig 1-4a) has been utilized to create SLBs.[16,57] This approach has several advantages, including the ability to create monolayers or bilayers depending on which deposition method(s) are applied. As is shown in Fig 1-4a, withdrawal of the vertically mounted substrate to effect LB deposition produces a monolayer on each side of the

substrate. With LS deposition, horizontal contact with a surface adlayer occurs. The substrate is suspended and contacts a surface layer held at a specific surface pressure. Performing this horizontal dip on a substrate that already contains a lipid layer deposited using LB methodology produces a lipid bilayer structure.[57] This approach allows for the formation of comparatively well organized bilayers.[57] SLBs can form on hydrophilic substrates of various composition[16] because lipid headgroups will be attracted to such surfaces, facilitating lipid adlayer organization. Though LB/LS deposition methodology does have many advantages, it is time consuming and labor intensive, and from a chemical standpoint it is sensitive to chemical contaminants.

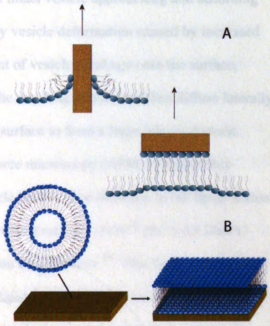

Fig. 1-4: A) Langmuir-Blodgett and Langmuir-Schaefer lipid deposition. B) Vesicle fusion

An alternative to the step-wise construction of SLBs is to deposit lipid bilayers on hydrophilic surfaces using vesicle fusion. This technique is useful because it allows for the solution phase creation of the lipid bilyers with wide control over vesicle composition, followed by the single-step deposition of the bilayer onto the substrate of interest. Vesicle fusion is a self assembly technique that starts with the lipids in vesicle format and, upon contact with the appropriate hydrophilic surface, the vesicles open and bind, either by physisorption or chemisorption, to the surface. Experimentally, vesicle fusion is a relatively quick and straightforward means to deposit SLBs and has been utilized in a variety of studies.[58,59] The details of vesicle fusion are not understood fully

at this point. It is believed to proceed with an intact vesicle approaching and adsorbing to a hydrophilic substrate surface, followed by vesicle deformation caused by increased lipid interaction with the substrate, to the point of vesicle breakage onto the surface, producing a region covered with a bilayer. The resulting bilayer can then diffuse laterally and merge with other bilayer domains on the surface to form a large bilayer domain. Schönherr and coworkers[59] utilized atomic force microscopy (AFM) to follow this process and develop this mechanism for vesicle fusion. The diffusion of the lipids across a substrate surface has been found to be fast, with a rate of 1-8x10^{-8} cm^2/s for DMPC and DOPC bilayers above their phase transition temperatures.[16] This finding may imply relatively fast lipid dynamics within a single lipid leaflet. Vesicle fusion has been shown to be adsorption limited; higher concentrations of vesicles in solution do not produce faster vesicle fusion.[58]

1-3.2: Inter-Layer Exchange (Translocation)

In addition to the substantial effort dedicated to the examination of dynamics and composition within a single lipid leaflet, there has also been an effort to understand inter-leaflet dynamics in bilayer structures.[28,60,61] Inter-layer exchange, termed translocation, is the movement of a lipid from one layer or "leaflet" to the other layer in a bilayer system. Translocation is important for several reasons, including lipid renewal,[62] lipid organization and packing,[63] protein sorting, and even raft formation.[64] The literature extant provides apparently contradictory information, with some reports suggesting that a "flippase" protein is required to mediate the translocation process,[65-68] and other reports using probe molecules, indicating that spontaneous translocation can occur. It is known that plasma membranes are asymmetric,[63,64,69] a situation that could argue either for or against lipid translocation. There are a variety of ways in which translocation can

proceed, with protein mediation being the most widely accepted means.[70] There are two types of mediating proteins: ATP-independent and ATP-dependent. ATP-independent proteins are thought to move lipids to/from either bilayer leaflet, but not against a compositional gradient.[67] ATP-dependent proteins can overcome compositional gradients, allowing lipids to be moved across a bilayer regardless of compositional differences between the layers.[67,69] There is also a body of work that indicates spontaneous translocation, but in cases where "probe" lipids were used, the structural issues associated with the probes called into question the time constants derived from such work.[67,71] The most elegant investigation of lipid translocation involved the use of nonlinear sum-frequency vibrational spectroscopy.[72] In that work, the "probes" were perdeuterated phosphocholines, which could differ in mass from the proteolipids by as much as 10%,[72] depending on acyl chain length. From this there is still room for understanding in terms of SLB lipid dynamics.

1-4: Controlling Vesicle Fusion

With the dynamics of supported bilayers in mind, in order to make useful structures it is necessary to have some from of control over the vesicle fusion process. Vesicle fusion on unmodified polar supporting substrates does not yield significant control over lipid organization or structure of the bilayer. To address this limitation, several techniques have been developed that range from physical manipulation to chemical modification of the substrate. Initial work in this area utilized a physical barrier that was grafted onto the substrates to prevent lipid spreading and covering all of the substrate.[48] That study focused on creating barriers of aluminum oxide, ITO, chromium, and gold on a silica substrate which would then be exposed to vesicles. Varying the identity of the barriers produced a range of results upon lipid exposure. Aluminum oxide inhibits vesicle

fusion to areas with accessible silica and would act as a barrier where no lipid could pass. The remaining barriers (ITO, chromium, and gold) can adsorb the lipids from the vesicle however, the lipids become tacked to those barriers and lateral diffusion becomes blocked.[48] These barriers allow control over vesicle fusion to the substrate by controlling the locations where fusion can proceed, allowing in turn patterns of lipid bilayer to be formed on the silica substrate. This work does suffer from the fact that while one can achieve control the overall physical structure of the SLB, there remains a lack of control over the type or quality of SLB formed, thus limiting their utility.

It is also of interest to gain control over the ability of the surface to support the formation of a monolayer or bilayer, or to control the quality of the adlayer formed. Chemical modification of the substrate is required to achieve this level of control. As the work discussed above has shown, forming bilayers on hydrophilic substrates by vesicle fusion is relatively straightforward. However, modifying the surface of a SiO_2 substrate with either self-assembled monolayers (SAMs) or by controlling the oxidation level of the SiO_2 surface, it is possible to control lipid adlayer deposition and improve the quality of the adlayers formed.[73,74] Hydrophilic lipid headgroups interact with the SiO_2 surface causing the lipids to adsorb onto the surface via the lipid head group, causing vesicle rupture and the subsequent deposition of a bilayer. This approch is useful to form bilayer structures however as mentioned modification of the surface can allow for control of the structure formed as well which could lead to further possibilities that must be explored. The resulting hydrophobic SAM modified surface does not interact strongly with lipid headgroups from other vesicles but can interact with lipid acyl tail regions yielding significantly different results form the bare SiO_2 surface discussed preveously.[73,74] If the hydrophobic region of the vesicle is exposed to the SAM modified surface, through either the fusion of the vesicle on to a clear SiO_2 area on the surface and lateral diffusion over

the SAM region or free lipid in solution absorbing to the SAM, the resulting Van Der Waal's interactions of the SAMs and lipid acyl tails causes the formation of a lipid monolayer over top the SAM.[73] This approach now allows for structural control over lipid adlayer formation.

To facilitate better bilayer formation it is necessary to make the surface as hydrophilic as possible. Thorough oxidation of the surface and minimal opportunity for contamination are important factors in producing a hydrophilic surface.[72] In the study conducted by Isono and coworkers, it was found that the extent of SiO_2 surface oxidation can influence the quality of the bilayers formed upon vesicle exposure.[74] Bilayer formation in this study was followed by fluorescence imaging with NBD-PC and, upon chemical oxidation, showed a significant increase in bilayer quality compared to that of a hydrogen terminated silica surface which served to demonstrate the existence of unruptured vesicles. Thermal oxidation over a long period of time further improved upon that bilayer quality significantly.[74] What this indicates is the use of SAMs and other forms of chemical surface modification allows for some level of control over the lipid adlayers formed as well as the quality of those layers.

1-5: Introduction of Work Performed

The ability to form SLBs has allowed for opportunities to investigate some of the details of lipid mono- and bilayer organization. SLBs can be made to be stable in air and can be formed in multiple ways and the supported substrate can be modified to allow for more selective control over the lipid layers formed. These studies have provided some level of insight regarding the dynamics of membrane adlayer constituents. A limitation of this area of work is that many of the known supported bilayer systems are fragile and cannot pass through the water/air interface without degradation. This degradation in-

cludes the formation of defects in the bilayer to complete collapse of the the bilayer structure. A lack of stability in air makes further examination of supported limited bilayers significantly more difficult. All analysis of the bilayers formed has to be in situ, limiting several spectroscopic techniques that could be useful in probing the details of lipid/lipid interactions within the bilayer structure.

The work reported here is intended to achieve a better understanding of the formation of selected lipid adlayers. Specifically, the formation of air stable bilayers was a primary focus of this work based on the hypothesis that the strength of lipid-substrate interactions was the primary factor that limited the formation of stable lipid adlayers. To create robust interactions between the lipid adlayer and the substrate, a well organized, hydrophilic substrate is required, and hydroxythiol SAMs on Au are one such surface. It is also a comparatively simple matter to react the terminal SAM hydroxyl groups to form a phosphate group, followed by zirconation of the phosphate group. The strategy to creating strong lipid-substrate interactions is to utilize robust interaction chemistry. A goal of this dissertation is to establish how well zirconium phosphate/bisphosphate (ZP) chemistry can be used to bind phospholipid head groups. The acyl tails of the lipids are composed of carbon-carbon and carbon-hydrogen bonds, leaving little interaction other that Van der Waals forces to mediate organization and stability. As previous studies have shown, these forces are central to the phase transitions in lipid bilayers and are important in the development of self-assembling monolayer systems. The lipid headgroups allow for the use of polar and/or ionic interactions to develop energetically favorable structures that are capable of maintaining their structural integrity under a wider range of environmental conditions that are hostile to physisorbed lipid bilayer assemblies.

Results from this work could point the way toward several possible opportunities in interface-mediated science, such as chemical/biological sensing and chemical sepa-

rations. It is also necessary to develop an understanding of the interactions that could give rise to lipid-specific surfaces, which could be utilized in lipid separations. Utilizing hydroxythiol SAMs and ZP chemistry to modify Au substrates allowed probing of interactions that lead to stable lipid adlayer formation. The initial aspect of this work were to investigate these surface/lipid interactions and move towards development of reproducible, air stable lipid adlayers.

Chapter 2

Formation of Air-Stable Supported Lipid Monolayers and Bilayers

2-1: Introduction to Air-Stable SLBs

The creation of planar supported lipid bilayers (SLBs) has been pursued because of their potential to function as biomimetic structures to facilitate studies aimed at understanding the function of transmembrane proteins. Such supported bilayers can be used to help understand the structural complexity and compositional heterogeneity of multicomponent lipid bilayer systems. Lipid bilayers, as discused earlier, are quasi-two dimensional structures characterized by both structural heterogeneity and fluidity, and it is this latter property that adds significant complexity to the study of these systems.[4-16]

While a great deal of work has been done in creating biomimetic bilayer films, the current understanding in the field is that such films cannot maintain their structural integrity upon exposure to air.[75] The instability of the bilayers in air is thought to originate at the point when the bilayer crosses the water/air interface following deposition, giving rise to bilayer disorganization and/or decomposition that is ultimately determined by the limited strength of interaction(s) between the bilayer and the supporting substrate. Several techniques have been explored to synthesize air-stable SLBs, including polymerization of the lipids that comprise the bilayers, the addition of stabilizing components such as cholesterol to the lipid mixture, or even the creation of physical boundaries on the solid support to prevent uncontrolled lipid spreading on the support surface.[75-77] Substantial effort has been dedicated to examining the dynamics and composition of single lipid leaflets in-situ, and there have also been efforts to understand inter-leaflet dynamics in bilayer structures.[28,60,61] However, the intrinsic structural and stability limitations of SLBs have prevented analogous experiments from being performed on that

fami

erati

crea

subs

imm

phos

show

be po

sition

to prep

groups

strongl

surface

exposu

action o

strong i

terface,

a ca. 20

using op

T

tammetry

character

faces. Th

family of structures.

Among the issues of concern is the extent to which the bilayer leaflets act cooperatively to stabilize the overall structure. It would be useful to have a facile means of creating either a monolayer or bilayer structure by simply controlling the identity of the substrate on which the layer is deposited. The use of Zr-bisphosphate (ZP) chemistry to immobilize lipid headgroups is an inviting possibility. This chemistry is known to bind phosphates and phosphonates strongly,[78-86] and if phosphocholine headgroups can be shown to bind to a zirconated surface, the creation of supported lipid monolayers would be possible without resorting to Langmuir-Blodgett (LB) or Langmuir-Shafer (LS) deposition methods.

In the work presented in this chapter, monolayer interfacial chemistry is used to prepare two surfaces; a polar interface capable of interacting with lipid bilayer headgroups noncovalently, and a second interface capable of binding the lipid headgroups strongly. Bilayers form readily and are stable for extended periods of time on an Au surface modified with 6-mercapto-1-hexanol, even following removal from solution and exposure to air. For Au substrates modified with 6-mercapto-1-hexanol, followed by reaction of the terminal –OH groups with $POCl_3$, H_2O and Zr^{+4}, it is observed that there are strong interactions between Zr^{+4} and the phosphocholine lipid headgroup.[87] For this interface, lipids originally present as a partial bilayer evolve to a monolayer structure over a ca. 20 minute time period. This partial bilayer-to-monolayer conversion was monitered using optical ellipsometry and contact angle measurements.

To develop a full understanding of the interactions taking place FTIR, cyclic voltammetry, time-resolved ellipsometry and contact angle data are utilized, allowing for the characterization of the formation of lipid adlayers on the two chemically modified interfaces. The coupling of phospholipids to the Zr-terminated surface was demonstrate using

^{31}P NMR measurements.

2-2: Materials and Instrumentation Utilized

The lipid used for these experiments was 1,2-dimyristoyl-sn-glycero-3-phosphocholine (DMPC) dissolved in chloroform obtained from Avanti Polar Lipids, Inc. The solvents acetonitrile, ethanol (100%) and ethyl acetate, as well as the reagents 6-mercapto-1-hexanol, phosphorus oxychloride ($POCl_3$), zirconyl chloride octahydrate ($ZrOCl_2 \cdot 8\ H_2O$), 2,4,6-collidine, potassium ferrocyanide trihydrate, lithium perchlorate, hexammineruthenium(III) chloride, and potassium chloride were all obtained from Sigma-Aldrich in the highest purity grade available. 18 MΩ Water was used for all experiments and all reagents were used as received, without further purification.

The specific instrumentation used is as follows: Reflectance FTIR spectra of modified gold substrates were collected with a Nicolet Magna-IR 560 spectrometer in reflection mode with 2 cm^{-1} spectral resolution. The data are presented as normalized absorbance spectra. Electrochemical data were acquired using a CH Instruments 650 Electrochemical Analyzer. All optical ellipsometry measurements were recorded with a J. A. Woollam Co., Inc. spectroscopic ellipsometer with a wavelength range of 185-1100 nm utilizing 44 wavelengths at a time. Water contact angle measurements were recorded on an ACT Products Inc. VCA 200 Video Contact Angle System. Except where noted experiments were performed at 20°C.

2-3: Experimental Setup

For the electrochemical measurements two electrochemically active probes were used to characterize the interfaces. These were $K_3Fe(CN)_6 \cdot 3\ H_2O$ (1.32 mM) in 0.1 M $LiClO_4$ and $Ru(NH_3)_6Cl_3$ (1.00 mM) in 0.1 M KCl. These two probes were chosen

because of their different electron transfer kinetics.[88] Cyclic voltammetry was performed with each probe being cycled three times at a scan rate of 0.1 V/s. The $Fe(CN)_6^{3-/4-}$ probe was scanned from -0.1 to 0.5 V and the $Ru(NH_3)_6^{3+/2+}$ probe was scanned from -0.4 to 0.1 V vs. Ag/AgCl using a Pt counter electrode.

Each substrate was prepared in a similar fashion. Gold substrates were prepared using a procedure described previously.[89] Briefly, the substrates were rinsed with water and ethanol, cleaned in a UV-cleaner for 15 min., then exposed to 10 mM 6-mercapto-1-hexanol in ethanol for 6 hrs. The resulting interface was rinsed with ethyl acetate and ethanol, then dried under a stream of N_2(g). For Zr-modified interfaces, the mercapto-hexanol monolayer was reacted with $POCl_3$ (0.4 mL) in dry acetonitrile (10 mL), and catalyzed with 2,4,6-collidine (0.4 mL) for 3 hrs. The phosphate-modified monolayer was rinsed with ethanol and water, dried with N_2(g), and exposed to 5 mM $ZrOCl_2$ in a 60:40 ethanol/water solution for 12 hrs. The zirconated monolayer was dried under N_2(g), then exposed to the solution containing DMPC unilamellar vesicles.

To prep the DMPC for adlayer formation, unilamellar vesicles of DMPC were prepared first as described previously.[60] The vesicles used are comprised solely of DMPC. Chloroform was first evaporated from the DMPC solution using a N_2 stream. The lipids were then exposed to vacuum to remove any remaining chloroform. The solid DMPC was next dissolved in a 10 mM Tris(hydroxymethyl)-aminomethane hydrochloride (Tris®, Aldrich) pH 7.5 buffer solution to a final concentration of 1 mg/mL. The solution was treated with five freeze-thaw-vortex cycles to ensure thorough suspension of the lipids prior to extrusion.[90] A syringe-based mini-extruder was used to form uniform unilamellar vesicles (Avanti Polar Lipids, Inc.).[91-93] The lipid suspension was passed eleven times through a polycarbonate filter with an average pore diameter of 400 nm to produce unilamellar vesicles of that diameter.

With the unilamellar vesicles of DMPC formed, mono- and bilayer formation can then proceed. Planar DMPC adlayers were formed by spontaneous fusion of the unilamellar vesicles formed.[75] The clean gold substrates were placed in a custom-made Teflon® flow cell (Fig. 2-1) with an approximate volume of 1 mL. A flow cell was employed to ensure that the lipid suspension was in full contact with the substrate during bilayer formation. Tris® buffer was flowed over the substrate at approximately 5 mL/min prior to lipid deposition, followed by the lipid suspension, flowed at the same rate until the buffer solution is displaced. The lipid-containing solution is then held in place to allow exposure to the substrate for a given time. Following exposure, the substrate was washed with water at the same flow rate, the water is then removed from the cell at a rate of 1 mL/min, and the substrate is removed from the flow cell and allowed to air dry by hanging the substrate by one end.

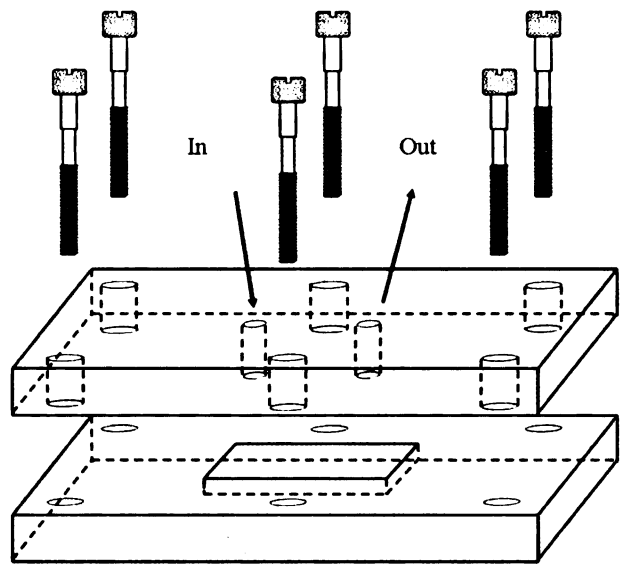

Fig. 2-1. Schematic of the Teflon® flow-cell used for the deposition of DMPC adlayers by vesicle fusion. The depth of the reservoir is ca. 2 mm.

In order to confirm the coordination of the lipid headgroup with the Zr substrate ^{31}P-NMR was performed. Solid-state NMR samples were prepared as described previously.[86] One gram of silica gel 60 (40-60 μm, 470-530 m^2/g surface area, EMD) was dried and placed under an Ar atmosphere. Silica gel was chosen as a substrate as it has the necessary –OH groups to perform the phosphonation and zirconation reaction; $POCl_3$ (2 mL) and dry acetonitrile (10 mL) were added to the silica gel and mixed. 2,4,6-Colli-

dine (2 mL) was added to this silica gel suspension and the solution was reacted for 3 hrs. The resulting suspension was dried and washed with acetonitrile to rinse away excess $POCl_3$ or other phosphorus oxides. A 5 mM $ZrOCl_2$ solution in 60:40 ethanol/water solvent was added to the silica gel, and the suspension was mixed for 12 hrs. The resulting suspension was dried and washed with ethanol and water. A 1 M DMPC solution in Tris® buffer was prepared and exposed to the silica gel for several hours. The resulting suspension was dried by filtration and washed with water. A sample of the functionalized silica gel was then taken at each of the drying steps in this process. The solution phase NMR sample was prepared using a 1 M DMPC solution. The chloroform was first evaporated from an aliquot of the stock DMPC solution and the resulting solid phase lipids were placed under vacuum to remove any remaining chloroform. The lipids were then dissolved in chloroform-d for NMR analysis.

Two different NMR instruments were utilized to collect the NMR measurements. ^{31}P MAS NMR measurements were made using a 400 MHz Varian Infinity Plus NMR spectrometer. The ^{31}P nuclei resonance frequency was 161.82 MHz for all spectra acquired with this instrument. Each sample was packed in a 6 mm diameter zirconium rotor and spinning speed was set to 4 kHz. MAS-NMR spectra were not proton-decoupled, and the nuclei were excited using a 90° pulse for a duration of 15 μs and an internal pulse delay of 1 s. 100 Hz of line-broadening was applied prior to processing the spectra to increase the S/N of the spectra.

Solution phase ^{31}P-NMR measurements were performed using a Varian UNITY-plus 500 MHz NMR spectrometer with a ^{31}P resonance frequency of 202.38 MHz. The spectra were proton-decoupled and the nuclei were excited with a 60° pulse for 7 μs and a recycle delay of 2 s. 1 Hz of line-broadening was applied prior to Fourier transform to increase the S/N of the spectra.

2-4: Results

The primary purposes of this work was to demonstrate a supported lipid bilayer that is stable in air, and to explore the consequences of a phosphocholine binding to a zirconated surface. Discussed first is the formation of an air-stable supported lipid bilayer, and then the formation of a supported lipid monolayer. With these interfacial structures characterized, the energetics of transition of an initially-deposited DMPC bilayer to monolayer on the zirconated surface is considered.

2-4.1: Air Stable Supported Bilayer Formation.

The creation of a supported lipid bilayer structure that is stable in air has been sought widely, with many attempts yielding interfacial lipid organization that is characterized by defects and possibly void regions.[75] There have been several methods devised for creating bilayers capable of surviving the passage through the air-water interface following their formation,[75-77,94] with methods for their formation ranging from the use of complex, multi-component systems to the growth of the bilayers on substrates such as PDMS.[94] In the work presented here, lipid bilayers comprised of DMPC are used, and these bilayers have been deposited via vesicle fusion onto substrates that are characterized by comparatively high densities of polar terminal functionalities. It is believed that the ability to form these air-stable supported lipid layer structures is dependent on the interfaces use.

DMPC has been deposited on a gold surface that has been modified with a self-assembled monolayer (SAM) of 6-mercapto-1-hexanol to produce a hydroxyl-terminated interface yielding a lipid bilayer. Present in Fig. 2-2a the FTIR spectrum of the interface prior to deposition of the bilayer. It should be noted that the background correction applied to these data has produced an artefactual sloping background that has no physical

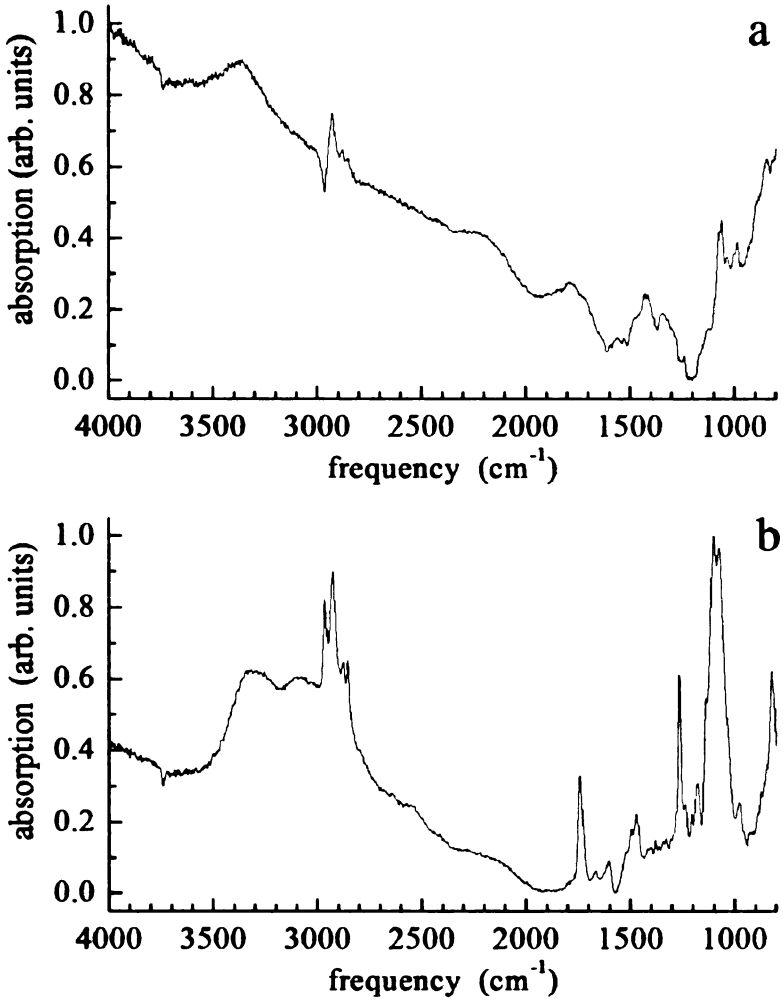

Fig. 2-2: FTIR spectra of (a) a 6-mercapto-1-hexanol self-assembled monolayer deposited on a gold surface. (b) a DMPC adlayer deposited on the 6-mercapto-1-hexanol-modified gold inter-face.

or chemical significance. It is the band positions that provide the relevant chemical information. These data reveal aliphatic resonances at 2854 cm^{-1} and 2928 cm^{-1}, characteristic of a comparatively disordered SAM aliphatic region. This is not a surprising result, based on the knowledge that aliphatic chains shorter than C_9 produce analogous results in alkanethiol self-assembled monolayers.[95] Also noted are the presences of a broad band centered at ca. 3300 cm^{-1}, indicative of hydrogen-bonded –OH functionality.

To gauge the quality of this film, cyclic voltammograms of these interfaces were measured in the presence of the electrochemical probes $Fe(CN)_6^{3-/4-}$ (Fig. 2-3a, solid line) and $Ru(NH_3)_6^{3+/2+}$ (Fig. 2-3b, solid line). Krysinski and Brzostowska-Smolska[88] have demonstrated these two probes produce different results at monolayer interfaces, owing to the modest difference in electron transfer kinetics that characterize the two probes, as

well as their formal charges.[88] Using both probes thus provides a gauge on the quality of the interfaces. The data report here are typical for thiol-modified interfaces where some amount of disorder is present. Specifically, for the $Fe(CN)_6^{3-/4-}$ probe and the 6-mercapto-1-hexanol monolayer, it is observed that no discernible redox waves (Fig. 2-3a, solid line), but for the $Ru(NH_3)_6^{3+/2+}$ redox couple (Fig. 2-3b, solid line), there is a measured midpoint potential of -154 mV, with a peak separation of 120 mV. These findings underscore the higher sensitivity of the $Ru(NH_3)_6^{3+/2+}$ redox couple to SAM quality and indicate that the adlayer is mediating electron transfer kinetics.

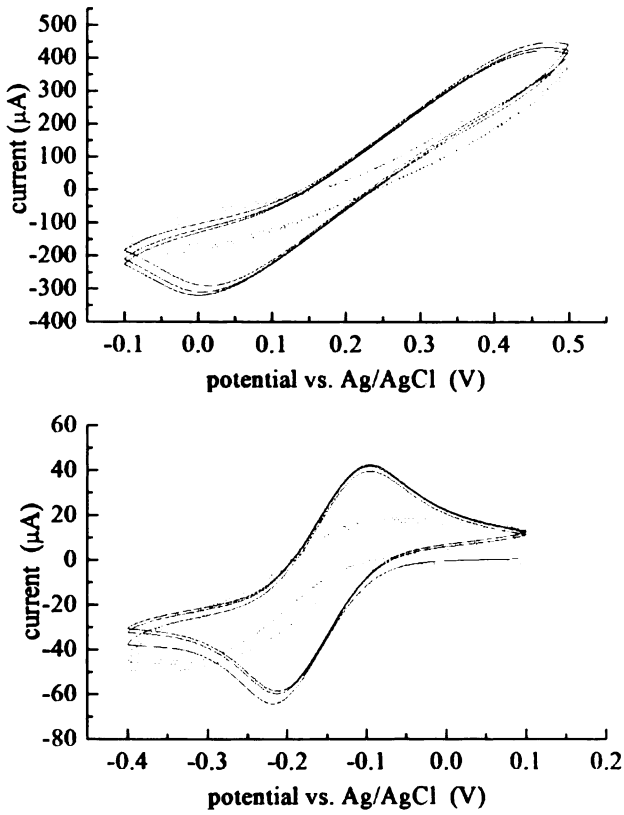

Fig. 2-3: Cyclic voltammograms of a 6-mercapto-1-hexanol self-assembled monolayer deposited on a gold surface (solid line) and of the same interface with an adlayer of DMPC deposited (dashed line), recorded using (a) 1 mM $K_4[Fe(CN)_6]$ in 0.1 M $LiClO_4$ and (b) 1 mM $[Ru(NH_3)_6]Cl_3$ in 0.1 M KCl as electrochemical probes.

Using substrates prepared in this manner, bilayers have been formed on them by means of vesicle fusion (vide infra). This procedure is well established, but what is unique about these results is that once the bilayers are formed in an aqueous environment, they have been successfully been removed from that environment and the bilayer is exposed to air. The resulting bilayer has been characterized using FTIR, cyclic voltam-

metry, optical ellipsometry and water contact angle measurements, all ex-situ from the vessel in which they were formed. The FTIR spectrum of the resulting bilayer is presented in Fig. 2-2b. These data show C-H stretching resonances at 2854 cm^{-1} and 2925 cm^{-1}, suggesting the bilayer acyl chains are somewhat disordered. This is not surprising given the gel-to-fluid transition temperature for DMPC is 24°C, and the internal temperature of the FTIR spectrometer is at or above 24°C. It is also important to note the presence of phosphate peaks at 1265, ~1100, and 820 cm^{-1}, further supporting the presence of the lipid bilayer.

The cyclic voltammetry data for the bilayer, using both the $Fe(CN)_6^{3-/4-}$ and $Ru(NH3)_6^{2+/3+}$ probes are presented as the dashed lines in Fig. 2-3. These data indicate that the presence of the bilayer provides some additional screening for the $Fe(CN)_6^{3-/4-}$ probe, but without the presence of redox peaks, it is not possible to quantitate these differences. For the $Ru(NH_3)_6^{2+/3+}$ probe, there is both a diminution in current and a substantial increase in peak separation, with a midpoint potential of -200 mV and a peak separation of 255 mV. This is not surprising and indicates that the resulting bilayer contains some imperfections and further impedes the electron transfer kinetics. Recognizing that it would be preferable to acquire CV data for adlayers both before and after removal from the flow cell in which they were deposited, due to design restrictions of the flow cell used, it is not possible to acquire CV data in situ at the present time.

Optical ellipsometry is used to measure the thickness of the DMPC bilayer as a function of exposure time to a solution of vesicles. This approach has been used before to measure bilayer formation kinetics.[58] Each surface was exposed to DMPC for a specific period of time before being removed from the solution, then washed, dried and measured. Initial measurements of the substrates after reaction with 6-mercapto-1-hexanol showed thicknesses of ca. 12 Å, and thicknesses of ca. 76 Å were observed following de-

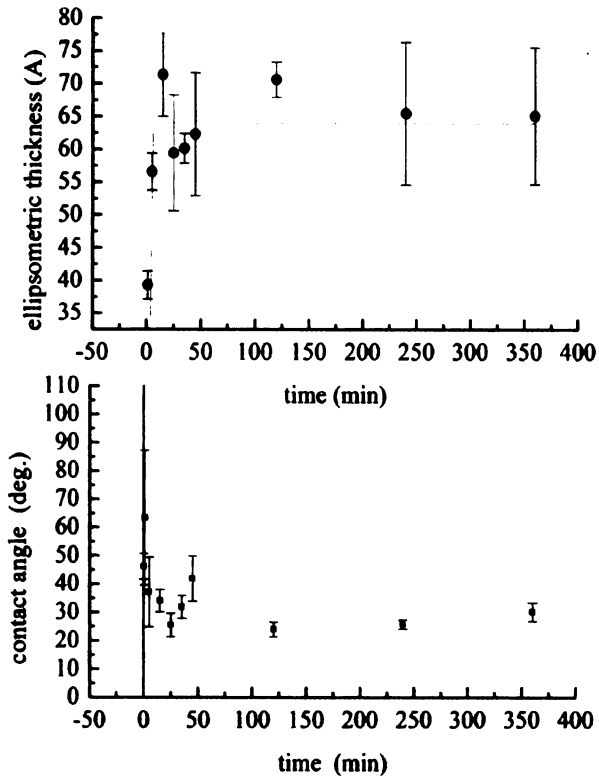

Fig. 2-4: (a) Ellipsometric thickness measurements for a 6-mercapto-1-hexanol-modified Au surface, acquired at a series of reaction times to follow DMPC deposition. (b) Water contact angle measurements acquired at a series of reaction times to follow DMPC deposition the same inter-face. For both panels, initial data points correspond to t=0.

position of DMPC. Fig. 2-4a shows the change in ellipsometric thickness of the interface as a function of time of exposure to a vesicle-containing solution. The data are characterized by a rapid build-up, with a time constant of 67 ± 5 sec to a thickness that is consistent with that of a DMPC bilayer (64 ± 2 Å) based on molecular mechanics calculations and experimental data.[96] While there is uncertainty in each data point, resulting from multiple measurements on a given sample and the use of multiple samples, the plateau value is consistent with a DMPC lipid bilayer.

Contact angle measurements have been used extensively for both the study of lipid interactions with surfaces as well as for the determination of the degree of surface coverage.[72,97-99] Water contact angle measurements are performed to further evaluate the polarity and uniformity of the bilayers. The measured water contact angle of the bilayer-containing interface was found to have a value of ca. 30° (Fig. 2-4b). The contact angle of an Au surface modified with 6-mercapto-1-hexanol was measured to be ca. 54°. These data are thus consistent with a polar interface being formed by the phosphocholine head groups.[77] The contact angle variation across the substrate is ca. 2° for all measurements, and the contact angle hys-

teresi

micro

electr

of the

chara

the bi

to air.

2-4.2:

layer F

zircon

fundam

face. I

treated

ness of

angle o

DMPC

were re

layer th

from the

evaluate

Fig. 2-5

evolutio

thickne

teresis (advancing – receding) is ca. 5°, indicating a comparatively uniform bilayer, both microscopically and macroscopically. These findings are consistent with the FTIR and electrochemical data, and indicate that a DMPC lipid bilayer forms rapidly upon exposure of the hydroxythiol-terminated surface to a vesicle containing solution. The fact that the characterization steps were performed following removal from the initial vessel in which the bilayer was deposited demonstrates that the resulting bilayer is stable upon exposure to air.

2-4.2: Air-Stable Lipid Monolayer Formation

Vesicle exposure to a zirconated surface results in a fundamentally different interface. Initial values for the ZP treated surface showed a thickness of ca. 20 Å with a contact angle of ca. 72°. Following DMPC exposure, measurements were repeated and the ZP-adlayer thickness was subtracted from the total thickness to evaluate the adlayer thickness. Fig. 2-5a shows the temporal evolution of the ellipsometric thickness of the interface fol-

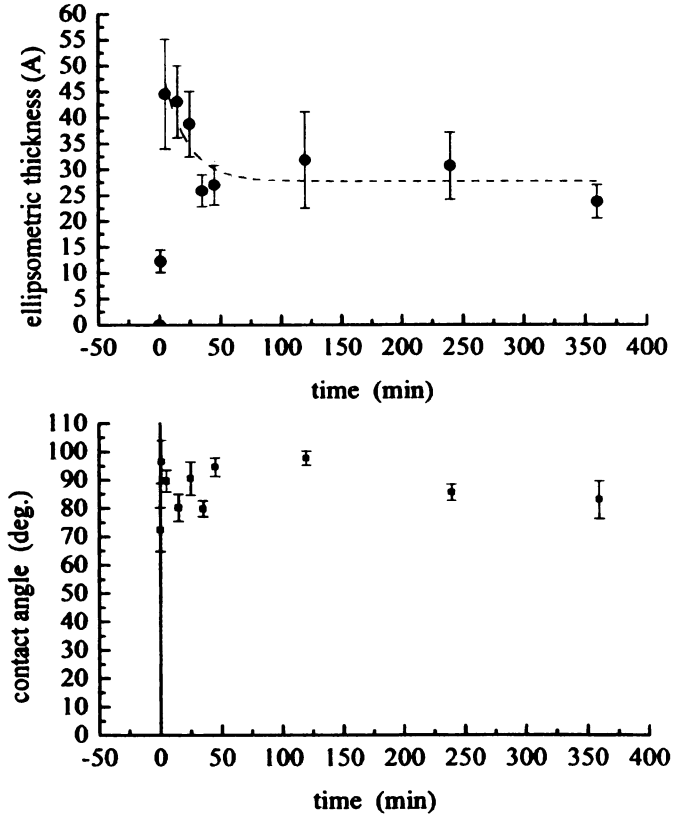

Fig. 2-5: (a) Ellipsometric thickness measurements for a zirconated 6-mercapto-1-hexanol/Au self-assembled monolayer, acquired at a series of reaction times to follow DMPC deposition. (b) Water contact angle measurements acquired at a series of reaction times for the same interface. For both panels, initial data points correspond to t=0.

lowing exposure to DMPC vesicles. By fitting these data, an initial growth to 53 ± 8 Å was obtained, followed by a decay in thickness to a value of 28 ± 3 Å. The time constant of the decay is 1200 ± 720 s. This uncertainty may seem large but, due to the nature of the measurements, such uncertainty is unavoidable. Water contact angle data reveal a nonpolar, homogeneous interface, with a contact angle of ca. 90° (Fig. 2-5b), with a variation across the substrate of ± 2° and a hysteresis of ca. 5°. These data, taken collectively, are consistent with the resulting interface being comprised of a monolayer of DMPC, where the polar headgroup of the lipid complexes essentially irreversibly with the Zr-phosphate surface and the nonpolar acyl tails are exposed.

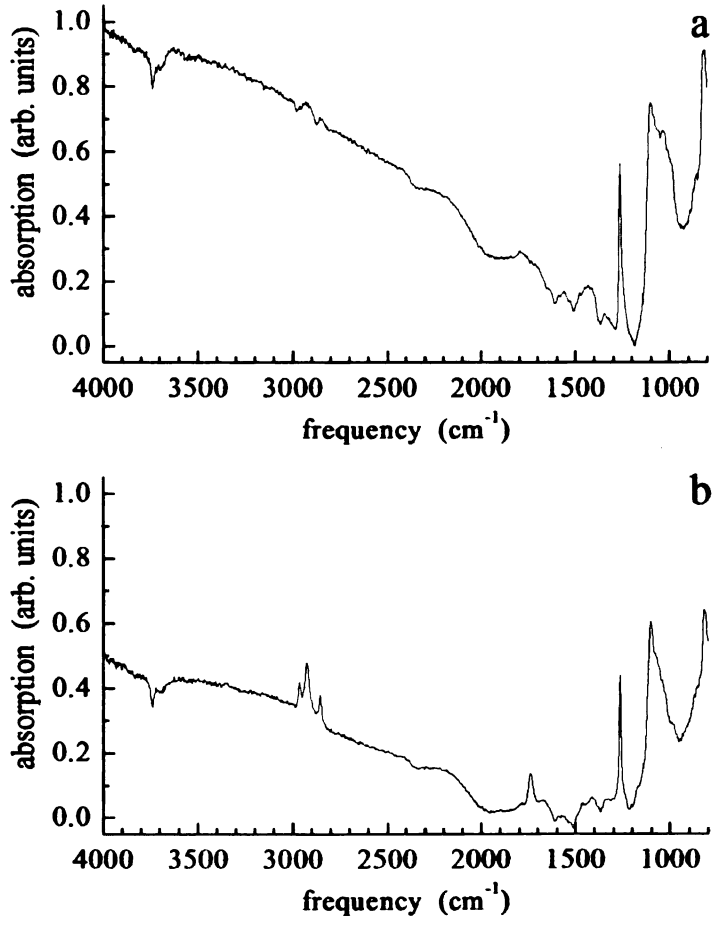

Fig. 2-6. FTIR spectra of (a) a zirconated 6-mercapto-1-hexylphosphate self-assembled mono-layer deposited on a gold surface. (b) a DMPC adlayer deposited on the zirconated 6-mercapto-1-hexylphosphate-modified gold interface.

The FTIR spectra of the zirconated interfaces are shown in Fig. 2-6a. The $POCl_3$ reacts essentially completely with the 6-mercapto-1-hexanol terminal -OH groups, and after zirconation only the phosphate peaks at 1265 cm^{-1}, ~1100 cm^{-1} and 820 cm^{-1} are observed. Upon exposure to DMPC, the monolayer that is formed shows the same

phosphate peaks with the addition of acyl chain peaks (Fig. 6b). These data also show C-H stretching resonances at 2854 cm^{-1} and 2926 cm^{-1}, suggesting the monolayer acyl chains are somewhat disordered. Interestingly however, these peaks, when compared to the bilayer acyl chain peaks, are slightly different and show more disorder in the monolayer than in the bilayer. This expected result is likely due to the monolayer acyl chains being exposed to the hydrophilic environment were the bilayer has the hydrophilic head groups exposed protecting the acyl chains from the hydrophilic environment making the bilayer slightly more crystalline.

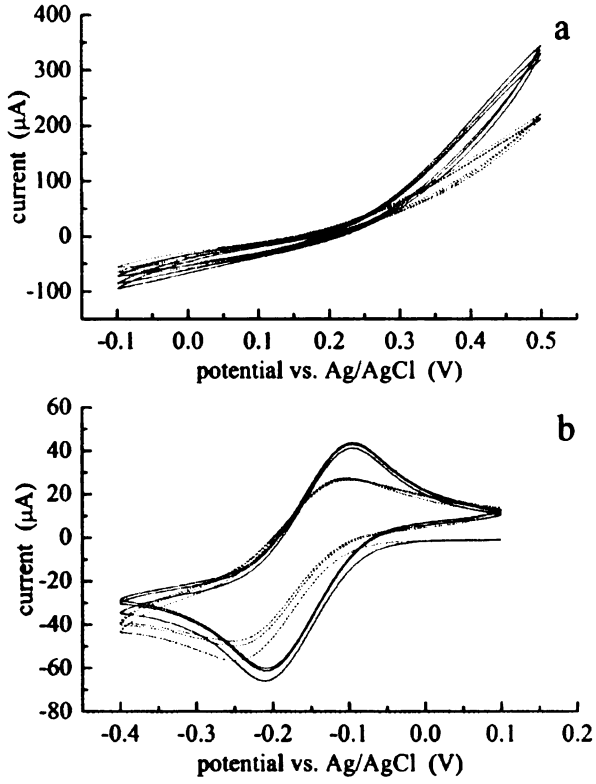

Fig. 2-7: Cyclic voltammograms of a 6-mercapto-1-hexanol/Au self-assembled monolayer reacted with $POCl_3$ and $ZrOCl_2$ to zirconate the interface (solid line) and of the same interface with an adlayer of DMPC deposited (dashed line), recorded using (a) 1 mM $K_4[Fe(CN)_6]$ in 0.1 M $LiClO_4$ and (b) 1 mM $[Ru(NH_3)_6]Cl_3$ in 0.1 M KCl as electrochemical probes.

While contact angle and ellipsometry measurements are useful in providing a mesoscopic gauge on the properties of the interfacial layer(s), electrochemical measurements are critical to evaluating their molecular-scale organization. Cyclic voltammetric measurements were performed on each lipid layer to probe the mono- or bilayer structures for defects. Figs. 2-3 show the cyclic voltammograms of the hydroxythiol-terminated interfaces with a DMPC bilayer using $Fe(CN)_6^{3-/4-}$ (Fig. 2-3a, dashed line) and $Ru(NH_3)_6^{3+/2+}$ (Fig. 2-3b, dashed line)

as probes. Figs. 2-7 shows the cyclic voltammograms of the zirconated interfaces with DMPC using $Fe(CN)_6^{3-/4-}$ (Fig. 2-7a) and $Ru(NH_3)_6^{3+/2+}$ (Fig. 2-7b) as the probes. The peak splittings and positions for both electrochemical probes are consonant with literature data,[57] and it is possible to gain some insight into the interface through a detailed examination of the CV data.

First, it should be noted that the capacitance for these interfaces was found to be 0.0074 $\mu F/cm^2$ for the bilayer on the 6-mercapto-1-hexanol SAM interface and 0.0087 $\mu F/cm^2$ for the monolayer on the zirconated SAM interface. This finding would suggest that the interfaces are close to the same thickness, provided their defect densities are similar. The ellipsometric data (vide infra) indicate that there is a factor of two difference in the interface thickness, implying that the adlayer capacitance we measure is defect-mediated for both systems. The $Fe(CN)_6^{3-/4-}$ CV data for the 6-mercapto-1-hexanol SAM indicate better blocking of the probe than the same interface with the lipid adlayer deposited (Fig. 2-3a). There is a large splitting (> 400 mV) of a weak wave seen for the lipid adlayer, suggesting very slow electron transfer kinetics at this interface. The presence of the wave following the addition of the lipid adlayer, which is not present with the SAM alone, implies that the adlayer is perturbing the organization of the SAM to some extent upon deposition.

The corresponding data for the $Ru(NH_3)_6^{3+/2+}$ probe reveal the presence of a redox wave for both adlayers as well as for the SAMs on which the adlayers are deposited (Figs. 2-3b, 2-7b). It is not surprising to observe this electrochemical behavior because lipid adlayers are likely to be characterized by some defect sites, and the $Ru(NH_3)_6^{3+/4+}$ probe is more sensitive to interface defect sites. It is clear for both interfaces that the electron transfer kinetics are slowed significantly by the presence of the lipid adlayer. As noted above, for the 6-mercapto-1-hexanol SAM, the peak separation

for the $Ru(NH_3)_6^{3+/2+}$ waves is ca. 120 mV with a midpoint potential of -154 mV, and this separation increases to ca. 255 mV (and the midpoint potential shifts to -200 mV) with the addition of the lipid bilayer (Fig. 2-3b). For the zirconated interface (Fig. 2-7), the redox peak splitting is ca. 117 mV (midpoint potential -153 mV) and the addition of the lipid adlayer increases the splitting to ca. 143 mV (midpoint potential -179 mV). For a reaction that is reversible on the time scale of the potential scan, the expected (E_{pa}-E_{pc}) splitting should be 59/n mV at 25° C. The values obtained for these interfaces are all in excess of 59 mV, indicating that the kinetics of the electron transfer are mediated by the interfacial adlayers in all cases. The splitting and midpoint potentials are essentially the same for both the 6-mercapto-1-hexanol and zirconated SAMs, which is not surprising. It is also not surprising that the lipid bilayer impedes the electron transfer kinetics to a greater extent than the lipid monolayer, as manifested by a comparison of the peak splitting and midpoint potential data. The electrochemical data are in qualitative agreement with the ellipsometric and contact angle data, and are consistent with the formation of a lipid bilayer structure on the 6-mercapto-1-hexanol SAM and a lipid monolayer on the zirconated SAM.

2-4.3: NMR Analysis

The ZP-lipid interactions that are central to understanding the formation of the monolayer data can be characterized using ^{31}P NMR measurements. ^{31}P NMR measurements have been used in the past to characterize ZP multilayer structures, and this work follows those same procedures.[87] All NMR spectra were referenced to 85% phosphoric acid (δ=0ppm). Fig. 2-8 shows the ^{31}P NMR spectrum for each step of interface preparation and DMPC exposure. For this work silica gel was used as the substrate for interface growth because of the surface area advantage. As seen in Fig. 2-8a, after exposure of

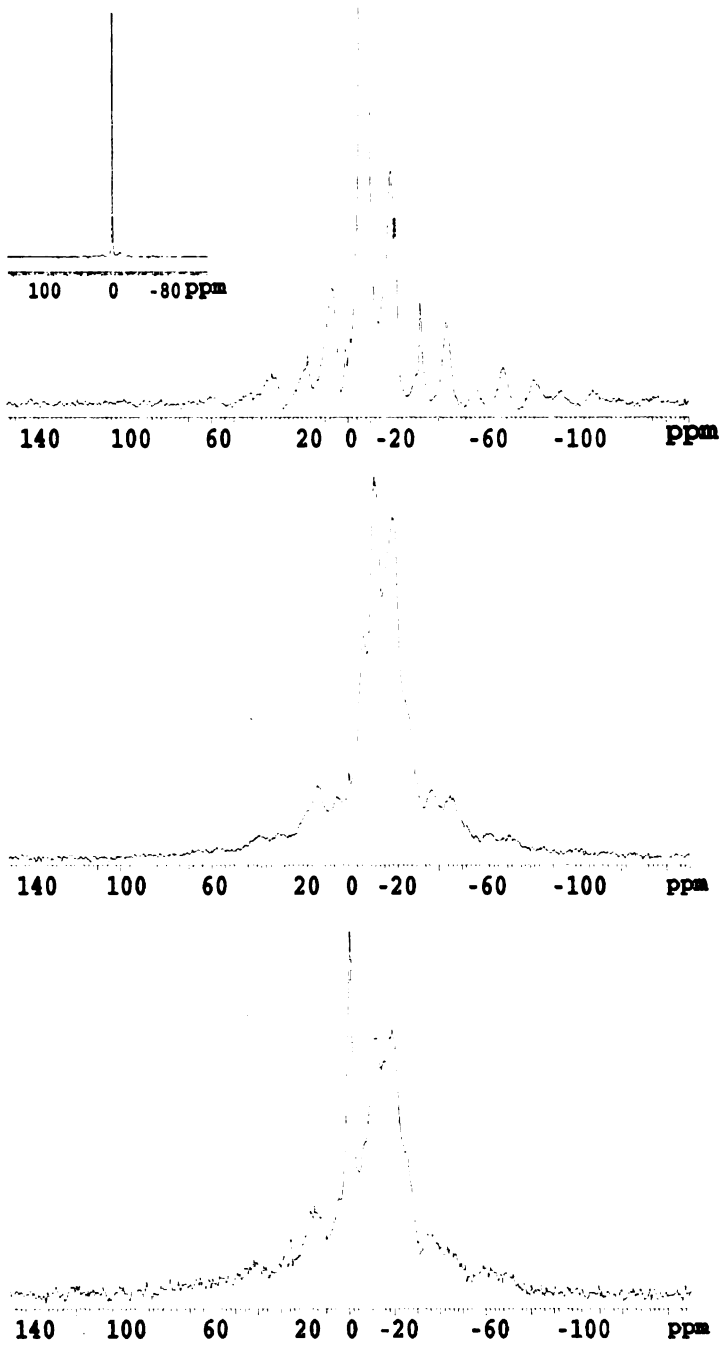

Fig. 2-8: ^{31}P MAS NMR spectra. (a) Silica gel coated with $POCl_3$, (b) surface shown in panel a exposed to $ZrOCl_2$(aq), (c) surface shown in panel b exposed to DMPC.

the silica gel to $POCl_3$ a strong resonance is observed at δ=-1.1 ppm, and a smaller resonance is seen at δ=-14.9 ppm, corresponding to physisorbed and chemically bound phosphate at the silica gel surface, respectively. The resonance at -1.1 ppm is extremely strong because the physisorbed phosphate cannot be removed easily. The remaining bands are due to the spectra not being proton decoupled, and the presence of spinning side bands.[87] On exposure to $ZrOCl_2$, the spectra exhibit a characteristic shift (Fig. 2-8b).[87] Poorly resolved peaks at δ=-4.7, -12.0, and -19.7 ppm result from zirconium coordination with a phosphate. The prominent peak at -1.1 ppm is eliminated because the Zr^{+4} in solution complexes the physisorbed phosphate, removing it from the silica gel surface. The spectrum shown in Fig. 2-8c was recorded following exposure of the zirconated surface to DMPC. The

broad peaks at δ=-12.1 and -19.4 ppm correspond to the zirconium-phosphate complex, and the sharp resonance at -0.5 ppm is due to zirconium complexation by the phosphocholine headgroup of DMPC. This assignment is made by comparing these data to a solution phase DMPC spectrum, which has a single peak at δ=-0.32 ppm (not shown). Washing the silica gel with water does not remove the resonance at -0.5 ppm, indicating that the DMPC phosphocholine moiety complexes with the Zr^{+4} present at the interface. While this is not a surprising result when viewed in the context of the literature on ZP chemistry,[78,79,81-86,100-103] it is one of the first reports that is available showing a direct complexation between a phospholipid and a zirconated substrate.

2-5: Discussion

The FTIR, ellipsometry, electrochemistry, contact angle and ^{31}P NMR data provide a self-consistent picture of these interfaces. A stable DMPC lipid bilayer is formed by vesicle fusion on the 6-mercapto-1-hexanol-coated Au substrate and a DMPC lipid monolayer is ultimately formed on the zirconated substrate, with the phospholipid headgroup interacting strongly with the Zr^{+4}. The FTIR data confirm the presence of phospholipids on the surfaces through the carbonyl stretches, which could be there only as a result of phospholipid deposition. Ellipsometric thickness data are consistent with the presence of a lipid bilayer on the mercaptohexanol-terminated surface and a lipid monolayer on the zirconated phosphate surface. These data however, do not provide explicit information on the organization of the phospholipids. The FTIR data suggest that the acyl chains of DMPC are not in a fully crystalline state, as gauged by the band positions of the asymmetric and symmetric CH_2 stretches. The cyclic voltammetry data, using two different electrochemical probes, demonstrate that the DMPC mono- and bilayers are not free of defects, but they do cover the interface to a significant extent. Water contact angle

data are complementary to the ellipsometric and electrochemical data and show that the bilayer is hydrophilic while the monolayer is hydrophobic. Taken collectively, the FTIR, ellipsometry, contact angle, and electrochemical data confirms that a DMPC bilayer is being formed on the 6-mercapto-1-hexanol coated substrate and a monolayer is formed on the zirconated substrate and that these interfacial structures remain even after being removed from the aqueous environment in which they are formed. The ^{31}P NMR data demonstrate that there is a measurable interaction between the DMPC head group and the zirconated interface, consistent with the known chemistry of Zr-bisphosphonate systems and the ellipsometric and contact angle data presented here.

There is limited precedent for the formation of air-stable bilayers. The approach to creating air-stable bilayers described here relies on the formation of a well organized interface on which the phospholipid mono- or bilayer can form. The mercaptohexanol base layer is comparatively well organized and tightly packed, based on the CV data (Figs. 2-3). Such an interface allows for substantial interaction of the terminal –OH functionalities with the phospholipid head group. For the case of the zirconated interface, the dominant chemical interaction is the formation of a ZP-like complex with the phospholipid headgroup, as confirmed by ^{31}P NMR measurements. For both interfaces, the interactions between the terminal chemical functionality and the phospholipid headgroups are sufficiently strong to allow the formation of structures that are stable in a range of environments.

2-6: How Mono- and Bilayers Form on the Modified Au Substrates

The interpretation of this data in the context of a lipid bilayer forming on a 6-mercapto-1-hexanol SAM and a lipid monolayer ultimately forming on a zirconated SAM requires a consideration of how each of these structures can form and has implications

in terms of the mass of phospholipid that ultimately deposits at the interface. For lipid adlayer formation on the 6-mercapto-1-hexanol SAM, vesicle fusion gives rise to the formation of a bilayer structure. When a vesicle contacts the interface, then spreads on that interface, there is the opportunity for lateral mobility of the bilayer constituents owing to the nature of the interface-lipid interactions. Because of the translational mobility of the planar bilayer on the 6-mercapto-1-hexanol SAM, vesicle fusion can proceed on open regions of the SAM until an essentially complete bilayer forms.

It is asserted that the physical "picture" for the zirconated interface is fundamentally different. While vesicle fusion proceeds on the zirconated interface, once the phospholipid headgroups of the bottom leaflet of the planar bilayer contact the zirconated interface, they bind and are not free to execute translational motion. Thus the interface coverage is heterogeneous initially, and the interstices between covered regions are, of necessity, left open once they become smaller than an area that can accommodate vesicle deposition and fusion. Over time, mediated by translational motion of the top lipid leaflet and translocation of the top leaflet constituents once they reach the edges of the bottom-leaflet "islands", the open interstitial regions are filled in with phospholipid molecules and a lipid monolayer results.

The coverage of a planar surface achieved by vesicle fusion is difficult to model, but if it is assumed that the spherical vesicle fuses to form a circular bilayer which is not free to translate on the surface, one can estimate the maximum achievable surface coverage. For a hexagonal close-packed array of circles, the maximum coverage would be 94% and for a face-centered cubic arrangement, coverage would be ca. 78%, based on simple geometric models. Because of the nominally random deposition of the vesicles on the zirconated surface, it is improbable that such high initial surface coverage is achieved. There may ultimately be a slight excess of lipid molecules present by the end of the par-

tial bilayer deposition and monolayer formation process. Any excess "top leaflet" molecules will likely dissolve into the bulk solvent and/or reincorporate into lipid vesicles that remain in solution.

2-7: Kinetics of Lipid Adlayer Formation

With this model of the interface in mind, one can consider the energetics and kinetics of lipid monolayer formation on the zirconated interface. From the data shown in Fig. 2-5a, there appears to be a time constant associated with the formation of the lipid monolayer. Initially it appears that a partial lipid bilayer structure forms on the surface, and over time the partial bilayer converts to a monolayer. Through the use of a zirconated interface, a condition has been established where a lipid initially in the top leaflet will bind to the zirconated surface essentially irreversibly once it migrates to an edge of the lipid island and executes a translocation to the bottom leaflet. The energetics associated with this process based on the time constant observed for the evolution of the monolayer structure can be estimated. Using the ansatz that, for the interactions of lipids with zirconated surfaces, the relevant unimolecular reaction[10,65,72] is

$$N_{top} \xrightarrow{k_{top-bottom}} N_{bottom} \qquad (2\text{-}1)$$

While it is possible that there is some dissociation from the lipid-ZP complex, the rate of dissociation is expected to be slow. The energy of formation for a Zr-bisphosphonate complex, which is similar to the lipid-ZP complex, is known to be ≥250 kJ/mol, corresponding to a dissociation constant at room temperature of ~$3x10^{-44}$ for 1:1 lipid:Zr stoichiometry.[80] The decay of interface thickness shown in Fig. 2-2a corresponds to the time constant for lipid top-to-bottom flipping, $k_{top\text{-}bottom} = \tau^{-1} = 8.3\ (+12.5, -3.1)\ x10^{-4}$

s^{-1}, a value that is similar to literature reports for lipid translocation.[10] By treating this interface evolution reaction as an activated process, the Arrhenius prefactor associated with such a reaction will lie within the range of $10^{10} - 10^{15}$ Hz. Because temperature-dependent data for the formation of these interfaces has not been examined, it is not possible to determine the prefactor experimentally. One can, however, determine the range of activation energies consistent with the unimolecular prefactor range (Table 2-1). Calculating the activation energies for DMPC lipid trans-leaflet migration using an Arrhenius prefactor in this range and with the experimental time constant measured, activation energies in the range of 73 – 101 kJ/mol are obtained. It is noted that the values for Ea are in relatively close correspondence with those reported by Kornberg and McConnell for translocation of a tagged lipid,[10] while Liu and Conboy[72] report Ea values on the order of 200 kJ/mol or more for lipid translocation.

A (s^{-1})	Ea (kJ/mol)
10^{10}	73.3
10^{11}	79.0
10^{12}	84.6
10^{13}	90.2
10^{14}	95.8
10^{15}	101.4

Table 2-1. Calculated activation energy for lipid flipping as a function of Arrhenius prefactor.

$k_{top\text{-}bottom} = \tau^{-1} = A*\exp(-Ea/RT)$, where $k_{top\text{-}bottom} = 8.3 \times 10\text{-}4\ s^{-1}$, $T = 300$ K, and $R = 8.314$ J/mol-K.

The fact that phosphocholines interact strongly with a zirconated interface suggests the ability to scavenge certain phospholipids from multi-component solutions using the appropriate interface chemistry. At the present time it is not clear that all phospholipids will interact equally well with the zirconated interface, and the process of understanding the role of phospholipid headgroup identity on the strength of lipid binding to zirconated interfaces is discussed in the following chapter. The phospholipid headgroup is not all that is anticipated that regulates the formation of lipid monolayer structures, and this points the way toward evaluating the strength of interaction of phospholipids with other

metal ions as well.

2-8: Conclusion

Here was observed a means of forming lipid mono- and bilayer structures that can cross the air/water interface and remain intact. The interfaces formed have been characterized using FTIR spectroscopy, cyclic voltammetry, optical ellipsometry, contact angle measurements and ^{31}P NMR data. Reported here is the formation of interfacial lipid layers on substrates that are either polar (hydroxythiol on Au) or are capable of binding the phospholipid headgroup (phosphated and zirconated interface). Complexation of the DMPC phosphocholine headgroup to the zirconated interface was confirmed by ^{31}P NMR data, demonstrating for the first time, at the time of this writing, knowledge of the complexation of a phospholipid in such a manner. It has been found that for a DMPC bilayer on the zirconated surface, the time constant for partial bilayer-to-monolayer conversion is ca. 20 minutes, and for a unimolecular reaction,[10,65,72] this time constant is consistent with an activation energy between 75 and 100 kJ/mol. Given the interaction between phospholipids and ZP-terminated interfaces, it is important to understand how the interaction varies with the identity of the phospholipid headgroup, which is discussed next.

Chapter 3

Phospholipid Headgroup Dependent Assembly of Lipid Adlayers on Zirconium Phosphate-Terminated Interfaces

3-1: Introduction to Surface Modification

The basis for the formation of a lipid bilayer structure is the balance of intermolecular interactions between the lipid nonpolar acyl chain regions and the polar headgroup interactions with the (aqueous) medium with which the bilayers are in contact. Lipid bilayers that are present in biological systems are comprised of many constituents and are structurally complex. It is thought that this complexity plays a role in stabilizing the folding of transmembrane proteins and thus mediating their function.

There is a significant research effort involved with chemical sensing based on the use of biomolecules as the chemically selective elements. To succeed in using certain biomolecules as chemical sensing elements, an interface is required that can stabilize the structure of the biomolecule and at the same time function as part of a transduction system to relay the chemical signal of interest to instrumentation. Supported lipid bilayers are an appropriate choice for such purposes. The bilayer composition and the manner in which the bilayer interacts with the interface to which it is bound need to be investigated as an initial step in this effort. It is therefore of interest to bind selected phospholipids to chemically modified interfaces, and one way to perform this binding is through interactions between the phospholipid headgroup moieties and the supporting surface similarly to that discussed in chapter 2. The work discuss here however, is focused on the deposition and characterization of lipid monolayers, not bilayers of several phospholipids. Investigation in to lipid monolayers was pursued because they provide an interesting opportunity to develop an understanding of the interaction(s) between the substrate and

the lipid headgroups. This is valuable because it is these interactions that ultimately will govern the bilayer integrity and physical properties. Once the substrate-lipid interactions are understood, it is possible to add an outer phospholipid leaflet by Langmuir-Schaefer deposition,[104-108] for example.

Zr-bisphosphonate and Zr-bisphosphate (ZP) chemistry is again suitable for this work as it is a type of self-assembly that has been used in the formation of interfacial adlayers for some time.[79,81-84,87,88,109-115] The primary motivation for the use of ZP chemistry is that the Zr-phosphate/phosphonate association is energetically very favorable,[80] resulting in an essentially irreversible complexation that is characterized by fast reaction kinetics. It has been demonstrated recently that ZP complexation chemistry can be used to form phosphocholine lipid adlayers on surfaces terminated with a zirconium phosphate moiety.[116] In that work, 1,2-dimyristoyl-sn-glycero-3-phosphocholine (DMPC) complexed with Zr^{+4} bound to surface phosphate functionalities to produce a self-assembling lipid adlayer.[116] ^{31}P NMR data demonstrated that the lipid-interface interaction was through the phospholipid headgroup phosphate moiety. The resulting adlayer remained intact after removal from the solution in which it was deposited, and was stable in air, suggesting its use as a foundation for biomimetic films. The only phospholipid investigated in that work was DMPC. Because of the compositional complexity of plasma membranes,[117] it is of interest to understand how the structure of the phospholipid headgroup influences the self-assembly of lipid-ZP complexes at planar interfaces.

In addition to the importance of binding phospholipids to interfaces as a step in the creation of biomimetic interfaces, understanding such interactions may have immediate utility in characterizing lipid profiles in selected biological systems. Specifically, if an interface can be identified that binds one or more types of phospholipids selectively, its use would facilitate the rapid characterization of plasma membranes. The initial step

in this endeavor is to determine what intrinsic, chemical selectivity for phospholipids is manifested by the ZP interface. Phospholipid headgroups vary significantly in size, polarity, and charge. These factors can and will affect the binding affinity of the phosphate moiety to Zr^{+4}, and the chemical headgroup-dependent binding efficiency of selected lipids is discussed in this work.

The use of gold-thiol self-assembled monolayer chemistry[95,118-125] to build a monolayer on a gold surface that can be modified subsequently to bind selected phospholipids was utilized again in this study. Au substrates are first exposed to 6-mercapto-1-hexanol to form a self-assembled monolayer (SAM), followed by the reaction of the SAM terminal –OH group with $POCl_3$, H_2O and Zr^{+4}.[80,87,89] The resulting zirconated surface has been shown to bind DMPC,[116] and the focus of this work is on understanding the chemical and steric factors that are important to this lipid-binding process. Examined here are the affinity of lipids possessing the

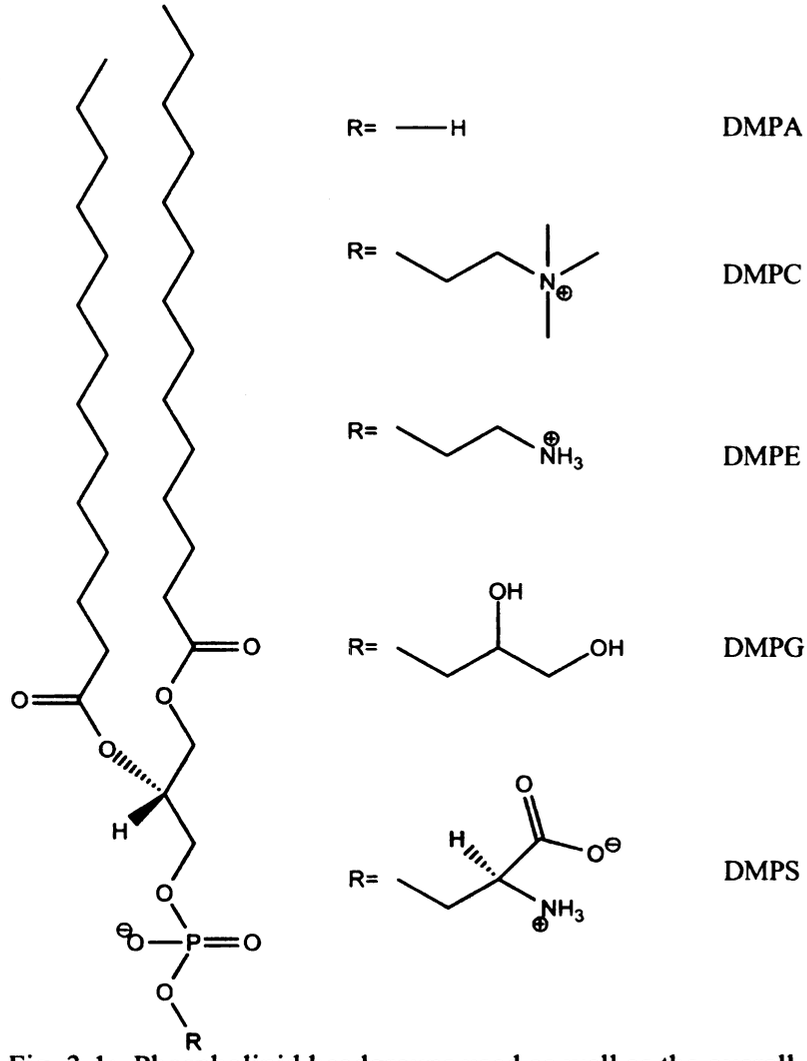

Fig. 3-1: Phospholipid headgroups used as well as the overall acyl chain. Base acyl chain does not change for each lipid with the R group being the different headgroups.

selected headgroups, including 1,2-dimyristoyl-sn-glycero-3-phosphatidic acid (DMPA), 1,2-dimyristoyl-sn-glycero-3-phosphocholine (DMPC), 1,2-dimyristoyl-sn-glycero-3-phosphoethanolamine (DMPE), 1,2-dimyristoyl-sn-glycero-3-[phospho-rac-(1-glycerol)] (DMPG), and 1,2-dimyristoyl-sn-glycero-3-[phospho-L-serine] (DMPS). The structures of these lipids are shown in Fig. 3-1. Acyl chains for all of the lipids were C_{14} with no unsaturations, allowing evaluation of the role of lipid headgroup structure on the surface-binding process.

The results for lipid-binding to a zirconated surface are presented here, including cyclic voltammetry, time resolved ellipsometry, and water contact angle data to elucidate the formation and to a limited extent, the organization of the monolayers. The data are consistent with structurally-based expectations, where steric factors and intermolecular interactions such as hydrogen-bonding can play a significant role in mediating surface-binding phenomena.

3-2: Experimental Set up and Materials Used

Materials utilized in these studies include the following and are similar to those used in the work discussed in chapter 2. They include: 1,2-dimyristoyl-sn-glycero-3-phosphatidic acid (DMPA, monosodium salt), 1,2-dimyristoyl-sn-glycero-3-phosphocholine (DMPC) dissolved in chloroform, 1,2-dimyristoyl-sn-glycero-3-phosphoethanolamine (DMPE), 1,2-dimyristoyl-sn-glycero-3-[phospho-rac-(1-glycerol)] (sodium salt) (DMPG), and 1,2-dimyristoyl-sn-glycero-3-[phospho-L-serine] (sodium salt) (DMPS), all in a mixture of chloroform, methanol and water, and are obtained from Avanti Polar Lipids, Inc. The solvents acetonitrile, ethanol (100%) and ethyl acetate, as well as the reagents 6-mercapto-1-hexanol, phosphorus oxychloride ($POCl_3$), zirconyl chloride octahydrate ($ZrOCl_2 \cdot 8\ H_2O$), 2,4,6-collidine, potassium ferrocyanide trihydrate,

lithium perchlorate, hexaminеruthenium(III) chloride, and potassium chloride, are all obtained from Sigma-Aldrich in the highest purity grade available. 18 MΩ Water was used for all of the experiments and all reagents were used as received, without further purification.

The instumentaion again was the same as the previous study as well and includes: a CH Instruments 650 electrochemical analyzer for electrochemical analysis, a J. A. Woollam Co., Inc. spectroscopic ellipsometer model EC110 with a wavelength range of 185-1100 nm, utilizing 44 wavelengths simultaneously for optical ellipsometry measurements, and an ACT Products Inc. VCA 200 video contact angle system for all water contact angle measurements. Unless noted otherwise, experiments were performed at 20°C.

Two electrochemically active probes were used to characterize the interfaces; $K_3Fe(CN)_6 \cdot 3\ H_2O$ (1.32 mM) in 0.1 M $LiClO_4$ and $Ru(NH_3)_6Cl_3$ (1.00 mM) in 0.1 M KCl. These two probes were chosen because of their different electron transfer kinetics and ionic charges.[88] Cyclic voltammetry (CV) was performed with each probe being cycled three times at a scan rate of 0.1 V/s. The $Fe(CN)_6^{3-/4-}$ probe was scanned from -0.1 to 0.5 V and the $Ru(NH_3)_6^{3+/2+}$ probe was scanned from -0.4 to 0.1 V vs. Ag/AgCl using a Pt counter electrode. It should be noted that due to calculation error, 10 times the iron probe concentration was used initially leading to larger then expected currents.

3-2.1: Sample Preparation

Gold substrates were prepared using a procedure described previously.[89] Briefly, the substrates are rinsed with water and ethanol, cleaned in a UV-cleaner for 15 min., then exposed to 10 mM 6-mercapto-1-hexanol in ethanol for 6 hrs. The resulting interface is then rinsed with ethanol and ethyl acetate, then dried under a stream of $N_2(g)$. For Zr-modified interfaces, the 6-mercapto-1-hexanol monolayer is reacted with $POCl_3$ (0.4 mL)

in dry acetonitrile (10 mL), and catalyzed with 2,4,6-collidine (0.4 mL) for 3 hrs. The phosphate-modified monolayer formed is then rinsed with ethanol and water, dried with N_2(g), and exposed to 5 mM $ZrOCl_2$ in a 60:40 ethanol/water solution for 12 hrs. The zirconated monolayer is then finaly dried under N_2(g), then is ready for exposure to the solution containing lipid unilamellar vesicles.

Unilamellar vesicles of each lipid are prepared as described previously.[60] The vesicles used here are comprised of phospholipid only, with no other constituents. Chloroform or the chloroform:methanol:water ternary system is first evaporated from the lipid solution using a N_2 stream, and any remaining solvent was removed under vacuum. The dried lipid is next dissolved in a 10 mM tris(hydroxymethyl)-aminomethane hydrochloride (Tris®, Aldrich) pH 7.5 buffer solution to a final concentration of 1 mg/mL. The solution is treated with five freeze-thaw-vortex cycles to ensure thorough suspension of the lipids prior to extrusion.[90] To form unilamellar vesicles with a narrow size distribution, a syringe-based mini-extruder is used (Avanti Polar Lipids, Inc.).[91-93] The lipid suspension is passed through a polycarbonate filter with an average pore diameter of 400 nm eleven times to produce unilamellar vesicles of that diameter.

Planar lipid adlayers are formed by spontaneous fusion of unilamellar vesicles.[75] The modified gold substrates are placed in a custom-made Teflon® flow cell (Fig. 2-1) with an approximate volume of 1 mL that has been described in detail in the previous chapter.[116] The flow cell is used to ensure the lipid vesicle suspension was in full contact with the substrate during adlayer formation. Tris® buffer is flowed over the substrate at ca. 5 mL/min. prior to lipid deposition, followed by the lipid suspension, flowed through the cell at the same rate, until the buffer solution is displaced. The vesicle-containing solution is then allowed to remain in contact with the substrate for a fixed period of time. For the electrochemical experiments, the vesicle-containing solution is in contact with the

substrate for at least six hours to allow for the maximum adlayer formation. After exposure to vesicle solution, the substrates are washed with water at the same flow rate. The water is then aspirated from the cell at 1 mL/min, and the substrate is removed from the flow cell and allowed to air dry by hanging vertically.

3-3: Individual Lipid Results

The primary purpose of this work is to evaluate the affinities of selected phospholipid headgroups for a zirconated surface and thus gauge the extent to which lipid adlayer self-assembly occurs. Considered first is the experimental data for the different phospholipids individually, then by comparing these results, it is possible to assess which factors are of primary importance in determining lipid-interface interactions.

3-3.1: DMPA

The planar substrate used in this work are Au that is first reacted with a 6-mercapto-1-hexanol to form a hydroxyl-terminated SAM. The resulting interface is subsequently reacted with $ZrOCl_2$ to produce a zirconated surface. The zirconated substrate is then exposed to a solution containing DMPA vesicles, and optical ellipsometry is used to measure the thickness of the resulting adlayer ex situ as a function of vesicle exposure time. DMPA exhibits a rapid build-up to a thickness of 30±2 Å (Fig. 3-2a), consistent with the formation of a lipid monolayer.[96] Once the lipid adlayer formed, the thickness remained constant as a function of vesicle exposure time. Water contact angle measurements are performed on these same interfaces, providing some insight into their polarity and homogeneity.[72,97-99] The water contact angle for a DMPA adlayer is 104°, with a hysteresis (the difference between advancing and receding contact angles) of ca. 7° (Fig. 3-2b). The value of 104° indicates that the chemical functionality of the adlayer in contact with the

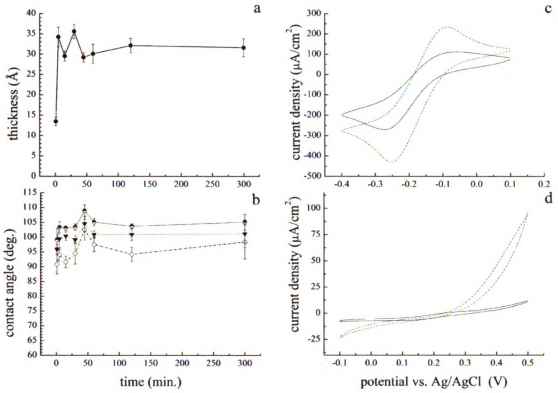

Fig. 3-2: DMPA results. A) Ellipsometric thickness measurement in time. B) Water contact angle in time with the solid line being the initial drop angle, the dashed line is advancing, and the dotted line is receding. C) CV of DMPA monolayer (solid line) and blank substrate (dashed line) when exposed to $Ru(NH_3)_6Cl_3$. D) CV of DMPA monolayer (solid line) and blank substrate (dashed line) when exposed to $K_3Fe(CN)_6$.

water droplet is nonpolar, suggesting the lipid acyl chains are the outermost component of the adlayer. By comparison, the blank ZP surface is characterized by a contact angle of ca. 72°. The hysteresis seen for the DMPA adlayer suggests modest spatial heterogeneity in the organization of the adlayer.

Cyclic voltammetry of electroactive probes in solution over the adlayers is also performed to evaluate interface uniformity. Two electrochemical probes are utilized, with CV data for $Ru(NH_3)_6Cl_3$ (Ru probe) shown in Fig. 3-2c and $K_3Fe(CN)_6$ (Fe probe) in Fig. 3-2d. For adlayers and probes where redox waves were detectable, the reactions are found to be reversible, redox waves for both probes, with peak splitting for both probes

being consistent with literature reports.[57] For the zirconated adlayer, probe access to the electrode is limited for the Ru probe and is heavily attenuated for the Fe probe. The measured peak splitting is found to be 128 mV with a midpoint potential of 190 mV vs. Ag/AgCl for the Fe probe with the ZP treated 6-mercapto-1-hexanol SAM surface. For the DMPA-terminated interface, it is observed that little to no Fe probe electrochemical response is found. The Ru probe yields a peak splitting of 164 mV and a mid-point potential of -170 mV vs. Ag/AgCl for the ZP treated 6-mercapto-1-hexanol SAM. The Ru probe electrochemical signal is attenuated slightly for the DMPA-terminated interface, yielding a splitting of 212 mV and a midpoint potential of -167 mV vs. Ag/AgCl. These results are compiled for both probes and all adlayers studied in Table 3-1 which is discussed later in this chapter. The splitting data for all measurements suggests interfacial adlayer mediation of the probe electron transfer kinetics. A peak splitting of 59 mV is expected for a fully reversible reaction with fast electron transfer kinetics. This increase in peak splitting data could also contain a contribution from hindered diffusion, but this is believe to be less likely to account for these reported findings than mediation of electron transfer kinetics by the adlayer. This statement is based on the fact that the diffusional properties of both probes are similar, and the electron transfer kinetics for the Ru probe are somewhat faster than for the Fe probe. If hindered diffusion accounted for these data, greater similarity in the peak splitting for both probes, and a dependence of the peak splitting on adlayer identity which follows the ellipsometry and/or contact angle data would be expected. This is not observe for either of these trends (Table 3-1). For the Ru probe, it is clear that the lipid adlayer is slowing the electron transfer kinetics to a greater extent than for the 6-mercapto-1-hexanol SAM-terminated interface alone. The electrochemical and water contact angle data point collectively to the DMPA monolayer containing a measurable quantity of defects. There is precedent for the formation of a lipid monolayer

at a zirconated interface. Recent work on DMPC interactions with a zirconated interface show that a monolayer does form, with the dominant chemical interaction being shown by ^{31}P NMR to be the complexation of the Zr^{+5} by the lipid phosphocholine group.[116]

3-3.2: DMPC

DMPC forms a stable adlayer on the zirconated Au surface, following a ca. 20 minute equilibration time.[116] The ellipsometric thickness of the DMPC adlayer was measured to be 28±3 Å,[116] (Fig. 3-3a) similar to that found for DMPA and consistent with a lipid monolayer being deposited at the interface. The water contact angle for the result-

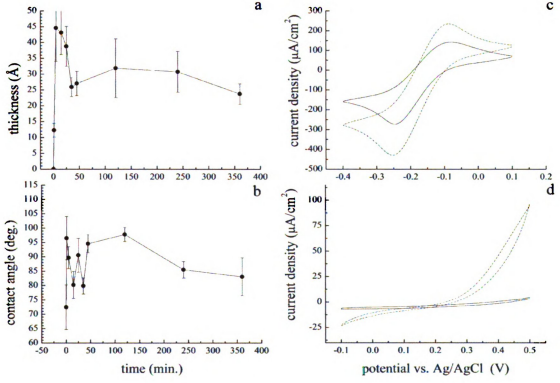

Fig. 3-3: DMPC results. A) Ellipsometric thickness measurement in time. B) Water contact angle in time with the solid line being the initial drop angle, the dashed line is advancing, and the dotted line is receding. C) CV of DMPC monolayer (solid line) and blank substrate (dashed line) when exposed to $Ru(NH_3)_6Cl_3$. D) CV of DMPC monolayer (solid line) and blank substrate (dashed line) when exposed to $K_3Fe(CN)_6$.

ing interface is ca. 90° (Fig. 3-3b) with a hysteresis of 5°. While the water contact angle is slightly less than that seen for the DMPA adlayer, it is consistent with the lipid acyl chains being the moiety which defines the outer portion of the adlayer. The comparatively low hysteresis is consistent with the existence of a slightly more homogeneous adlayer than was seen for DMPA, in keeping with the electrochemical data. Cyclic voltammetry data for the DMPC interface using the Ru and Fe electrochemical probes (Figs. 3-3c and 3-3d, respectively) indicate that the DMPC adlayer effectively blocks access of the Fe probe to the Au surface, while allowing the Ru probe access. For the Ru probe, the ZP treated 6-mercapto-1-hexanol interface yields a splitting of 166 mV with a midpoint potential of -164 mV vs. Ag/AgCl (Fig. 3-3c). For the DMPC-terminated interface, we observe 167 mV of peak splitting and a midpoint of -170 mV vs. Ag/AgCl. Both interfaces mediate the electron transfer kinetics of the probe to the electrode, and given the similarity of the data, it appears that DMPC does not influence the organization of the underlying 6-mercapto-1-hexanol SAM adversely, as is seen for the DMPE-terminated interface (vide infra). These electrochemical findings are also consistent with a well organized adlayer, because the Ru probe is energetically favored over the Fe probe in terms of being able to penetrate the interfacial adlayer.[88]

3-3.3: DMPE

Ellipsometry and water contact angle measurements for the zirconated substrate exposed to DMPE unilamellar vesicles yielded data consistent with a somewhat less organized adlayer than that of either DMPA or DMPC. The ellipsometric thickness was measured to be 16±1 Å (Fig. 3-4a) suggesting either sub-monolayer coverage or a relatively uniform lipid adlayer exhibiting a ca. 45° tilt angle with respect to the surface normal. Water contact angle data for the DMPE adlayer reveals a hydrophobic interface

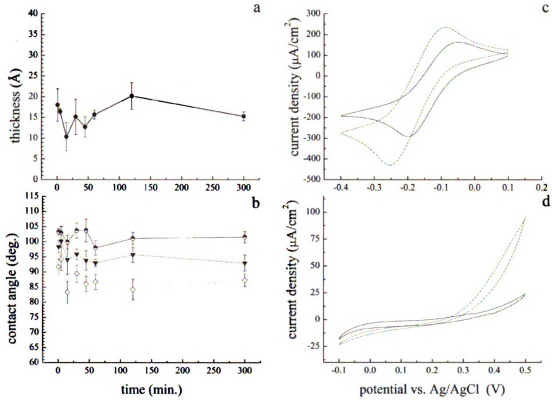

Fig. 3-4. DMPE result. A) Ellipsometric thickness measurement in time. B) Water contact angle in time with the solid line being the initial drop angle, the dashed line is advancing, and the dotted line is receding. C) CV of DMPE monolayer (solid line) and blank substrate (dashed line) when exposed to $Ru(NH_3)_6Cl_3$. D) CV of DMPE monolayer (solid line) and blank substrate (dashed line) when exposed to $K_3Fe(CN)_6$.

with a contact angle of ca. 103° (Fig. 3-4b). The contact angle hysteresis for the DMPE interface is >10°, a value consistent with a heterogeneous surface and arguing for sub-monolayer coverage. The ellipsometry and water contact angle data are both consistent with a DMPE interfacial adlayer that is measurably less well organized than either the DMPA or DMPC adlayers, and likely present as a partial adlayer. Cyclic voltammetry data for the DMPE interface (Figs. 3-4c and d) reveal a more prominent Ru redox wave than was seen for DMPA or DMPC, but for the Fe probe, no signal is seen for either the ZP treated SAM or the DMPE-terminated interface. The Ru probe data exhibit a peak splitting of 164 mV and a midpoint potential of -170 mV vs. Ag/AgCl for the ZP treated

SAM, and a peak splitting of 151 mV with a midpoint potential of -124 mV vs. Ag/AgCl for the DMPE-terminated interface. The addition of the DMPE adlayer apparently facilitates the electron transfer kinetics compared to the 6-mercapto-1-hexanol SAM, implying that the DMPE disrupts the organization of the underlying SAM. These data point collectively to the existence of a heterogeneous interface, consistent with partial monolayer coverage by DMPE.

3-3.4: DMPG

Adlayers formed using DMPG exhibited properties that are significantly different from those observed for DMPA and DMPC adlayers, and more akin to that seen for

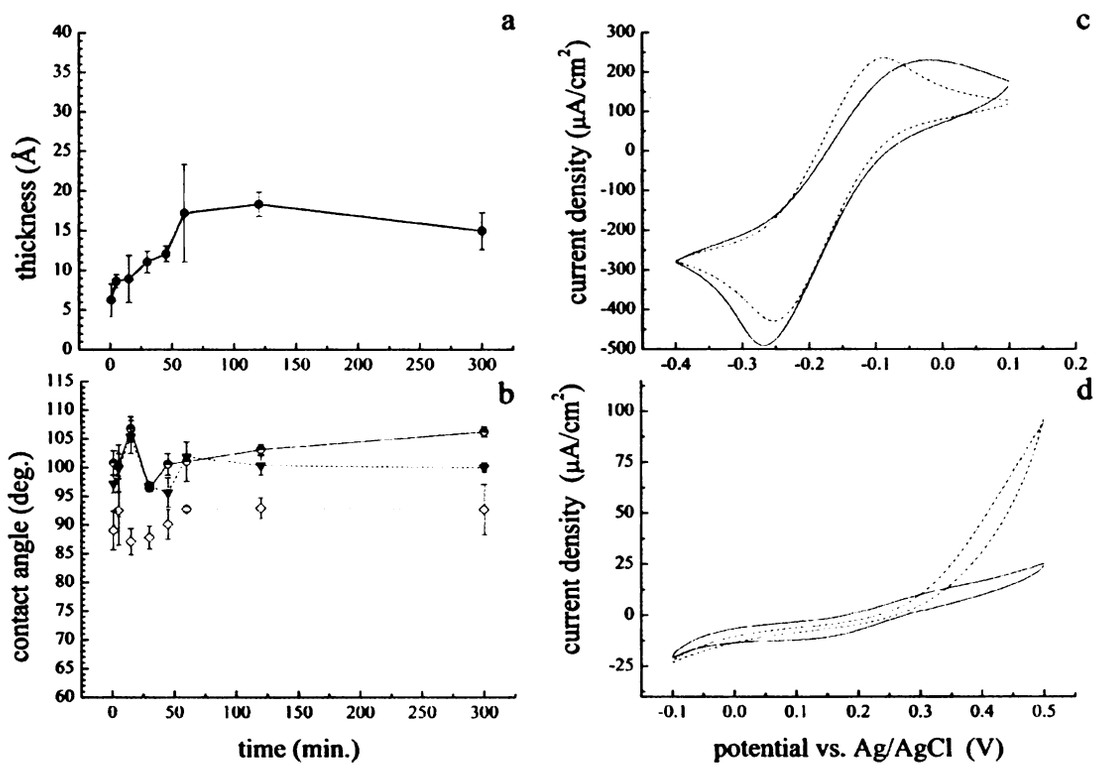

Fig. 3-5: DMPG results. A) Ellipsometric thickness measurement in time. B) Water contact angle in time with the solid line being the initial drop angle, the dashed line is advancing, and the dotted line is receding. C) CV of DMPG monolayer (solid line) and blank substrate (dashed line) when exposed to $Ru(NH_3)_6Cl_3$. D) CV of DMPG monolayer (solid line) and blank substrate (dashed line) when exposed to $K_3Fe(CN)_6$.

DMPE. The ellipsometric thickness of the DMPG adlayers is 16±3 Å, requiring an hour to form (Fig. 3-5a). This thickness value is similar to that seen for DMPE and is consistent either with a partial, spatially heterogeneous adlayer, or an adlayer that displays a ca. 45° tilt angle relative to the interface normal for its acyl chains. The water contact angle value for the DMPG adlayer is ca. 101° (Fig. 3-5b), with a hysteresis of ca. 10°. The interface is clearly nonpolar but the magnitude of the hysteresis indicates the presence of spatial heterogeneity in the adlayer, consistent with fractional coverage. Cyclic voltammetry data for the Ru and Fe probes indicate that the addition of the lipid adlayer can diminish the organization of the thiol SAM (Fig. 3-5d). It is found that for the Ru probe there is a peak splitting of 166 mV for the ZP treated SAM, with a midpoint potential of -169 mV vs. Ag/AgCl. With the addition of the DMPG adlayer, an increase in splitting to 254 mV and a midpoint potential of -143 mV vs. Ag/AgCl are observed. It is clear that the presence of the DMPG adlayer is mediating the electron transfer kinetics at this interface, but perhaps more important is the observation that the magnitude of the current is the same for both interfaces. In all cases, the Ru probe has significant access to the electrode. For the Fe probe, it is found that the thiol adlayer yields a small Fe redox wave, with a peak splitting of 152 mV and a midpoint potential of 225 mV vs. Ag/AgCl. In this case, the presence of the DMPG adlayer hinders access of the Fe probe to the electrode surface. These data indicate, collectively, that there can be significant access of the electrochemical probe to the electrode, implying a disordered, incomplete adlayer that can influence the organization of the 6-mercapto-1-hexanol SAM is formed by DMPG.

3-3.5: DMPS

DMPS is also used to evaluate its propensity for adlayer formation on a zirconated interface. Ellipsometric thickness measurements yielded erratic results with data ranging

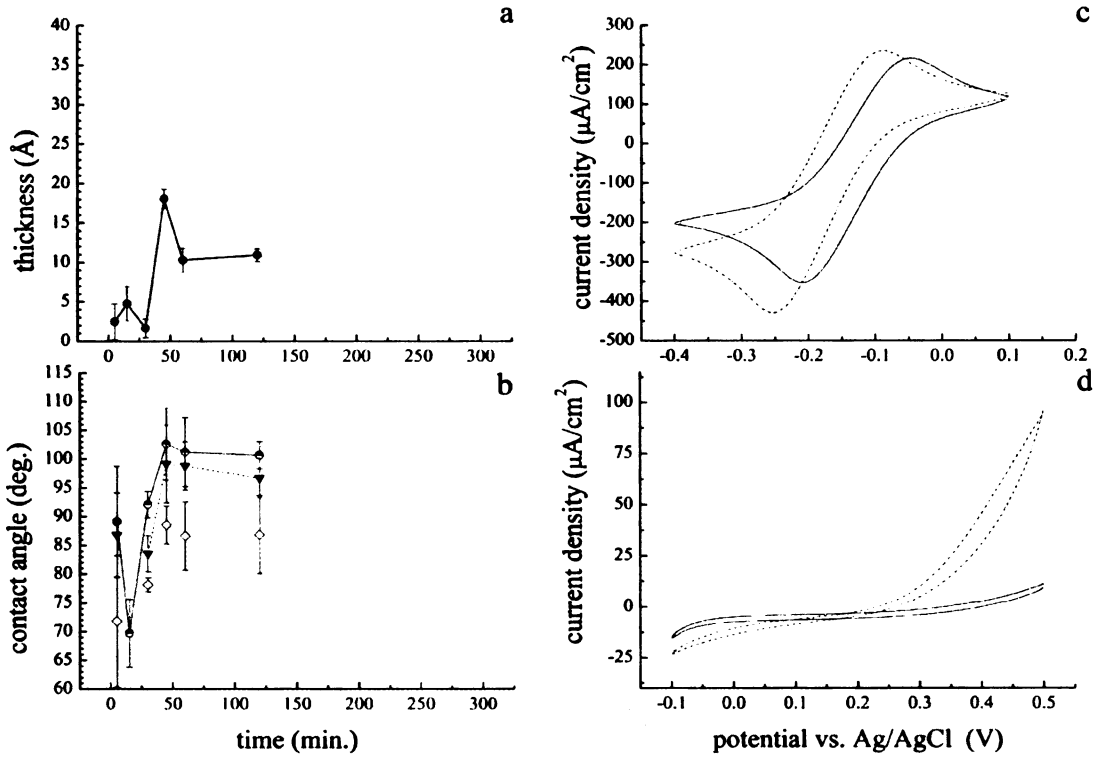

Fig. 3-6: DMPS results. A) Ellipsometric thickness measurement in time. B) Water contact angle in time with the solid line being the initial drop angle, the dashed line is advancing, and the dotted line is receding. C) CV of DMPS monolayer (solid line) and blank substrate (dashed line) when exposed to $Ru(NH_3)_6Cl_3$. D) CV of DMPS monolayer (solid line) and blank substrate (dashed line) when exposed to $K_3Fe(CN)_6$.

from 4 Å to ca. 10 Å (Fig. 3-6a). These data indicate the formation of what could optimistically be termed a partial adlayer. Water contact angle data on these same interfaces indicated the existence of a hydrophobic adlayer being formed (Fig. 3-6b), with a contact angle of ca. 100° and a hysteresis of ca. 15°. Such a large hysteresis indicates a highly nonuniform interface, consistent with the ellipsometric thickness data. The interaction of DMPS with a zirconated interface is not sufficiently favorable to produce an identifiable adlayer, and what does adsorb onto the zirconated interface does so only after extended exposure time. Cyclic voltammetry data using the Ru and Fe probes indicate an adlayer with fractional interface coverage. Redox waves are seen for the Ru probe but not for Fe probe (Fig. 3-6c,d). For the ZP treated SAM, the Ru probe produces a peak splitting

of 166 mV and a midpoint potential of -171 mV vs. Ag/AgCl. With the addition of the DMPS adlayer, the splitting is 162 mV and the midpoint potential shifts to -128 mV vs. Ag/AgCl. Given the comparative magnitudes of the voltammograms for the SAM and DMPS interfaces and peak splitting data, it is possible that lipid deposition disrupts the organization of the zirconated SAM.

3-4: Overall Lipid Observations

With an overview of the ellipsometry, water contact angle and CV data for each of the lipid adlayers that have been studied, the next consideration is how these data compare to one another. Specifically, of concern is how the phospholipid headgroup identity mediates lipid adlayer formation. All data collected for each phospholipid headgroup is overlaid in Fig. 3-7 in order to gain further insights on the variations between headgroups. The data point to the division of the lipids into two broad categories; those phospholipids characterized by comparatively strong headgroup interactions with the zirconated interface (DMPA, DMPC), and those phospholipids that interact only to a limited extent with the zirconated interface (DMPE, DMPG, DMPS). This draws on the assertion that there is both a steric component and an "interaction" component (e.g. hydrogen bonding) that account for these findings.

A word is in order at this point on the formation of lipid monolayers rather than bilayers in this study. The physical picture for monolayer formation as discused in chapter 2, is believed to proceed as follows: initially, vesicle fusion proceeds on the zirconated interface, and once the phospholipid headgroups of the bottom leaflet of the planar bilayer contact the zirconated interface, they bind in an essentially irreversible manner, provided the headgroup structure allows for this interaction to occur. The bottom leaflet is thus not free to execute translational motion. It is believed that the interface coverage

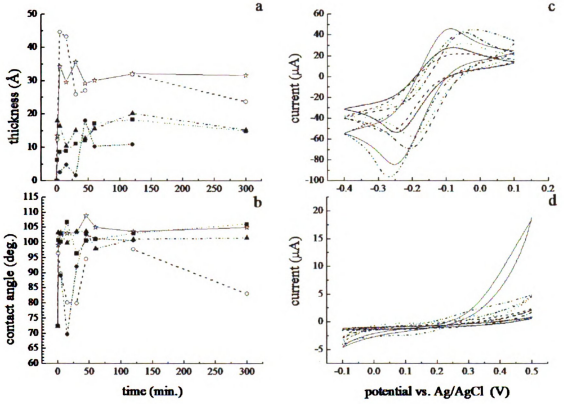

Fig. 3-7: A) Overlay of all thickness measurements in time with DMPA (solid line), DMPC (dashed line), DMPE (dash-dot-dot-dash line), DMPG (dotted line), DMPS (dash-dot-dash line). B) Overlay of initial drop water contact angle measurements with DMPA (solid line), DMPC (dashed line), DMPE (dash-dot-dot-dash line), DMPG (dotted line), DMPS (dash-dot-dash line). C) Overlay of $Ru(NH_3)_6Cl_3$ probe CVs with Blank (solid line), DMPA (dashed line), DMPC (bold solid line), DMPE (dotted line), DMPG (dash-dot-dot-dash line), DMPS (dash-dot-dash line). D) Overlay of $K_3Fe(CN)_6$ probe CVs with Blank (solid line), DMPA (dashed line), DMPC (bold solid line), DMPE (dotted line), DMPG (dash-dot-dot-dash line), DMPS (dash-dot-dash line).

of lipids is heterogeneous initially, and the interstices between covered regions remain open if they are smaller than the area required for vesicle adsorption and fusion. Subsequent to initial deposition, translational motion of the top lipid leaflet, and translocation of those lipids, once they reach the edges of the bottom-leaflet islands, serves to fill in the open interstitial regions with phospholipid molecules, resulting in a lipid monolayer. In cases where the phospholipid headgroup interaction is weak (vide infra), the formation of a partial adlayer is achieved.

3-4.1: Lipids with Strong Headgroup Interactions

The phospholipids DMPA and DMPC both exhibit strong interactions with the zirconated interface. Both adlayers produce ellipsometric thicknesses of ca. 30 Å, consistent with a monolayer of C_{14} phospholipid based on molecular mechanics calculations and experimental data.[96] While all phospholipids yielded a water contact angle of $\geq 90°$, implying a very hydrophobic interface, contact angle hysteresis has proven to be more informative in terms of adlayer quality. The magnitude of the contact angle hysteresis scales with interface heterogeneity, with a hysteresis of 5° or less implying a comparatively homogeneous interface, and a hysteresis of 10° or more, implying significant structural heterogeneity.[126] The DMPA and DMPC adlayers yield the lowest contact angle hysteresis of all the lipid adlayers studied, and these findings are in qualitative agreement with the electrochemical data, which indicate that these two adlayers are the least permeable to the $Ru(NH_3)_6Cl_3$ and $K_3Fe(CN)_6$ probes.

3-4.2: Lipids with Weak Headgroup Interactions

The second group of lipids, DMPE, DMPG and DMPS, are all characterized by comparatively thin (ca. 15 Å) adlayer thicknesses, and contact angle hysteresis of 10° or more. The CV data point to a measurable ability of the electrochemical probes to undergo electron transfer with the Au electrode. In some cases (e.g. DMPE), the addition of the lipid adlayer appeared to diminish the integrity of the underlying SAM. Taken collectively, the data point to a heterogeneous interface with sub-monolayer coverage of the lipids. Considered next is the physical and chemical basis for these findings.

3-5: Discussion

There is an important feature of the electrochemical data which can be understood

in terms of access of the electrochemical probes to the zirconated layer (Table 3-1). It is noted that the midpoint potential for all of the zirconated interfaces is located at ca. -170 mV vs. Ag/AgCl. For a zirconated interface, it is expected that the Zr^{+4} will be coordinated by either OH- or Cl- ions in solution, and it is also likely that non-stoichiometric water will be associated with the interface terminal group.[127,128] These ligands must be displaced upon complexation of the phospholipid headgroup to the Zr^{+4}. It has been established previously that the presence of Zr-phosphate at an electrode interface can shift the midpoint potential of a redox-active species to more positive values if the redox-

	$Ru(NH_3)_6^{3+/2+}$ probe				$Fe(CN)_6^{3-/4-}$ probe			
Lipid	SAM		SAM+lipid		SAM		SAM+lipid	
	Splitting (mV)	$E_{mi-dpoint}$ (mV)	Splitting (mV)	$E_{mi-dpoint}$ (mV)	Splitting (mV)	$E_{mi-dpoint}$ (mV)	Splitting (mV)	$E_{mi-dpoint}$ (mV)
DMPA	164	-170	212	-167	128	190	--	--
DMPC	166	-164	167	-170	--	--	--	--
DMPE	164	-170	151	-124	--	--	--	--
DMPG	166	-169	254	-143	152	225	--	--
DMPS	166	-171	162	-128	--	--	--	--

Table 3-1. Electrochemical data for $Ru(NH_3)_6^{3+/2+}$ and $Fe(CN)_6^{3-/4-}$ probes for interfaces studied here. The SAM indicated in the Table is 6-mercapto-1-hexanol. Endpoint values are reported vs. Ag/AgCl reference electrode.

active species can gain direct access to the ZP moiety.[129] These experimental midpoint potential data show no change for DMPA and DMPC interfaces and a ca. 40 mV positive shift for DMPE, DMPG and DMPS interfaces. For structurally heterogeneous, partial lipid adlayers, such a shift is expected, and this finding is consistent with the ellipsometry and contact angle results.

When possible, the Zr-bisphosphate (ZP) structure will form because of the substantial thermodynamic driving force for this reaction.[130] The formation of the ZP structure can be precluded by either steric interference or by competition from other intermolecular interactions. As mentioned above, it is known that ZP interfaces with Zr^{+4}

as the topmost layer will attract non-stoichiometric water, presumably due to the hydrophilic nature of the Zr^{+4} ion.[127,128] When a ligand complexes with the Zr^{+4} ion, it must first displace the water surrounding the metal ion. If the ligand also has a propensity for interaction with water, the water may not be displaced or may be competitively bound by the ligand, leading to diminished complexation between the metal and the phosphate moiety. This situation could lead to structural disruption of the ZP interface. Considering the phospholipids in the context of their propensity for H-bonding interactions, it is anticipated that the phospholipids DMPA, DMPE, DMPG and DMPS can all undergo extensive H-bonding with water due to the presence of phosphate, amine, hydroxyl and carboxylate moieties, respectively. In the case of DMPC, analogous H-bonding with water is hindered by the terminal trimethylamine moiety, and experimentally it is found that the existence of the choline substituent on the lipid phosphate group does not sterically preclude formation of the ZP complex. For DMPA, the formation of a ZP complex with a sterically unhindered phosphate can occur, displacing H_2O in the process. For the substituted phospholipids DMPE, DMPG and DMPS, the side groups are capable of H-bond formation with any water in the vicinity of the ZP group, and can thus maintain the phosphonate moieties physically separate from the Zr^{+4}. For these lipids, it is possible that the formation of a partial adlayer disrupts the organization of the underlying SAM, leading to enhanced exposure of the ZP moieties to the electrochemical probes, as manifested by the observed ca. 40 mV positive shift in the midpoint potential. For phospholipids that either do not participate substantially in aqueous H-bonding (DMPC) or for those where there is no steric issue with respect to access to the phosphate moiety (DMPA), we observe comparatively strong chemical interactions with the zirconated surface, resulting in the formation of a structure that resembles a monolayer of lipid. Under these conditions, electrochemical probe access to the ZP moieties and underlying Au electrode surface is

precluded by the presence of the lipid and the midpoint potential seen for these interfaces resembles that seen for the (presumably well organized) ZP-terminated interface, where the ZP moieties are likely coordinated to OH^- and/or Cl^-. For phospholipids with phosphate pendant functionalities capable of significant H-bonding, less well organized adlayers are observed. The data for the phospholipids that fall into this group (DMPE, DMPG, DMPS) suggest the formation of a spatially heterogeneous partial adlayer on the zirconated interface.

The results obtained for the DMPS adlayer is somewhat surprising in light of the fact that Zr-phosphate-carboxylate (ZPC) complexation is known to occur.[89,131,132] While this complexation is not as energetically favorable as ZP complexation, the presence of two functionalities in the DMPS headgroup offers the opportunity for multiple types of complexation, neither of which are found to contribute significantly, based on our experimental results.

3-6: Conclusions

In this study the time-dependent ellipsometric thickness and contact angle of a series of phospholipid adlayers bound to a zirconated interface have been measured. These data, in concert with cyclic voltammetry data using two electrochemical probes of the resulting interfaces, serve to characterize the comparative binding efficiency and quality of the lipid adlayers. The data reveal that DMPA and DMPC form the most organized adlayers with DMPE, DMPG, and DMPS producing adlayers characterized by spatial heterogeneity and sub-monolayer coverage. The adlayer properties are then related to the ability of the phospholipid substituted phosphate moiety to interact with the zirconated interface. Both steric issues and the propensity of the phospholipid headgroups to H-bond with water and possibly other lipids in the proximity of the interface likely play

roles in determining the quality of the phospholipid adlayers. One issue that remains to be investigated is whether or not the means of lipid adlayer deposition influences the observed interfacial film thickness and uniformity. Lipid fusion is used to effect the self-assembly process. It is possible that the pre-assembly of lipid adlayers as Langmuir-Blodgett films could influence the properties of films deposited on the same substrates used here, and an effort is underway to explore this possibility.

It is clear that the understanding of this novel class of self-assembling adlayers would benefit from imaging measurements, and this is an effort that is ongoing. It is hoped that these adlayers will find use in the formation of supported lipid bilayer structures where the extent of interaction between the lipid adlayer and the support can be adjusted chemically through the composition of the lipids used.

It is important however, just like with the varying lipid headgroups, to explore varying substrates. By changing the metal on the surface from Zr to other various metals, different lipid-metal interactions could be observed. This could then translate to the ability to have multi-metal surfaces that have tailored effects on mixed lipid solutions. Initially however, it is important to gain an understanding of how different metals interact with a lipid headgroup, which is discussed in the following chapter.

Chapter 4

Ionic Binding of Phospholipids to Interfaces: Dependence on Metal Ion Identity

4-1: Introduction

The goal of creating bilayer systems is to utilize them to simulate the plasma membrane in a manner that allows for the presence of trans-membrane proteins in their active form(s).[57] Success in this area requires that the lipid bilayer and the immediate environment on both sides of the bilayer be sufficiently hydrophilic to mimic a cellular system, and this issue has led to the design of bilayer structures that reside on hydrophilic underlayers, for example.[59,74,77] In addition to these structural requirements, there are the issues of lipid bilayer fluidity and the manner in which the bilayer is bound to the underlayer many of these issues already have been addressed. Simple physisorption of bilayers onto most substrates yields an interface that is not sufficiently robust to maintain its structural integrity in the long term. It is thus important to identify ways to make more robust the lipid bilayer interaction(s) with the support on which they reside. In the previous chapters this has been explored, with this work showing that Zr^{+4} can interact with phospholipid phosphate headgroups,[116,133] and there is anecdotal evidence that Ca^{+2} is required to achieve a high quality lipid bilayer under conditions where the bilayer is physisorbed to the interface. For these reasons it is also of interest to explore the strength of interactions between other interfacial metal ions and selected phospholipids, and these findings are reported here.

To reiterate, mammalian plasma membranes are complex systems that are comprised of more than 100 different components.[1] This compositional complexity is thought to be essential for housing transmembrane proteins as well as making the bilayer

structure sufficiently robust that it is capable of maintaining its structural integrity upon exposure to air.[75-77,116] It is found in the earlier work presented that it is possible to create a hydrophilic interfacial adlayer with a high density of surface hydroxyl groups, and this interface can support a physisorbed phospholipid bilayer. The resulting interface is important for the creation of a well organized and robust biomimetic interface.[116] By modifying the hydroxylated interface to create a Zr-phosphate (ZP) functionality, it was determined that structurally robust lipid monolayers were formed because of the interaction of phosphocholine head groups with the surface-bound ZP functionality. The formation of a Zr-bisphosphate complex was verified by ^{31}P NMR measurements.[116] The use of Zr^{+4}-phosphate/phosphonate complex formation to create organized mono- and multilayer interfacial structures is well known, and the success of this approach to controlled adlayer formation is based on the essentially irreversible Zr^{+4} interaction with the phosphate moieties.[89,134]

With the establishment of phospholipid binding to zirconated interfaces, a key issue to evaluate was the role of phospholipid headgroup identity in mediating the complexation process. Utilizing the gold-thiol self-assembled monolayer chemistry used in earlier studies[95,118-125] to build a monolayer on a gold surface. This can be modified subsequently to bind selected phospholipids. Au substrates are first exposed to 6-mercapto-1-hexanol to form a self-assembled monolayer (SAM), followed by reaction of the SAM terminal –OH group with $POCl_3$, H_2O, and then $ZrOCl_2$. It was found that phosphocholine and phosphatidic acid lipids complexed with Zr^{+4} ions strongly, while phosphoethanolamine, phosphoglycerol and phosphoserine lipids did not form organized lipid adlayers.[133] Contact angle and optical ellipsometry data indicate that the adlayers formed using these lipids were incomplete and spatially heterogeneous. These findings are understood in the context of the propensity of the lipid headgroups to hydrogen bond with

water in the vicinity of the Zr-phosphate interface. Lipids with H-bonding headgroups do not complex substantially with the surface-bound Zr^{+4} because of competitive interactions with nonstoichiometric water in the vicinity of the interface. In this next group of experiments, phosphatidic acid was chosen to eliminate issues that could be related to steric contributions to ZP complex formation.

4-2: Metals for Modification of Au Substrates

It is clear that, for reasons of the phospholipid headgroup structure, there is intrinsic chemical selectivity associated with the formation of lipid adlayers in this manner. It is also important to consider whether the metal ion used in the formation of the interfacial metal-phosphate structure will play a role in mediating the interface-lipid interactions. Metal-phosphates are known for a range of metal ions.[78,135-142] Most of the metal ions tested have been divalent transition metals, and Mg^{+2} and Ca^{+2} have also been used.[136-139] Following the same methods used in the modification of Au substrates with Zr^{+4},[116] the examination of the ability of several metal ions, some with biological significance, to form interfacial complexes with phosphatidic acid has been chosen. Metal ions Ca^{+2}, Mg^{+2}, Zn^{+2}, Ni^{+2} and Cu^{+2} are chosen based on their known propensity for interactions with phosphates. Fe^{+3} was chosen because iron coordinates phosphate strongly.[136] Because of the oxidative instability of Fe^{+2}, it was necessary to work with Fe^{+3} due to the fact that experiments are performed in air or in an aqueous medium where no effort had been made to deoxygenate the solution. To gain further insight the phosphate interactions with Cu^{+} was examined in an attempt to understand whether or not metal ionic charge played a significant role in the formation of the supported lipid adlayer. Since lipid interactions with Zr^{+4} have been characterized,[133] the data reported here are compared to the Zr^{+4}-modified interface.

The results for lipid binding to a metal modified surface include X-ray photo-electron spectroscopy (XPS), cyclic voltammetry, optical ellipsometry and water contact angle data, to elucidate the formation and, to a limited extent, the organization of the lipid adlayers. The data indicate that lipid-metal coordination is a complex process that is mediated by the identity and loading density of the metal ion that coordinates to the surface-bound phosphate groups.

4-3: Experimental Setup and Instrumentation Utilized

The lipid chosen for these experiments was 1,2-dimyristoyl-sn-glycero-3-phosphatidic acid (DMPA, monosodium salt) and was obtained from Avanti Polar Lipids, Inc. The solvents and reactants: Acetonitrile, ethanol (100%), ethyl acetate, 6-mercapto-1-hexanol, phosphorus oxychloride ($POCl_3$), zirconyl chloride octahydrate ($ZrOCl_2 \cdot 8 H_2O$), 2,4,6-collidine, lithium perchlorate, potassium chloride, as well as the electrochemical probes potassium ferrocyanide trihydrate and hexaminerutheniun(III) chloride were obtained from Sigma-Aldrich in the highest purity grade available. The metal salts calcium chloride ($CaCl_2$), zinc chloride ($ZnCl_2$), nickel chloride ($NiCl_2$), magnesium chloride ($MgCl_2$) and ferric chloride ($FeCl_3$) were obtained from Spectrum Chemicals. While cupric chloride ($CuCl_2$) was obtained from J.T. Baker Inc. and cuprous chloride (CuCl) obtained from Mallinckrodt. All metal salts were purchased in the highest purity grade available and used as received. 18 MΩ Water was obtained from an in-house Barnstead system and used for all experiments.

The instrumentation utilized is as follows: all electrochemical data were acquired using a CH Instruments 650 electrochemical bench. Optical ellipsometry measurements were performed using a J. A. Woollam Co., Inc. model EC110 spectroscopic ellipsometer with a wavelength range of 185-1100 nm, utilizing 44 wavelengths simultaneously. The

water contact angle measurements were performed on an ACT Products Inc. VCA 200 video contact angle system. XPS measurements were performed on a Perkin Elmer Phi 5400 instrument equipped with a Mg-Kα X-ray source. Samples were analyzed at pressures between 10^{-9} and 10^{-8} Torr with a pass energy of 29.35 eV and a take-off angle of 45°. The spot size is ca. 250 mm^2. Atomic concentrations were determined using known sensitivity factors. All peaks were referenced to the C1s peak associated with adventitious C at 284.6 eV. Unless noted otherwise, experiments were performed at 20°C.

The electrochemical measurements were performed similarly to the experiments in chapter 2 and 3.[116,133] Two electrochemically active probes were used to characterize the interfaces that were studied; $K_3Fe(CN)_6 \cdot 3\ H_2O$ (1.32 mM) in 0.1 M $LiClO_4$ and $Ru(NH_3)_6Cl_3$ (1.00 mM) in 0.1 M KCl. These two probes were chosen because of their different electron transfer kinetics across alkanethiol SAMs and their different ionic charges.[88] Cyclic voltammetry (CV) was performed with each probe being cycled three times at a scan rate of 0.1 V/s. The $Fe(CN)_6^{3-/4-}$ probe was scanned from -0.1 V to +0.5 V vs. Ag/AgCl and the $Ru(NH_3)_6^{3+/2+}$ probe was scanned from -0.4 V to +0.1 V vs. Ag/AgCl, using a Pt counter electrode.

4-3.1: Substrate Preparation

Gold substrates were prepared using a procedure described previously.[89] Briefly, the substrates were rinsed with water and ethanol, cleaned in a UV-cleaner for 15 min., then exposed to 10 mM 6-mercapto-1-hexanol in ethanol for 6 hrs. The resulting interface was rinsed with ethanol and ethyl acetate, then dried under a stream of $N_2(g)$. For metal modified interfaces, the 6-mercapto-1-hexanol monolayer was reacted with $POCl_3$ (0.4 mL) in dry acetonitrile (10 mL), and catalyzed with 2,4,6-collidine (0.4 mL) for 3 hrs. The phosphate-modified monolayer was rinsed with ethanol and water, dried with

N_2(g), and exposed to 5 mM concentrations of one metal salt in a 60:40 ethanol/water solution for 12 hrs. For each metal ion used, the substrate was prepared in the same manner utilizing metal chloride salts (except for Zr^{+4}, where $ZrOCl_2$ was used). The resulting metal ion-containing monolayer was dried under N_2(g), then exposed to a solution containing a DMPA unilamellar lipid vesicles.

4-3.2: DMPA Vesicle Preparation.

Unilamellar vesicles of DMPA were prepared as described previously.[60] The vesicles were comprised of the phospholipid only, with no other constituents. The chloroform:methanol:water solvent system was first evaporated from the lipid solution using a N_2 stream. The lipid was then exposed to vacuum to remove any remaining solvent. The dried lipid was dissolved in a 10 mM tris(hydroxymethyl)-aminomethane hydrochloride (Tris®, Aldrich) pH 7.5 buffer solution to a final concentration of 1 mg/mL. The solution was then mixed using five freeze-thaw-vortex cycles to ensure suspension of the lipids prior to extrusion.[90] A syringe-based mini-extruder was used to form unilamellar vesicles with a narrow size distribution (Avanti Polar Lipids, Inc.).[91-93] The lipid suspension was then passed through a polycarbonate filter (average pore diameter 400 nm) eleven times to produce unilamellar vesicles of that diameter.

4-3.3: Adlayer Formation

Planar DMPA adlayers were formed by spontaneous fusion of unilamellar vesicles.[75] The modified gold substrates were placed in a custom-made Teflon® flow cell that has been described in chapter 2.[116] The flow cell was used to ensure the lipid vesicle-containing solution was in full contact with the substrate during bilayer formation. Tris® buffer was flowed over the substrate at ca. 5 mL/min. prior to DMPA deposition,

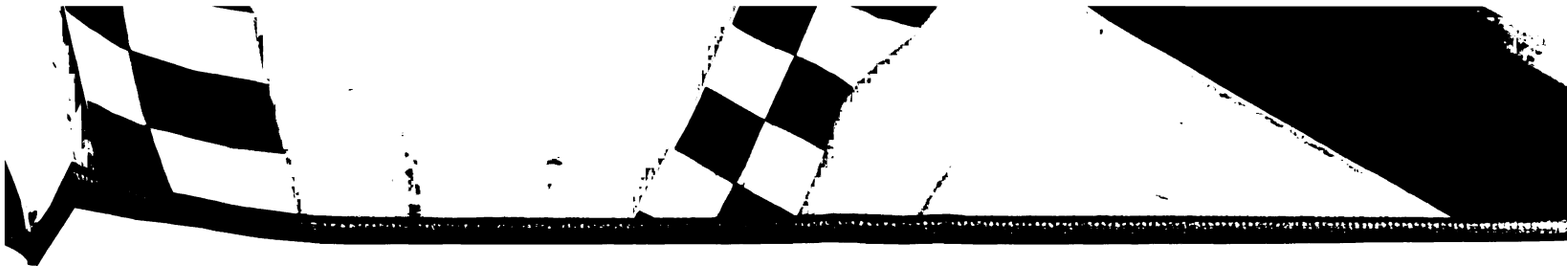

then the vesicle-containing solution was flowed through the cell at the same rate until the buffer solution was displaced, and this solution remained in contact with the substrate for two hours. After exposure to the vesicle-containing solution, the substrate was washed with water. Following washing, the water was aspirated from the cell. The substrate was then removed from the flow cell and allowed to dry in air while being held vertically.

4-4: Results of DMPA Exposure

The primary purpose of this work is to evaluate the interactions between the DMPA headgroup and selected metal ions bound to surfaces through a phosphate group, and thus gauge the extent to which lipid adlayer self-assembly proceeds. First the experimental data for the metal ions individually is discussed, then the comparison of these results to assess which metal ions give rise to phospholipid self-assembly, and which factors are of primary importance in determining the lipid-interface interaction is looked into.

4-4.1: Zirconium

As noted above, phosphate-terminated SAMs as the substrate for vesicle deposition were used. By reacting the phosphate-terminated interface with $ZrOCl_2$, it is possible to produce a Zr^{+4}-terminated surface. XPS was used to determine Zr-surface coverage. Analysis of the ratio of Zr:Au4f concentrations yields a value of 0.34 (Fig. 4-1a), which we take to indicate substantially complete surface coverage based on the known strongly favored complex formation behavior of Zr^{+4} with $ROPO_3^{-2}$.[80,134] It should be recognized that this concentration ratio is not quantitative due to the fact that the signal from a monolayer (or less) of metal ions is compared to the signal from a comparatively thick Au layer, but these ratio data for the different metal ions serve as a useful com-

parison. The zirconated substrate was exposed to a solution containing DMPA vesicles, and optical ellipsometry was used to measure the thickness of the resulting lipid adlayer ex situ (30±2 Å), consistent with the formation of a lipid monolayer.[96] Water contact angle measurements were performed on these same interfaces, providing insight into their polarity and homogeneity.[72,97-99] The water contact angle for a DMPA adlayer is 104°, with a hysteresis (the difference between advancing and receding contact angles) of ca. 7°. The value of 104° indicates that the chemical functionality of the adlayer in contact with the water droplet is nonpolar, consistent with the lipid acyl chains being the outermost component of the adlayer.[133] The hysteresis seen for the DMPA adlayer sug-

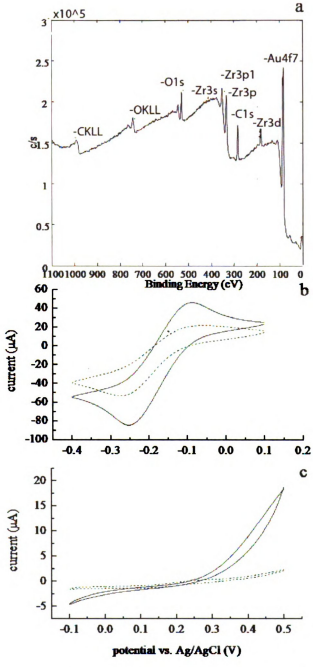

Fig. 4-1: a) XPS spectrum of Zr^{+4}-modified thiol/gold substrate. b) CV of $Ru(NH_3)_6Cl_3$ for a DMPA monolayer on Zr^{+4}-terminated interface (dashed line) and for the Zr^{+4}-terminated inter-face with no adlayer (solid line). c) CV of $K_3Fe(CN)_6$ for a DMPA monolayer on Zr^{+4}-terminated interface (dashed line) and for the Zr^{+4}-terminated interface with no adlayer (solid line).

gests modest spatial heterogeneity in the organization of the adlayer. Typically, hysteresis of ca. 2-3° is taken to indicate a homogeneous interface, and hysteresis of 10° or more indicates a structurally heterogeneous interface.

Cyclic voltammetry of electroactive probes in solution was also used to gauge the presence of defects in the lipid interface. Two electrochemical probes were utilized because of their different ionic charges and consequent abilities to penetrate nonpolar adlayers,[88] with CV data for $Ru(NH_3)_6Cl_3$ (Ru probe) shown in Fig. 4-1b and $K_3Fe(CN)_6$ (Fe probe) in Fig. 4-1c. The data reveal reversible redox waves for both probes, with peak splitting for both probes being consistent with literature reports.[57] Probe access to the electrode is limited for the Ru probe and is essentially blocked for the Fe probe with the Zr-lipid adlayer. For the Ru probe, it was found to have a measured peak splitting of 164 mV for the ZP treated 6-mercapto-1-hexanol SAM. The Ru probe electrochemical signal is attenuated slightly for the DMPA-terminated interface, and characterized by a splitting of 212 mV. It is noted that the splitting data for all measurements indicate interfacial adlayer mediation of the probe electron transfer kinetics. A peak splitting of 59 mV would be the expected peak splitting for a fully reversible reaction with fast electron transfer kinetics. For the Ru probe, it is clear that the lipid adlayer is influencing the electron transfer kinetics to a greater extent than for the 6-mercapto-1-hexanol SAM-terminated interface alone. For the DMPA-terminated interface, the ratio of non-Faradaic current to the non-Faradaic current of the blank was found to be 0.54. The lipid adlayer that is formed on the surface is analogous to the dielectric medium in a parallel plate capacitor, with the gold substrate and the water/lipid interface as the plates. The spacing between the plates determines the capacitance of the system. The ratio of the capacitive current measured for the lipid-adlayer terminated interface to that of the blank (Zr^{+4}-terminated) interface allows for an estimate of the lipid layer thickness, in the limit

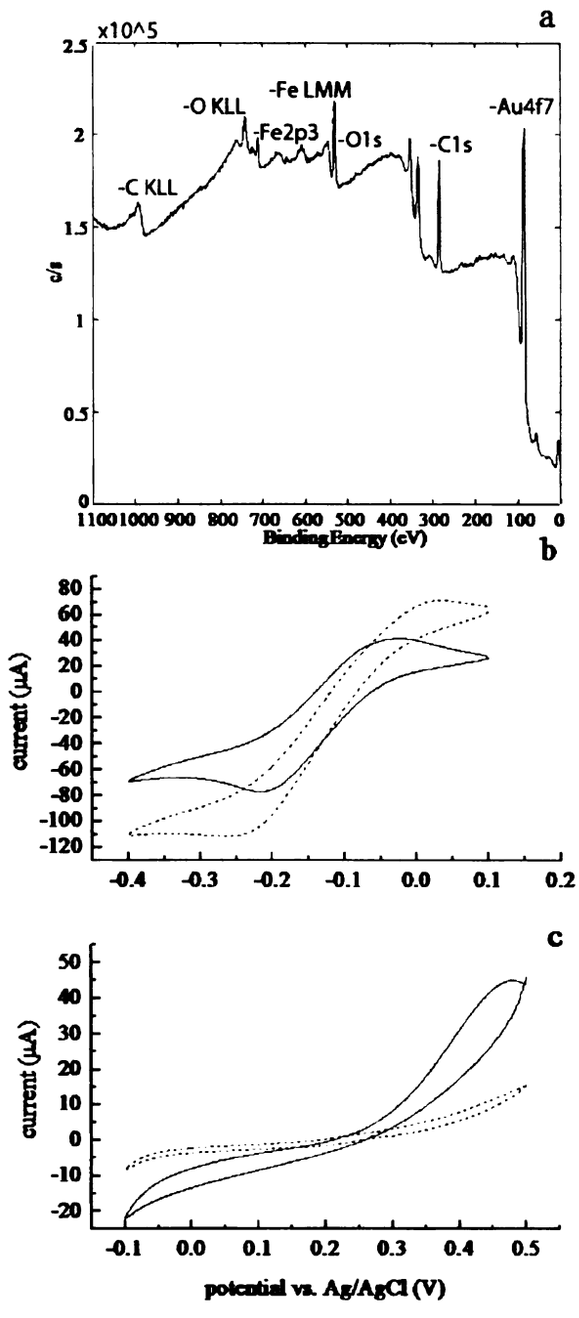

Fig. 4-2: a) XPS spectrum of Fe^{+3}-modified thiol/ gold substrate. b) CV of $Ru(NH_3)_6Cl_3$ for a DMPA monolayer on Fe^{+3}-terminated interface (dashed line) and for the Fe^{+3}-terminated inter-face with no adlayer (solid line). c) CV of $K_3Fe(CN)_6$ for a DMPA monolayer on Fe^{+3}-terminated interface (dashed line) and for the Fe^{+3}-terminated interface with no adlayer (solid line)

of an interface characterized by very few defects. The capacitive current ratio of the non-Faradaic currents for the DMPA-terminated interface to the Zr^{+4}–terminated substrate indicates adlayer deposition. The cyclic voltammetry and water contact angle data point collectively to the DMPA monolayer containing a measurable quantity of defects. There is precedent for the formation of a lipid monolayer at a zirconated interface.[116] Recent work on DMPC interactions with a zirconated interface showed that a monolayer does form, with the dominant chemical interaction being shown by ^{31}P NMR to be the complexation of the Zr^{+4} by the lipid phosphocholine group.[116]

4-4.2: Iron III

Fe^{+3} is an important metal ion from a biological perspective, and it is known to form metal bisphosphonate structures.[143] XPS

measurements of the Fe modified surface revealed a ratio of Fe:Au of 0.46 (Fig. 4-2a), similar to the surface coverage seen for Zr^{+4} (vide infra). Complexation of Fe^{+3} with DMPA is also observed by the formation of a lipid adlayer with a thickness of 26±2 Å. Water contact angle measurements of the lipid-terminated Fe^{+3} interface yield a contact angle of 102±2°, indicating a hydrophobic lipid monolayer oriented such that the acyl chains form the outer surface. The contact angle hysteresis for this substrate was found to be 7°, the same as was found for the Zr^{+4} interface and indicative of a macroscopically moderately well organized lipid monolayer. Cyclic voltammetry measurements for the Fe^{+3} interface were performed with the two redox probes to gain a insight on the microscopic organization. The Ru probe data reveal that the Fe modified interface is characterized by a peak splitting of 175 mV (Fig. 4-2b) and the DMPA-terminated interface produces a 277 mV peak splitting. The non-Faradaic current ratio calculated for the Fe probe was found to be 0.57 (Fig. 4-2c). The electrochemical data are in good agreement with the contact angle and ellipsometric data. These measurements point collectively to the formation of a DMPA monolayer that is characterized by a modest defect density. The Fe^{+3} modified surface is similar to the Zr^{+4} modified surface, indicating the formation of a substantially complete lipid monolayer. It should be noted that the examination of the Fe^{+3}-modified substrate is potentially complicated by the use of the $Fe(CN)_6^{-3/-4}$ probe. During potential cycling, the surface-bound Fe^{+3} will be reduced, but the current from this species will be small relative to that of the solution-phase probe, and because Fe^{+3} is present on both the blank and the DMPA-terminated interfaces, it will represent a constant contribution to any interface-dependence seen in the data.

4-3.3: Nickel

XPS analysis of nickel coordination with the modified gold substrate found a

surface coverage ratio of 0.08 Ni:Au (Fig 4-3a). There appears to be minimal Ni^{+2} bound to the phosphate-terminated the interface. In contrast to the behavior of the Cu^{+2}-terminated interface (vide infra), the Ni^{+2}-terminated interface is seen to form a complex with the DMPA headgroup. The thickness of the DMPA adlayer is 27±3 Å, with a water contact angle of 50±3°. By comparison, the Ni^{+2}-terminated interface yields a contact angle of 62±4°. The contact angle hysteresis for this system is ca. 2°, suggestive of a uniform interface. These data are apparently contradictory, with an adlayer thickness consistent with a lipid monolayer and contact angle data pointing to a polar interface. For a heterogeneous interface characterized by bare or coated domain sizes that are large (ca. μm scale), contact angle hysteresis is not an accurate gauge of surface heterogeneity. It is possible to have

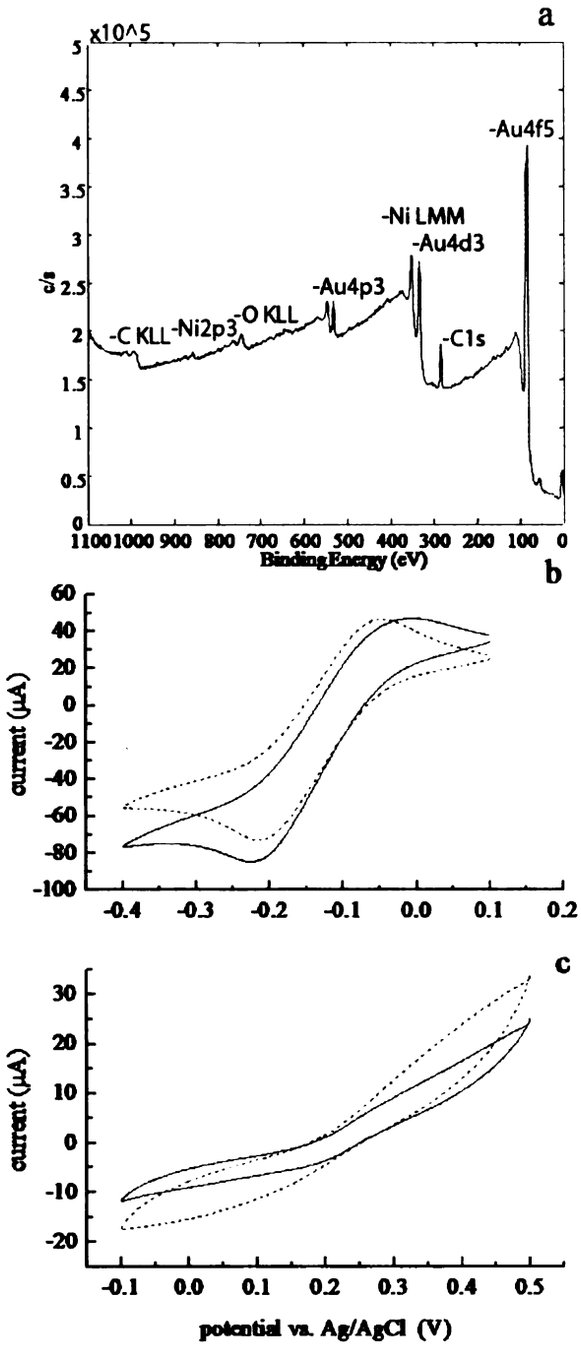

Fig. 4-3: a) XPS spectrum of Ni^{+2}-modified thiol/gold substrate. b) CV of $Ru(NH_3)_6Cl_3$ for a DMPA monolayer on Ni^{+2}-terminated interface (dashed line) and for the Ni^{+2}-terminated inter-face with no adlayer (solid line). c) CV of $K_3Fe(CN)_6$ for a DMPA monolayer on Ni+2-terminated interface (dashed line) and for the Ni^{+2}-terminated interface with no adlayer (solid line).

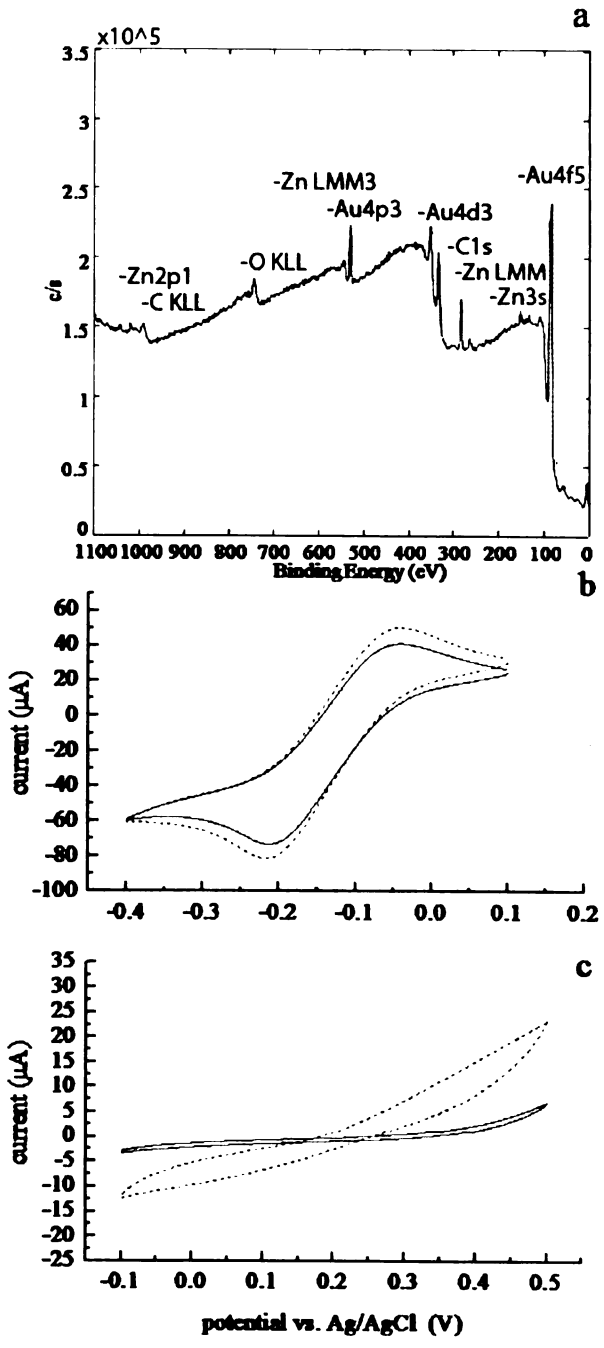

Fig. 4-4: a) XPS spectrum of Zn^{+2}-modified thiol/gold substrate. b) CV of $Ru(NH_3)_6Cl_3$ for a DMPA monolayer on Zn^{+2}-terminated interface (dashed line) and for the Zn^{+2}-terminated inter-face with no adlayer (solid line). c) CV of $K_3Fe(CN)_6$ for a DMPA monolayer on Zn^{+2}-terminated interface (dashed line) and for the Zn^{+2}-terminated interface with no adlayer (solid line).

a macroscopically heterogeneous interface that produces such results, and electrochemical data are useful in resolving whether or not this is the case for the Ni^{+2}-terminated interface. Using the Ru probe, the Ni^{+2}-terminated interface produces a splitting of 209 mV (Fig. 4-3b) and upon exposure to DMPA, a peak splitting of 171 mV is observed. Such a significant decrease in peak splitting would suggest that, upon the initial exposure of the Ni to the substrate, the Ni coordinates with multiple interfacial phosphate groups, limiting access of the Ru probe to the electrode surface. The addition of a DMPA adlayer perturbs this organization and enhances access of the probe to the electrode surface. The ratio of the DMPA interface-to-Ni^{+2}-terminated interface capacitance is 1.28 for interfaces examined with the Fe probe (Fig. 4-3c), a value indi-

cating a thickness intermediate between that of a monolayer and a bilayer based on data obtained for both types of adlayers, suggesting that the DMPA adlayer formed is spatially heterogeneous with a relatively large characteristic domain size.

4-4.4: Zinc

The behavior of Zn^{+2} is similar to that of Ni^{+2}, suggesting sub-monolayer coverage of the phosphate-terminated interface, and yielding a XPS Zn:Au concentration ratio of 0.08 (Fig. 4-4a). Ellipsometry data point to a DMPA adlayer thickness of 31±2 Å. Water contact angle measurements show a contact angle of 66±1° with a hysteresis of ca. 8°, suggesting some amount of surface heterogeneity. These data, taken collectively, point to a heterogeneous interface with a thickness slightly greater than that expected for a uniform monolayer and a water contact angle similar to that of the unmodified Zn^{+2}-terminated interface, which is characterized by a contact angle of 58±4°. Electrochemical data for the Zn^{+2}-terminated interface, collected with the Ru probe, show a splitting of 166 mV (Fig. 4-4b) and the DMPA-terminated interface exhibits a 214 mV peak splitting. Again, the presence of the lipid adlayer mediates electron transport at the interface, and the ratio of capacitance for the DMPA-terminated interface to the Zn^{+2}-terminated interface was found to be 4.72 using the Fe probe (Fig. 4-4c). The electrochemical capacitance data point to the DMPA adlayer enhancing the organization of the Zn^{+2}-terminated supporting SAM. The capacitance data, by themselves, suggest a thick DMPA adlayer. Based on all of the data collected for this system, it is more likely that a heterogeneous surface comprised of regions of DMPA bilayer is formed, and that defect areas as well as possibly poorly organized regions of the lipid adlayer contribute to these findings. In any case, Zn^{+2} appears to produce only modest interactions with the DMPA headgroup.

4-1.5: C

it is kn

phosp

on pla

unilar

held t

at an

intera

headg

sonab

adlay

Ca^{+2}

the s

Zn^{+}

0.05

me

m

in

th

h

r

c

4-4.5: Calcium

Ca^{+2} is of interest because it is known that calcium facilitates phospholipid bilayer formation on planar substrates formed from unilamellar vesicles.[74,144] It is held that the presence of Ca^{+2} ions at an interface somehow mediates interactions of the phospholipid headgroups and produces a reasonably uniform interfacial lipid adlayer. The surface coverage of Ca^{+2} was measured by XPS to be the same as that seen for Ni^{+2} and Zn^{+2}, with a metal-to-Au ratio of 0.08, indicating low coverage of metal ion (Fig. 4-5a). Ellipsometry measurements performed following DMPA exposure yielded a thickness of 39±2 Å, significantly higher than that seen for a DMPA monolayer, and approaching that of a bilayer. The presence of a partial bilayer is further indicated by the contact angle data, with a

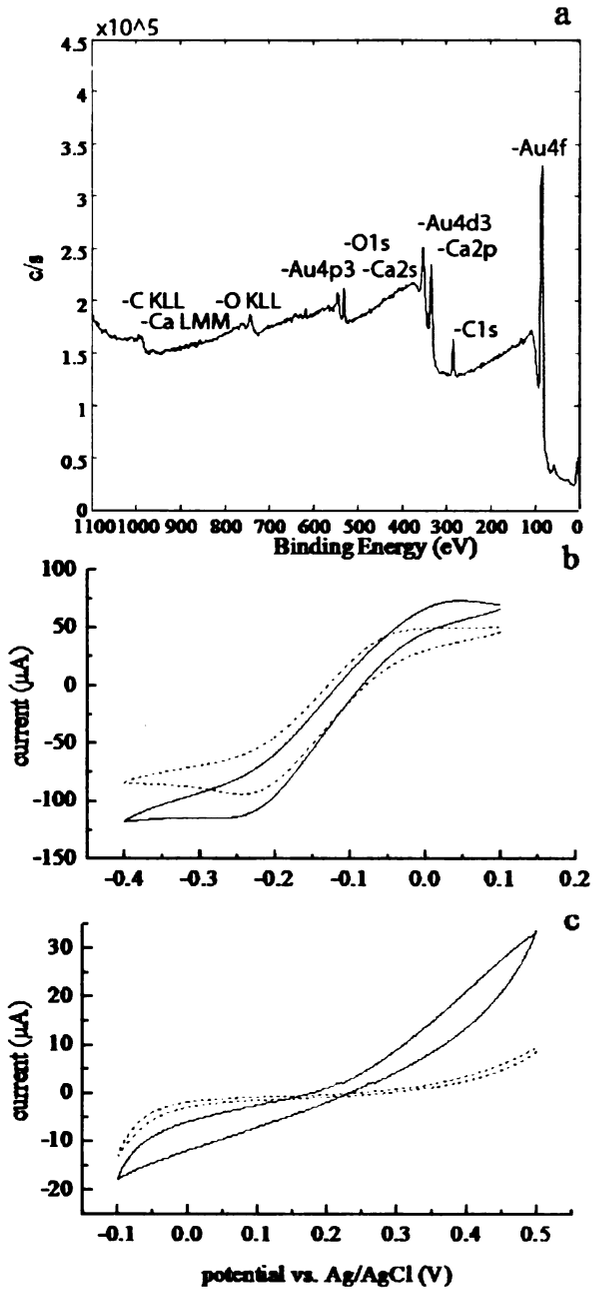

Fig. 4-5: a) XPS spectrum of Ca^{+2}-modified thiol/gold substrate. b) CV of $Ru(NH_3)_6Cl_3$ for a DMPA monolayer on Ca^{+2}-terminated interface (dashed line) and for the Ca^{+2}-terminated inter-face with no adlayer (solid line). c) CV of $K_3Fe(CN)_6$ for a DMPA monolayer on Ca^{+2}-terminated interface (dashed line) and for the Ca^{+2}-terminated interface with no adlayer (solid line).

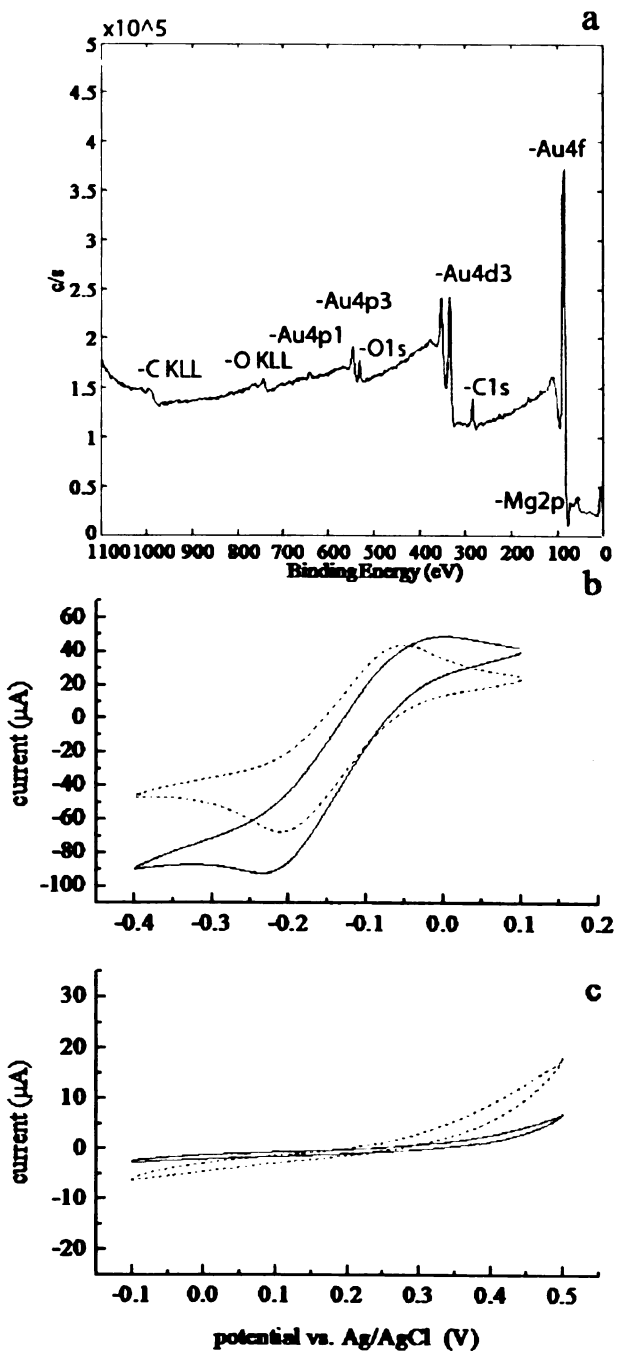

Fig. 4-6: a) XPS spectrum of Mg^{+2}-modified thiol/ gold substrate. b) CV of $Ru(NH_3)_6Cl_3$ for a DMPA monolayer on Mg^{+2}-terminated interface (dashed line) and for the Mg^{+2}-terminated inter-face with no adlayer (solid line). c) CV of $K_3Fe(CN)_6$ for a DMPA monolayer on Mg^{+2}-terminated interface (dashed line) and for the Mg^{+2}-terminated interface with no adlayer (solid line).

water contact angle of 37±6° and a hysteresis of 7°. Electrochemical data for the Ru probe at the Ca^{+2}-modified interface shows a peak splitting of 237 mV (Fig. 4-5b). The same interface, modified with a DMPA adlayer, exhibits a 224 mV peak splitting. The similarity of these splitting values argues for the unimportance of the DMPA adlayer in mediating the electron transfer process at this interface. Using the Fe probe, an observed capacitance ratio of 4.7 is found for the DMPA-terminated interface relative to the Ca^{+2}-terminated interface (Fig. 4-5c). These data point to comparatively strong interactions between the Ca^{+2} ions and the phosphates of both the underlying SAM and the lipid headgroup. Ca^{+2} appears to interact with the lipid headgroups but does not form a tightly bound interfacial structure. This point is considered below.

4-4.6: Magnesium

Mg^{+2} is a metal that is found widely in biological systems. XPS measurements of phosphate-terminated SAMs that had been exposed to Mg^{+2} were found to yield a Mg:Au concentration ratio of 0.08 from XPS data (Fig. 4-6a). This finding is consistent with measurements of the other divalent metals investigated in this work. An ellipsometric thickness of 38±1 Å, water contact angle of 61±10°, with a hysteresis of 8° was found for the DMPA-terminated Mg^{+2} interfaces. These results point to a lipid adlayer similar to that formed on the Ca^{+2}-modified substrates. Cyclic voltammetry data further indicate a similar surface being formed as that found with Zn^{+2}, with the Ru probe data for the Mg^{+2}-terminated interface yielding a peak splitting of 206 mV (Fig. 4-6b). The DMPA-terminated interface exhibited a 157 mV peak splitting, less than that of the Mg^{+2}-terminated interface. Capacitance measurements, performed with the Fe probe, show a ratio of the Mg^{+2}-terminated surface-to-DMPA-terminated surface to be 1.77 (Fig. 4-6c). These data point to the disruption of the supporting SAM structure upon exposure to of DMPA. This result is not surprising, because a decrease in the organization of the support monolayer is also seen for other divalent metals ions (vide infra). This is attributed to the loss of organization upon addition of the lipid adlayer in all of these cases (Ni, Zn, and Mg) to the charge carried by the metal ions and the consequent inability to accommodate the presence of two divalent ligands ($ROPO_3^{-2}$) while maintaining interfacial integrity. Initial exposure of the phosphate-terminated interface to Mg^{+2} produces coordination with the bound phosphates and a consequent increase in the organization of the interface by virtue of the metal ion coordinating with more than one phosphate moiety. Upon exposure to DMPA, the Mg^{+2}-terminated interface rearranges to accommodate the presence of the DMPA ligands, resulting in a decreased interaction with the phosphate moieties that are bound to the interface. The result is a decrease in the organization of the interface

with a consequent increased accessibility of the solution phase electrochemical probes to the electrode surface. Capacitance measurements performed with the Fe probe support the ellipsometry and contact data collected, indicating an interfacial thickness intermediate between that of the Cu^{+2}-containing DMPA adlayer (vide infra) and the Zr^{+4}-containing DMPA adlayer.

4-4.7: Copper I

Cu^{+} was found to bind to the phosphate-terminated SAM. XPS data showed that the ratio of Cu^{+}:Au was 0.31 indicating a substantially complete coverage of the interface with Cu^{+} (Fig. 4-7a). Following exposure of the Cu^{+}-terminated interface to DMPA, ellipsometry measurements yielded a thickness of 14±5 Å and the water contact angle for this interface was found to be 52±3° with a hysteresis of 6°. In

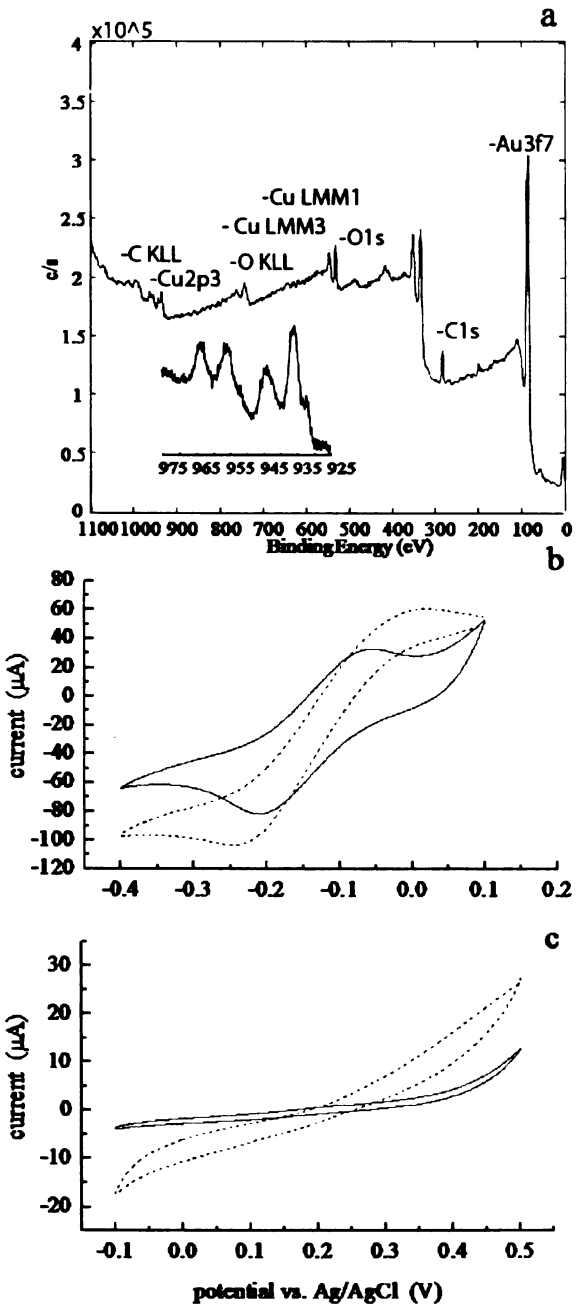

Fig. 4-7: a) XPS spectrum of Cu^{+}-modified thiol/gold substrate. Inset shows Cu2P spectral region. b) CV of $Ru(NH_3)_6Cl_3$ for a DMPA monolayer on Cu^{+}-terminated interface (dashed line) and for the Cu^{+}-terminated interface with no adlayer (solid line). c) CV of $K_3Fe(CN)_6$ for a DMPA monolayer on Cu^{+}-terminated interface (dashed line) and for the Cu^{+}-terminated interface with no adlayer (solid line).

comparison, the water contact angle of the Cu^+-terminated interface was measured to be 57±4°. The ellipsometry data point to fractional coverage of the interface with DMPA, giving rise to an interface that is dominated by unreacted sites. The contact angle data support this interpretation because there is not a measurable change in contact angle of the interface upon exposure to DMPA. Cyclic voltammetry data for the DMPA-terminated interface using the Ru and Fe electrochemical probes (Figs. 4-7b and 4-7c, respectively) indicate that the DMPA adlayer disrupts the underlying SAM. For the Ru probe, the Cu^+-terminated interface yields a splitting of 155 mV (Fig. 4-7b) and the DMPA-terminated interface exhibits a 256 mV peak splitting. These data suggest that Ru probe access to the electrode surface is hindered by the addition of the DMPA adlayer, but, as can be seen in Fig. 4-7b, the Cu^+-terminated interface produces two oxidative peaks. It is found that exposure of the phosphate-terminated interface to Cu^+ leaves a noticeable film on the interface, suggesting the presence of excess physisorbed Cu^+. Upon electrochemical cycling, the film desorbs, producing a second oxidative peak in addition to allowing the electrochemical probe access to the electrode. Examination of the surface with the Fe probe also indicates that the addition of DMPA disrupts interfacial organization, also allowing access of the probe to the electrode surface. Comparison of the non-Faradaic current of the DMPA terminated interface to that of the Cu^+-terminated interface yields a value of 2.21, suggesting a larger than expected DMPA-terminated adlayer thickness. This finding is attributed to the presence of non-stoichiometric Cu^+ at the interface. Upon exposure of the interface to DMPA, the phospholipid will coordinate to the non-stoichiometric Cu^+, which desorbs into solution, leaving hydrophilic open regions in the interface. Subsequently, DMPA in solution can interact with the hydrophilic interface, allowing the formation of bilayers.[116] It is these resulting bilayers that contribute to the cyclic voltammetry capacitance measurements.

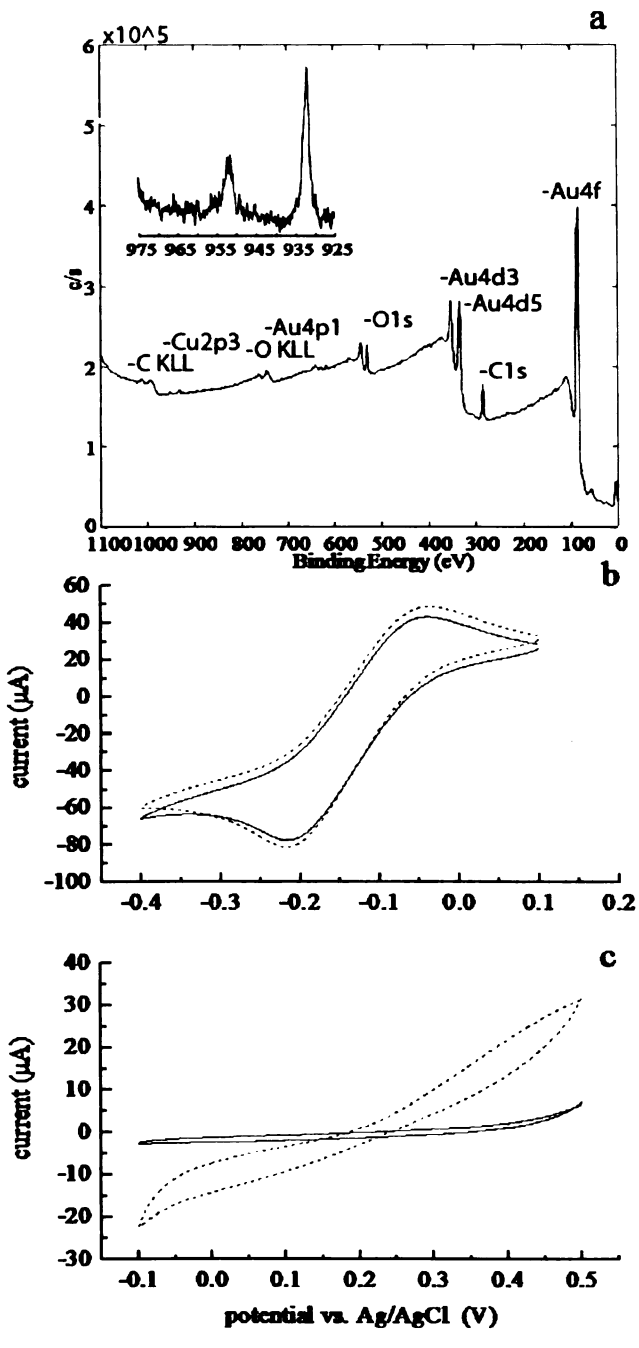

Fig. 4-8: a) XPS spectrum of Cu^{+2}-modified thiol/gold substrate. Inset shows Cu2P spectral region. b) CV of $Ru(NH_3)_6Cl_3$ for a DMPA monolayer on Cu^{+2}-terminated interface (dashed line) and for the Cu^{+2}-terminated interface with no adlayer (solid line). c) CV of $K_3Fe(CN)_6$ for a DMPA monolayer on Cu^{+2}-terminated interface (dashed line) and for the Cu^{+2}-terminated inter-face with no adlayer (solid line).

4-4.8: Copper II

Modification of the phosphate-terminated interface with Cu^{+2} produces a fundamentally different interaction upon DMPA exposure than is seen for the Cu^{+}-terminated interface. XPS measurements indicate very little Cu^{+2} being deposited on the phosphate-terminated interface, with a concentration ratio of Cu^{+2}:Au of 0.03 (Fig. 4-8a). This finding indicates little opportunity for adlayer formation in a manner similar to that seen for other divalent metal ions. Without the deposition of Cu^{+2} at the phosphate-terminated interface, the interface that will be available for interaction with DMPA will be dominated by the presence of phosphate, resulting in the formation of a lipid bilayer.[116] The ellipsometry and contact

angle confirm this assertion with the DMPA adlayer thickness being 63±5 Å and a water contact angle of 23±2°. Due to the significantly hydrophilic surface formed by this adlayer, hysteresis measurements could not be performed with any degree of accuracy. The CV measurements are consistent with the presence of a lipid bilayer at the interface. For the Ru probe, the Cu^{+2}-terminated interface produces a splitting of 178 mV (Fig. 4-8b) and the DMPA-terminated interface exhibits a 185 mV peak splitting. The absence of a measurable difference in the peak splitting for the two interfaces suggests a bilayer with a high defect density. Using the Fe probe, a capacitance ratio of 2.92 (Fig. 4-8c) was obtained, indicating a comparatively thick adlayer forms upon DMPA deposition.

4-5: Comparison of Metal-ion Modified Interfaces

With the data reported for the different metal ions, now it is time to consider how these results compare to one another. Table 4-1 shows the results for each interface. From these data it emerges that there are three classes of interface that form. Some metal ions (Fe^{+3}, Zr^{+4}) form a relatively well organized monolayer structure upon complexation with DMPA, some metal ions (Cu^{+2}) yield a bilayer structure, and some metal ions (Zn^{+2}, Ni^{+2}, Cu^{+}, Ca^{+2}, Mg^{+2}) produce a partial adlayer characterized by limited organization. These different characteristic interfaces are attributed to the result of the ability of the metal ions examined to form ionic complexes with phosphates, and this complex-forming ability is correlated for the most part with thecharge of the metal ion. For some metal ions (Ni^{+2}, Ca^{+2}, Mg^{+2}) the addition of the DMPA overlayer appears to produce a disruption of the organization of the supporting SAM. This disruption is attributed to a stoichiometric deficiency of the metal ion based on its formal charge and consequent inability to form a regular structure when sandwiched between two phosphate planes. Specifically, the issue of charge compensation likely plays a central role in deter

Metal	XPS Mn^{+n}:Au4f ratio	Ellipso-metric thickness (Å)	Water contact angle (deg.)	Contact angle hystere-sis (deg.)	$Ru^{+3/+4}$ splitting (mV) for M^{+n} surface	$Ru^{+3/+4}$ splitting (mV) for DMPA surface	$Fe^{+2/+3}$ non-Faradaic current ratio
Cu^{+}	0.21	14±5	52±3	6	155	256	2.21
Cu^{+2}	0.03	63±5	23±5	--	178	185	2.92
Ni^{+2}	0.08	27±3	50±3	2	209	171	1.28
Zn^{+2}	0.08	31±2	66±2	8	166	214	4.72
Ca^{+2}	0.08	39±2	37±6	7	237	224	0.19
Mg^{+2}	0.08	38±1	61±10	8	206	157	1.77
Fe^{+3}	0.46	26±2	102±2	7	175	277	0.57
Zr^{+4}	0.34	30±2	104±1	5	163	212	0.54

Table 4-1: Data for the interfaces examined in this work. In the first column, metal ion-surface coverage reported by the ratio of the XPS M^{+n} to Au4f signal intensities; second column, ellipsometric thickness in Å; Water contact angle of DMPA-terminated inter-faces, in degrees; water contact angle hysteresis in degrees; $Ru^{+3/+4}$ CV peak splitting for metal ion-terminated in-terface; $Ru^{+3/+4}$ CV peak splitting for DMPA-terminated inter-faces; $Fe^{+2/+3}$ CV ratio of non-Faradaic current for metal-terminated interface to DMPA-terminated interface. All CV data has an associated 0.5 mV error.

mining the organization of the interfaces. The divalent metal ions are characterized by comparatively low surface loading densities and, in order to achieve surface charge compensation upon reaction with metal ions, there must also be residual H^{+} present. Upon addition of the phospholipid, charge compensation becomes a more significant issue, with Na^{+} and/or tris(hydroxymethyl)-aminomethane cation from the buffer in the vesicle-containing solution being the only additional cationic species present that are capable of charge compensation. It is the structural accommodation of these additional cationic species that must be responsible at some level for the changes in organization of the self-assembled monolayer upon addition of DMPA, and this effect can be seen in certain of the CV results.

Fe^{+3} and Zr^{+4} are known to bind strongly to phosphate and have sufficiently high formal charge to accommodate the presence of the DMPA functionality without disrup-

tion of the underlying phosphate layer. Copper is unique because Cu^{+2} is found to bind to the phosphate-terminated SAM more weakly the Cu^{+}. The limited extent to which Cu^{+2} bonds to phosphate gives rise to the formation of a DMPA bilayer rather than a monolayer, consistent with very weak Cu^{+2} – phosphate interactions. This finding implies an interface that is closer to a hydroxyl-terminated interface in terms of the strength of interaction with the lipid adlayer.[116] Cu^{+} gives rise to the formation of a more monolayer-like lipid adlayer, albeit with extensive heterogeneity and likely regions of little or no DMPA deposition. It is apparent from this data that a prerequisite for the formation of a reasonably well organized lipid adlayer is the presence of sufficient metal ion loading density at the interface. XPS data shows comparatively high interface coverage for Fe^{+3} and Zr^{+4}. Metal ions that are deposited at the phosphate interface at lower loading density give rise to a lower quality lipid adlayer, as can be seen from contact angle data and especially electrochemical data.

4-6: Conclusions

In this study the interactions between selected metal ions, a phosphate-terminated interface and the phospholipid DMPA have been investigated. The chemical interactions investigated in this work are akin to those examined for metal bisphosphonate multilayer structures with selected metal ions, with similar results.[145] The goal of this work, however, is aimed at understanding the limits on the ability to form strongly bound supported lipid mono- and bilayer structures. This data point to the use of metal ions with high ionic charge and small ionic radius as being the most useful for forming lipid adlayer structures. In general, divalent metal ions give rise to partial, spatially heterogeneous structures that may or may not be useful in the creation of biomimetic interfaces, depending on the application.

Chapter 5
Conclusions

In this work the formation of air stable lipid monolayers and bilayers has been explored. The goal in forming these various adlayers is to create a one step approach utilizing vesicle fusion for the formation of lipid adlayer structures that can be removed from the aqueous environment in which they are formed. To act as a first step in creating an interface that could be useful in simulating a plasma membrane structure in a sensor format, these interfaces need to be stable in air and be comparatively free of structural defects. The imposition of a robust physical structure on a system that must perform as a two-dimensional fluid is a challenging prospect.

The initial step in this work was to explore how to create an air-stable lipid adlayer. To succeed in this attempt, (Chapter 2) it is necessary to maximize the intermolecular interactions between the phospholipid lipid headgroup and the supporting substrate. Two distinct but related interfaces were utilized for this purpose; 6-mercaptohexanol and zirconium phosphate modified gold substrates. These modifications allowed for different molecular interactions to be explored. The mercaptohexanol -OH terminal functionality allowed for polar interactions with the lipid headgroup, allowing for the deposition of a lipid bilayer structure. DMPC does not covalently bond to this surface, which then allows for lateral diffusion of the lipids to produce a bilayer structure. The Zr^{+4} modified surface utilized the known strong interaction of Zr ion to phosphates/bisphosphates (ZP chemistry). The phosphate group on DMPC coordinates to the bound Zr^{+4} preventing further lateral diffusion or translocation leaving the lipids in place. This molecular interaction was verified by ^{31}P-NMR spectroscopy. What is seen is that a partial bilayer initially formed would gradually decay over a period of 20 min. to a DMPC monolayer.

Monolayer formation is attributed to the irreversibility of the Zr^{+4}/lipid headgroup coordination. This work showed that, by maximizing strong intermolecular or ionic forces, it is possible to stabilize the lipid adlayer that is exposed to the substrate, making the corresponding adlayer air stable. This result is desirable for the formation of an air-stable lipid adlayer, and it is the use of ZP chemistry that allows this structural motif to be realized.

The initial step of this work lead to the ability to create air stable lipid bilayers and monolayers. What also resulted from this work was the observation that DMPC, a phosphocholine, would coordinate with the Zr^{+4} modified surface. To further understand the interactions at the Zr^{+4}/headgroup point of interaction, other lipid headgroups interactions must be explored (Chapter 3). It was desirable to examine lipids with headgroup functionalities that varied in both size and polarity. The operating hypothesis is that each headgroup would have a distinctly different interaction with the Zr^{+4} on the surface based on these lipid properties. It should be first noted that the bound Zr^{+4} will have excess coordinated water surrounding it because no attempt was made to make the substrates anhydrous. Therefore, if the phospholipid headgroup is to bind to the Zr^{+4}, the water must be displaced. This becomes problematic with headgroups that can hydrogen bond as they will interact with the surrounding water opposed to the Zr leaving weaker coordination and in turn poor adlayers. Steric and polar interactions will have a minor effect as well but are secondary to the H-bonding effects. As a result it was observed that PA and PC showed strong interaction with the surface, where PE, PG, and PS showed poor adlayer formation, consistent with less energetically favorable interactions with the surface-bound Zr. This is an expected result because PA is a small headgroup which eliminates steric factors contributing to it's interaction with Zr^{+4}, and while it is polar and can hydrogen bond with the excess water around the Zr^{+4}, the lack of steric hindrance allows for the PA to displace the coordinated water and coordinate strongly to the bound Zr. PC,

though being a larger headgroup, does not have the chemical functionality required to hydrogen bond substantially because there are three methyl groups on the amine portion of the choline headgroup. Phospholipid headgroups that do not undergo strong H-bonding interactions allow for displacement of the water and good coordination with the bound Zr^{+4}. PE, PG, and PS are all larger headgroups which will limit access of the headgroup organophosphate moiety to the Zr^{+4}, while polar interactions and to a greater extent the ability of these headgroups to form H-bonds with any surrounding water, minimizes interactions with the bound Zr, consequently producing poor adlayers. The comparison of the data illustrated the wide range of interactions that are possible with the various lipid headgroups and the Zr^{+4} surface. Given the headgroup-dependent nature of lipid interactions with the surface-bound Zr^{+4}, it is also likely that the interactions between lipid headgroups and selected metal ions will differ significantly.

The goal of the work presented in Chapter 4 was to investigate the effect the metal has on the lipid headgroups interaction and adlayer formation. As discussed above, previous studies have shown that metal ions other than Zr^{+4} can bind strongly with phosphates. The work presented in Chapter 4 was designed to explore the interactions between a phosphatidic acid and selected metal ions bound to a phosphate-terminated interface. Phosphatidic acids (PA) were found to have the strongest interaction with Zr^{+4} from the work presented in Chapter 3 and, therefore, PA was chosen for the metal ion-dependence study. The goal was to minimize steric contributions to the metal-phosphate interactions. The substrates were modified with biologically relevant metals in an effort to investigate the effect of the metal on the metal/phosphate interaction with the lipids and the surface bound metal. The interactions between DMPA and the several surface-bound metal ions that the strength of lipid-interface interaction depended significantly on the identity of the metal ion. The thickness and uniformity of the metal ion-bound DMPA adlayer was

found to depend on the formal charge of the metal ion used. The strongest metal ion-lipid interactions were found for metal ions with comparatively high (+3, +4) ionic charge and small ionic radius. Fe^{+3} and Zr^{+4} formed the strongest complexes with DMPA and thus the most uniform adlayers resulted. It is also found that the range of interactions of DMPA with the bound metal ions is limited by the quality of the surface-bound metal ion layer formed on the substrate. To form a surface-bound complex, the metal ions must interact with a bound phosphate group on the substrate and the phosphate functionality of DMPA. Owing to the requirement of macroscopic charge neutrality, divalent and monovalent metal ions would be more likely to compete with other ions (e.g. H^{+}, Na^{+}) and thus an interface with a comparatively high density of defects would result. If there is not enough charge to balance the PA anions, then poor adlayer formation is observed. This situation was found to obtain for Ca^{+2}, Mg^{+2}, Cu^{+}, Cu^{+2}, Zn^{+2}, and Ni^{+2}. Without a balance of charge that can be satisfied only by the metal ion and the phosphate moieties in the layer where complexation occurs, it is difficult to form high quality adlayers. This phenomenon is consistent with what is known about ZP layered materials and suggests that much of the knowledge relating to ZP layered materials can be applied to the formation of lipid adlayers by these means.

One issue that was not explored through these studies and would be a logical next step, is the effect of acyl chain length on adlayer formation. While it is most probable that the dominant molecular interaction in the deposition of metal ion-bound lipid adlayers is the interaction between the lipid headgroup and the metal ion, it is possible that the structure and conformation of the acyl chains could play a role. The gel-to-fluid phase transition for phospholipids is thought to be dominated by acyl chain length and extent of unsaturation, and the propensity of the acyl chains to organize in concert with the headgroup-metal ion complexation process could, in principle, play a role in the forma-

tion of lipid adlayers. An experiment that could be performed to evaluate the importance of lipid acyl chain length and structure would utilize selected phosphatidic acids and complexation would proceed with Zr-modified substrates. Choice of the PA to use would be important because the acyl chains impact several physical properties of the lipids that could potentially influence adlayer formation. First, the issue of the lipids solubility in water must be considered. Lipids exhibit limited solubility in water, and solubility will depend on acyl chain length. A decrease in lipid solubility could result in less efficient vesicle fusion. Additional factors that would factor into lipid choice would be the secondary organizational role that the acyl chain chains play in mediating adlayer organization. These considerations are reflected in the gel-to-fluid phase transition temperature T_m of the lipids. The work discussed in this dissertation has been performed with lipids chosen to have the same chain length (C_{14}) and thus similar transition temperatures T_m, near 24° C. While the use of a lipid with a higher T_m could interfere with adlayer deposition for reasons of solubility, the increased chain length of such a lipid may also serve to introduce organization to the adlayers, once they form. The careful choice of lipid acyl chain length and degree of unsaturation will likely allow these issues to be resolved in future experiments.

The work presented in this disertation provides insight into the factors that allow for the formation of air-stable, surface-bound lipid bilayers and monolayers. From this foundation, it will be possible to explore potential applications that utilize air stable bilayers and/or metal ion coordination with phospholipid headgroups. The availability of air-stable lipid adlayers may form the foundation for novel multilayer structures, and a key issue will be the extent to which the surface-bound adlayer can mimic the fluid nature of a plasma membrane. If the lipid adlayers can be organized and/or modified to become biomimetic, an effort that is presently underway in the Blanchard group, the next step

will be to explore the incorporation of biologically active molecules (*e.g.* transmembrane proteins) groups into the bilayer structure. Owing to the structural and compositional complexity of plasma membranes, the incorporation of multiple bilayer constituents, including cholesterol for example, will be required to produce a biomimetic interface. While this goal will likely not be realized for several years, initial studies to evaluate the stabilization of the bilayer with the addition of multiple components as well as the examination of any phase segregation which may take place, will be necessary.

It is also possible that further exploration of the interactions between interface-bound metal ions and phospholipids will lead to the creation of interfaces that adsorb lipids with different headgroups selectively. Since it has been established that various lipid headgroups interact differently to the presence of Zr^{4+}, it is possible that different interface structural motifs or the use of different metal ion complexing agents could produce higher lipid selectivity than has been seen to date. The effect of lipid acyl chain length and saturation could also influence the efficiency of interfacial lipid adsorption, an issue that bears investigation in the future (*vide infra*).

The work reported in this dissertation points to the benefits and possibilities that could result from creating modified substrates as support structures for lipid bilayers or monolayers. Through careful chemical control of the modified substrate, it is possible to create air stable bilayers and lipid monolayers using vesicle fusion. These findings point the way toward possible applications in chemical sensing and the design of biomimetic interfaces.

Literature Cited

(1) Edidin, M. Nature Reviews. Molecular Cell Biology 2003, 4, 414.

(2) Ikeda, M.; Kihara, A.; Igarashi, Y. Biological & Pharmaceutical Bulletin 2006, 29, 1542.

(3) Lee, A. Current Biology 2001, 11, R811.

(4) Anderson, T. G.; McConnell, H. M. Biophysical Journal 2001, 81, 2774.

(5) Anderson, T. G.; McConnell, H. M. Biophysical Journal 2002, 83, 2039.

(6) Benvegnu, D. J.; McConnell, H. M. Journal of Physical Chemistry 1993, 97, 6686.

(7) Brian, A. A.; McConnell, H. M. Proceedings of the National Academy of Sciences 1984, 81, 6159.

(8) Keller, S. L.; McConnell, H. M. Physical Review Letters 1999, 82, 1602.

(9) Keller, S. L.; Radhakrishnan, A.; McConnell, H. M. Journal of Physical Chemistry B 2000, 104, 7522.

(10) Kornberg, R. D.; McConnell, H. M. Biochemistry 1971, 10, 1111.

(11) Lee, K. Y. C.; Klingler, J. F.; McConnell, H. M. Nature 1994, 263, 655.

(12) Radhakrishnan, A.; McConnell, H. M. Journal of the American Chemical Society 1999, 121, 486.

(13) Radhakrishnan, A.; McConnell, H. M. Biophysical Journal 1999, 77, 1507.

(14) Radhakrishnan, A.; McConnell, H. M. Journal of Physical Chemistry B 2002, 106, 4755.

(15) Subramaniam, S.; McConnell, H. M. Journal of Physical Chemistry 1987, 91, 1715.

(16) Tamm, L. K.; McConnell, H. M. Biophysical Journal 1985, 47, 105.

(17) Xu, Y.; Shen, Z. Z.; Wiper, D. W.; Wu, M. Z.; Morton, R. E.; Elson, P.; Kennedy, A. W.; Belinson, J.; Markman, M.; Casey, G. Jama-Journal of

the American Medical Association 1998, 280, 719.

(18) Discher, B. M.; Maloney, K. M.; Grainger, D. W.; Sousa, C. A.; Hall, S. B. Biochemistry 1999, 38, 374.

(19) Samsonov, A. V.; Mihalyov, I.; Cohen, F. S. Biophysical Journal 2001, 81, 1486.

(20) Yechiel, E.; Edidin, M. Journal of Cell Biology 1987, 105, 755.

(21) Epand, R. M. Biochemical Society Transactions 1997, 25, 1073.

(22) Tocanne, J. F.; Cezanne, L.; Lopez, A.; Piknova, B.; Schram, V.; Tournier, J. F.; Welby, M. Chemistry and Physics of Lipids 1994, 73, 139.

(23) McMullen, T. P. W.; McElhaney, R. N. Biochimica Et Biophysica Acta-Biomembranes 1995, 1234, 90.

(24) Pabst, G.; Amenitsch, H.; Kharakoz, D. P.; Laggner, P.; Rappolt, M. Physical Review E 2004, 70.

(25) Stevens, B. C.; Ha, T. Journal of Chemical Physics 2004, 120, 3030.

(26) Prenner, E. J.; Lewis, R.; Kondejewski, L. H.; Hodges, R. S.; McElhaney, R. N. Biochimica Et Biophysica Acta-Biomembranes 1999, 1417, 211.

(27) Lewis, R.; McElhaney, R. N. Biophysical Journal 2000, 79, 2043.

(28) Koan, M. M.; Blanchard, G. J. Journal of Physical Chemistry B 2006, 110, 16584.

(29) Perrin, F. Journal De Physique Et Le Radium 1936, 7, 1.

(30) Debye, P. Polar Molecules; Chemical Catalog Co.: New York, 1929.

(31) Zwanzig, R.; Harrison, A. K. Journal of Chemical Physics 1985, 83, 5861.

(32) Edward, J. T. Journal of Chemical Education 1970, 47, 261.

(33) Khan, T. K.; Chong, P. L. G. Biophysical Journal 2000, 78, 1390.

(34) Lakowicz, J. R.; Knutson, J. R. Biochemistry 1980, 19, 905.

(35) Marsh, D. Handbook of Lipid Bilayers; CRC Press: Boca Raton, Fl, 1990.

(36) McConnell, H. Biophysical Journal 2005, 88, L23.

(37) Radhakrishnan, A.; McConnell, H. Proceedings of the National Academy of Sciences of the United States of America 2005, 102, 12662.

(38) McConnell, H. M.; Radhakrishnan, A. Biochimica Et Biophysica Acta-Biomembranes 2003, 1610, 159.

(39) Simons, K.; Ikonen, E. Nature 1997, 387, 569.

(40) Veatch, S. L.; Keller, S. L. Biophysical Journal 2003, 85, 3074.

(41) Veatch, S. L.; Keller, S. L. Physical Review Letters 2005, 94.

(42) Dietrich, C.; Bagatolli, L. A.; Volovyk, Z. N.; Thompson, N. L.; Levi, M.; Jacobson, K.; Gratton, E. Biophysical Journal 2001, 80, 1417.

(43) Veatch, S. L.; Polozov, I. V.; Gawrisch, K.; Keller, S. L. Biophysical Journal 2004, 86, 2910.

(44) Tenenhouse, H. S.; Murer, H. Journal of the American Society of Nephrology 2003, 14, 240.

(45) Inoue, M.; Digman, M. A.; Cheng, M.; Breusegem, S. Y.; Halaihel, N.; Sorribas, V.; Mantulin, W. W.; Gratton, E.; Barry, N. P.; Levi, M. Journal of Biological Chemistry 2004, 279, 49160.

(46) McConnell, H. M.; Watts, T. H.; Weis, R. M.; Brian, A. A. Biochimica Et Biophysica Acta 1986, 864, 95.

(47) Grakoui, A.; Bromley, S. K.; Sumen, C.; Davis, M. M.; Shaw, A. S.; Allen, P. M.; Dustin, M. L. Science 1999, 285, 221.

(48) Groves, J. T.; Boxer, S. G. Accounts of Chemical Research 2002, 35, 149.

(49) Plant, A. L. Langmuir 1993, 9, 2764.

(50) Sackmann, E. Science 1996, 271, 43.

(51) Cornell, B. A.; BraachMaksvytis, V. L. B.; King, L. G.; Osman, P. D. J.; Raguse, B.; Wieczorek, L.; Pace, R. J. Nature 1997, 387, 580.

(52) Groves, J. T.; Ulman, N.; Boxer, S. G. Science 1997, 275, 651.

(53) Jenkins, A. T. A.; Boden, N.; Bushby, R. J.; Evans, S. D.; Knowles, P. F.; Miles, R. E.; Ogier, S. D.; Schonherr, H.; Vancso, G. J. Journal of the American Chemical Society 1999, 121, 5274.

(54) Cremer, P. S.; Yang, T. L. Journal of the American Chemical Society 1999, 121, 8130.

(55) Ataka, K.; Giess, F.; Knoll, W.; Naumann, R.; Haber-Pohlmeier, S.; Richter, B.; Heberle, J. Journal of the American Chemical Society 2004, 126, 16199.

(56) Giess, F.; Friedrich, M. G.; Heberle, J.; Naumann, R. L.; Knoll, W. Bio physical Journal 2004, 87, 3213.

(57) Dominska, M.; Krysinski, P.; Blanchard, G. J. Langmuir 2008, 24, 8785.

(58) Stroumpoulis, D.; Parra, A.; Tirrell, M. Aiche Journal 2006, 52, 2931.

(59) Schonherr, H.; Johnson, J. M.; Lenz, P.; Frank, C. W.; Boxer, S. G. Langmuir 2004, 20, 11600.

(60) Greenough, K. P.; Blanchard, G. J. Journal of Physical Chemistry B 2006, 110, 6351.

(61) Lapinski, M. M.; Blanchard, G. J. Chemistry and Physics of Lipids 2007, 150, 12.

(62) Mohandas, N.; Wyatt, J.; Mel, S. F.; Rossi, M. E.; Shohet, S. B. Journal of Biological Chemistry 1982, 257, 6537.

(63) Pomorski, T.; Holthuis, J. C. M.; Herrmann, A.; van Meer, G. Journal of Cell Science 2004, 117, 805.

(64) Lin, W. C.; Blanchette, C. D.; Ratto, T. V.; Longo, M. L. Biophysical Journal 2006, 90, 228.

(65) Kol, M. A.; de Kruijff, B.; de Kroon, A. Seminars in Cell & Developmental Biology 2002, 13, 163.

(66) Menon, A. K.; Watkins, W. E.; Hrafnsdottir, S. Current Biology 2000, 10, 241.

(67) Raggers, R. J.; Pomorski, T.; Holthuis, J. C. M.; Kalin, N.; van Meer, G. Traffic 2000, 1, 226.

(68) Menon, A. Trends in Cell Biology 1995, 5, 355.

(69) Devaux, P. F.; Lopez-Montero, I.; Bryde, S. Chemistry and Physics of Lipids 2006, 141, 119.

(70) Anglin, T. C.; Liu, J.; Conboy, J. C. Biophysical Journal 2007, 92, L1.

(71) Liu, J.; Conboy, J. C. Biophysical Journal 2005, 89, 2522.

(72) Ross, E. E.; Rozanski, L. J.; Spratt, T.; Liu, S. C.; O'Brien, D. F.; Saavedra, S. S. Langmuir 2003, 19, 1752.

(73) Tero, R.; Takizawa, M.; Li, Y. J.; Yamazaki, M.; Urisu, T. Langmuir 2004, 20, 7526.

(74) Isono, T. T., H.; Ogino, T. Journal of Surface Science and Nanotechnology 2007, 5, 99.

(75) Groves, J. T.; Ulman, N.; Cremer, P. S.; Boxer, S. G. Langmuir 1998, 14, 3347.

(76) Deng, Y.; Wang, Y.; Holtz, B.; Li, J. Y.; Traaseth, N.; Veglia, G.; Stottrup, B. J.; Elde, R.; Pei, D. Q.; Guo, A.; Zhu, X. Y. Journal of the American Chemical Society 2008, 130, 6267.

(77) Ross, E. E.; Bondurant, B.; Spratt, T.; Conboy, J. C.; O'Brien, D. F.; Saavedra, S. S. Langmuir 2001, 17, 2305.

(78) Cao, G.; Hong, H. G.; Mallouk, T. E. Accounts of Chemical Research 1992, 25, 420.

(79) Katz, H. E.; Scheller, G.; Putvinski, T. M.; Schilling, M. L.; Wilson, W. L.; Chidsey, C. E. D. Science 1991, 254, 1485.

(80) Kohli, P.; Rini, M. C.; Major, J. S.; Blanchard, G. J. Journal of Materials Chemistry 2001, 11, 2996.

(81) Lee, H.; Kepley, L. J.; Hong, H. G.; Akhter, S.; Mallouk, T. E. Journal of Physical Chemistry 1988, 92, 2597.

(82) Putvinski, T. M.; Schilling, M. L.; Katz, H. E.; Chidsey, C. E. D.; Mujsce, A. M.; Emerson, A. B. Langmuir 1990, 6, 1567.

(83) Schilling, M. L.; Katz, H. E.; Stein, S. M.; Shane, S. F.; Wilson, W. L.; Buratto, S.; Ungashe, S. B.; Taylor, G. N.; Putvinski, T. M.; Chidsey, C. E. D. Langmuir 1993, 9, 2156.

(84) Vermeulen, L. A.; Snover, J. L.; Sapochak, L. S.; Thompson, M. E. Journal of the American Chemical Society 1993, 115, 11767.

(85) Vermeulen, L. A.; Thompson, M. E. Nature 1992, 358, 656.

(86) Vermeulen, L. A.; Thompson, M. E. Chemistry of Materials 1994, 6, 77.

(87) Kohli, P.; Blanchard, G. J. Langmuir 2000, 16, 695.

(88) Krysinski, P.; BrzostowskaSmolska, M. Journal of Electroanalytical Chemistry 1997, 424, 61.

(89) Mazur, M.; Krysinski, P.; Blanchard, G. J. Langmuir 2005, 21, 8802.

(90) Mayer, L. D.; Hope, M. J.; Cullis, P. R. Biochimica Et Biophysica Acta 1986, 858, 161.

(91) Hunter, D. G.; Frisken, B. J. Biophysical Journal 1998, 74, 2996.

(92) Moscho, A.; Orwar, O.; Chiu, D. T.; Modi, B. P.; Zare, R. N. Proceedings of the National Academy of Sciences of the United States of America 1996, 93, 11443.

(93) Patty, P. J.; Frisken, B. J. Biophysical Journal 2003, 85, 996.

(94) Holden, M. A.; Jung, S.-Y.; Yang, T.; Castellana, E. T.; Cremer, P. S. Journal of the American Chemical Society 2004, 126, 6512.

(95) Porter, M. D.; Bright, T. B.; Allara, D. L.; Chidsey, C. E. D. Journal of the American Chemical Society 1987, 109, 3559.

(96) Brechling, A.; Sundermann, M.; Kleineberg, U.; Heinzmann, U. Thin Solid Films 2003, 433, 281.

(97) Foss, B. J.; Sliwka, H. R.; Partali, V.; Naess, S. N.; Elgsaeter, A.; Melo, T. B.; Naqvi, K. R. Chemistry and Physics of Lipids 2005, 134, 85.

(98) Munro, J. C.; Frank, C. W. Langmuir 2004, 20, 3339.

(99) Toca-Herrera, J. L.; Krustev, R.; Muller, H. J.; Mohwald, H. Journal of Physical Chemistry B 2000, 104, 5486.

(100) Burwell, D. A.; Valentine, K. G.; Thompson, M. E. Journal of Magnetic Resonance 1992, 97, 498.

(101) Colon, J. L.; Yang, C. Y.; Clearfield, A.; Martin, C. R. Journal of Physical Chemistry 1988, 92, 5777.

(102) Hanken, D. G.; Corn, R. M. Analytical Chemistry 1997, 69, 3665.

(103) Horne, J. C.; Blanchard, G. J. Journal of the American Chemical Society

1998, 120, 6336.

(104) Conboy, J. C.; Liu, S.; O'Brien, D. F.; Saavedra, S. S. Biomacromolecules 2003, 4, 841.

(105) Liu, J.; Conboy, J. C. Langmuir 2005, 21, 9091.

(106) McConnell, H. M.; Watts, T. H.; Weis, R. M.; Brian, A. A. Biochim. Biophys. Acta 1986, 864, 95.

(107) Plant, A. L. Langmuir 1999, 15, 5128.

(108) Starr, T. E.; Thompson, N. L. Langmuir 2000, 16, 10301.

(109) Burwell, D. A.; Thompson, M. E. Chemistry of Materials 1991, 3, 730.

(110) Burwell, D. A.; Thompson, M. E. Acs Symposium Series 1992, 499, 166.

(111) Frey, B. L.; Hanken, D. G.; Corn, R. M. Langmuir 1993, 9, 1815.

(112) Hong, H. G.; Sackett, D. D.; Mallouk, T. E. Chemistry of Materials 1991, 3, 521.

(113) Katz, H. E.; Schilling, M. L. Chemistry of Materials 1993, 5, 1162.

(114) Ungashe, S. B.; Wilson, W. L.; Katz, H. E.; Scheller, G. R.; Putvinski, T. M. Journal of the American Chemical Society 1992, 114, 8717.

(115) Newman, J. D. S.; Roberts, J. M.; Blanchard, G. J. Analytica Chimica Acta 2007, 602, 101.

(116) Oberts, B. P., Blanchard, G. J. Langmuir 2009, 25, 2962.

(117) Edidin, M. Nature Reviews Molecular Cell Biology 2003, 4, 414.

(118) Chidsey, C. E. D.; Porter, M. D.; Allara, D. L. Journal of the Electrochemical Society 1986, 133, C130.

(119) Dubois, L. H.; Zegarski, B. R.; Nuzzo, R. G. Journal of Vacuum Science & Technology a-Vacuum Surfaces and Films 1987, 5, 634.

(120) Nuzzo, R. G.; Allara, D. L. Journal of the American Chemical Society 1983, 105, 4481.

(121) Nuzzo, R. G.; Fusco, F. A.; Allara, D. L. Journal of the American Chemical Society 1987, 109, 2358.

(122) Nuzzo, R. G.; Zegarski, B. R.; Dubois, L. H. Journal of the American Chemical Society 1987, 109, 733.

(123) Ulman, A. Chemical Reviews 1996, 96, 1533.

(124) Whitesides, G. M.; Troughton, E. B.; Bain, C.; Holmesfarley, S. R.; Wasserman, S. R.; Strong, L. H. Journal of the Electrochemical Society 1987, 134, C110.

(125) Xia, Y. N.; Whitesides, G. M. Annual Review of Materials Science 1998, 28, 153.

(126) Fang, C. P.; Drelich, J. Langmuir 2004, 20, 6679.

(127) Major, J. S.; Blanchard, G. J. Langmuir 2001, 17, 1163.

(128) Tulock, J. J.; Blanchard, G. J. Journal of Physical Chemistry B 2002, 106, 3568.

(129) Malinauskas, A.; Ruzgas, T.; Gorton, L. Bioelectrochemistry and Bioenergetics 1999, 49, 21.

(130) Pet'kov, V. I.; Asabina, E. A.; Markin, A. V.; Smirnova, N. N.; Kitaev, D. B. Journal of Thermal Analysis and Calorimetry 2005, 80, 695.

(131) Bakiamoh, S. B.; Blanchard, G. J. Langmuir 1999, 15, 6379.

(132) Bakiamoh, S. B.; Blanchard, G. J. Langmuir 2001, 17, 3438.

(133) Oberts, B. P., Blanchard, G. J. Langmuir 2009, XX, XXXX.

(134) Akhter, S.; Lee, H.; Hong, H. G.; Mallouk, T. E.; White, J. M. Journal of Vacuum Science & Technology a-Vacuum Surfaces and Films 1989, 7, 1608.

(135) Bujoli, B.; Courilleau, A.; Palvadeau, P.; Rouxel, J. European Journal of Solid State and Inorganic Chemistry 1992, 29, 171.

(136) Bujoli, B.; Pena, O.; Palvadeau, P.; Lebideau, J.; Payen, C.; Rouxel, J. Chemistry of Materials 1993, 5, 583.

(137) Cao, G.; Lee, H.; Lynch, V. M.; Mallouk, T. E. Inorganic Chemistry 1988, 27, 2781.

(138) Cao, G.; Lynch, V. M.; Swinnea, J. S.; Mallouk, T. E. Inorganic Chemistry 1990, 29, 2112.

(139) Cao, G.; Mallouk, T. E. Journal of Solid State Chemistry 1991, 94, 59.

(140) Cao, G.; Mallouk, T. E. Inorganic Chemistry 1991, 30, 1434.

(141) Cao, G.; Rabenberg, L. K.; Nunn, C. M.; Mallouk, T. E. Chemistry of Materials 1991, 3, 149.

(142) Cao, H.; Tokutake, N.; Regen, S. L. Journal of the American Chemical Society 2003, 125, 16182.

(143) Feldheim, D. L.; Mallouk, T. E. Chemical Communications 1996, 2591.

(144) Kim, Y. H.; Rahman, M. M.; Zhang, Z. L.; Misawa, N.; Tero, R.; Urisu, T. Chemical Physics Letters 2006, 420, 569.

(145) Yang, H. C.; Aoki, K.; Hong, H. G.; Sackett, D. D.; Arendt, M. F.; Yau, S. L.; Bell, C. M.; Mallouk, T. E. Journal of the American Chemical Society 1993, 115, 11855.